INDENTATION HARDNESS AND ITS RELATION TO MECHANICAL YIELD IN QUARTZ AND OLIVINE

by

JAMES BRIAN EVANS

B.S., University of Idaho (1968)

M.S., University of Minnesota (1975)

SUBMITTED IN PARTIAL FULFILLMENT

OF THE REQUIREMENTS FOR THE

DEGREE OF DOCTOR OF

PHILOSOPHY

at the

MASSACHUSETTS INSTITUTE OF TECHNOLOGY

AUGUST 1978

Signature of Author _____
Department of Earth and Planetary Sciences
August, 1978

Certified by _____
Thesis Supervisor

Accepted by _____
Chairman, Departmental Committee on Graduate Students

ABSTRACT

INDENTATION HARDNESS AND ITS RELATION TO MECHANICAL YIELD IN QUARTZ AND OLIVINE

by

JAMES BRIAN EVANS

Submitted to the Department of Earth and Planetary Sciences

The variation of indentation hardness with temperatures was measured for quartz and olivine up to temperatures of 800°C and 1500°C respectively. A comparative review of hardness data and compressive creep measurements done under high pressure show that the single crystal hardness measurements, when corrected for elastic strains, can be correlated to the fully ductile yielding of a polycrystal.

For olivine, the computed differential yield stresses, σ (in GPa), in the region above $\sigma = .2$ GPa were well represented by an equation of the form

$$\sigma = 9.1(\pm.3) - .23(\pm.01)T^{1/2}$$

where T is the absolute temperature (in K) and the quoted variances are for 1 standard deviation. For olivine and Frederick, Maryland diabase, the 15 second indentation test empirically corresponds to a polycrystalline yield test conducted at strain rate $\dot{\sigma} = 10^{-5}s^{-1}$. Using a semi-empirical method of dislocation rosette analysis, the critical resolved shear stress on the {110}[001] slip system was estimated to 20% over the temperature range 20°C to 780°C as 1.2 GPa and .3GPa respectively.

The hardness of seven quartz samples containing a range of structural hydroxyl impurities up to 400 H/10^6 Si was measured to 800°C. There was no significant variation of hardness for any impurity content at any temperature. Annealing the samples at 600°C for several hours in dry argon caused the hardness to increase by a factor of 1.6 at 500°C. The hardness data when reduced to hardness derived-yield stress and combined with previously published data, delineates an empirical yield stress curve for strain rate of $10^{-5\pm.5}$, but the data are insufficient to determine a constitutive flow law.

Indentation tests are most useful to obtain estimates of the variation of yield stress with temperature, to compare relative ductility of compositional variations of minerals, and as an adjunct to conventional creep tests to extend the range of stresses attainable in the laboratory.

Table of Contents

Figures

Tables

Acknowledgements

It is a humbling experience to reflect on the number of people who have helped me in one way or another and it is an honor to thank the many teachers that I have had, many of whom have been called by that title and some who were not but were teachers nevertheless. Chief among these was Chris Goetze. Even though his death was tragic and untimely he had a great effect on his students who will surely feel his influence far into the future. I am very glad to have been in that number.

This study would not have been undertaken had it not been preceded by the careful work of Professor Bill Brace, and would not have continued without his guidance. It is my hope that some of the high professional standards which routinely characterize his work can be found in some small way in this thesis.

Professor David L. Kohlstedt was very generous with his help, read through an early draft, and contributed several very useful comments. His visits to M.I.T. and always prompt replies to our emergency phone calls kept important parts of the lab running in Chris's absence.

Professor A. S. Argon is responsible for my being interested in the mechanical properties of rocks by virtue of his clear exposition of deformation mechanics in subject 3.22 and 3,23. I thank him for that and for consenting at very short notice to be on my committee. Professor Burns and Molnar are

also thanked for their stimulating courses and for serving on the committee. Conversations with Yves Caristan and Wong TengFong were interesting and enjoyable. Jock Hirst and Madge Slavin are both to be thanked for the professional way in which they conduct their jobs and for the good humor which they both seem to generate. Sheila Parker and Madge Slavin did an excellent job of typing even though my poor planning put them in extremis. Marcia Evans typed parts of the rough drafts, drafted many of the figures, xeroxed, ran small errands, and generally bent her back against the wheel. Somehow she managed to get me to do the same and made the whole thing enjoyable. Remarkable.

CHAPTER I

THE TEMPERATURE VARIATIONS OF HARDNESS OF OLIVINE AND ITS IMPLICATION FOR POLYCRYSTALLINE YIELD STRESS

Abstract. The variation of hardness with temperature was measured for olivine on a number of crystal faces by the Vickers diamond pyramid technique (up to 800°C) and by a mutual indentation technique (for temperatures up to 1500°C). A comparative review of hardness data and compressive creep measurements obtained under large confining pressures confirms the hypothesis of Rice [1971, in Kriegel, W.W., and Palmour III, H., Mat. Sci. Res., Vol. 5, pp. 195-229] that single crystal hardness measurements, corrected for elastic yielding, can be correlated to the fully plastic yielding of a polycrystal by intragranular dislocation mechanisms, including dislocation climb and glide. The computed differential yield stresses, σ (in GPa), which empirically correspond to a strain rate ($\dot{\varepsilon}$) of $10^{-5}s^{-1}$, were well represented by an equation of the form

$$\sigma = 9.1(\pm.3) - .23(\pm.01)T^{\frac{1}{2}}$$

where T is the absolute temperature (in K), and the quoted variances are for 1 standard deviation. The olivine data

therefore predict a high stress polycrystalline flow law that may be expressed as:

$$\dot{\varepsilon} = 1.3 \times 10^{12} \exp - \frac{60 \times 10^3}{T} \left(1 - \frac{\sigma}{9.1}\right)^2$$

where $\dot{\varepsilon}$ is the strain rate in s^{-1}. A similar functional dependence of strain rate on stress is indicated for Al_2O_3 for temperatures below 900°C, but is contraindicated for MgO and NaCl.

Using a semi-empirical method of dislocation rosette analysis, the critical resolved shear stress on the {110} [001] slip system was estimated (to 20%) over the temperature range 20°C to 780°C as 1.2 GPa and .3 GPa respectively.

This data is useful in providing an upper bound to the yield stress in a region of stress and temperature space not easily accessible by other experimental methods.

Introduction:

The Relationship of Microindentation Hardness and Yield Stress

The attractiveness of microindentation hardness testing as a quick and nearly nondestructive method of testing material resistance to deformation has caused a large and detailed literature to develop. Several books and articles give very clear and comprehensive reviews of hardness [McClintock and Argon, 1966; Tabor, 1951, 1956, 1970]; the standard equipment and test conditions are described in ASTM [1961]; Brace [1961, 1963, 1964] and others have discussed the application of microindentation hardness to geology; Westbrook [1957, 1958, 1966] as well as Atkins and Tabor [1966a,b] and Koester and Moak [1967] have published detailed works on high temperature (hot hardness) experiments and equipment.

Of the several indentor (brale) geometries in common use, this study utilizes the Vickers diamond pyramid (VDP) indentor for lower temperatures [McClintock and Argon, 1966] and a mutual indentation scheme designed to reduce chemical incompatibility problems attendant with high temperatures (a similar technique with slightly different geometry is described by Atkins and Tabor [1966a]). In the first method, a diamond pyramid of 136° included angle was pressed against the flat surface to be tested, while the second method utilized a cone of 150° apical angle pressed against a flat slab of the same material. In both cases, the hardness (H) is defined here as the load on the brale divided by the

actual pyramidal or conical contact area of the test material and the brale. For the Vickers geometry, H, which is sometimes denoted by DPH (diamond pyramid hardness), reduces to

$$H \equiv DPH = 1.854 \frac{W}{d^2} \tag{1}$$

where W is the load in kilograms (force) and d is the diagonal of the indent measured along the test surface in millimeters. For the conical mutual indentation geometry,

$$H = \frac{4W \cos \beta}{\pi (d_m)^2} = 1.23 \frac{W}{(d_m)^2} \tag{2}$$

where d_m is the diameter of the indent measured along the test surface, and β is the angle between the brale surface and the test surface (here, $\beta = 15°$).

Hardness and differential yield stress ($\sigma \equiv \sigma_1 - \sigma_3$) are related for many materials according to

$$H = C\sigma \tag{3}$$

where C is a constant referred to as the constraint factor. For the Vickers diamond pyramid (VDP) indentor C is approximately equal to 3.0 for most metals [McClintock and Argon, 1966; Tabor, 1970]. For materials which strain-harden, the yield stress derived from a hardness measurement and equation 3 is the yield stress at a strain (ε) of .08, which has been shown to be the equivalent strain for the Vickers test by Tabor [1951, 1970].

The effects of indentor geometry and elastic rebound on the constraint factor have been analyzed by Johnson [1970]. Using plasticity theory [for a review see Hill, 1950] Johnson

shows that for a flat surface indented by a cone-shaped brale the constraint factor is a function only of the geometry of the brale and the parameter $\frac{E}{\sigma}$ where E is Young's modulus and σ is the differential yield stress as given below:

$$C = \frac{H}{\sigma} = \frac{2}{3} \left[1 + \ln \left(\frac{1}{3} \frac{E}{\sigma} \tan \beta\right)\right] \qquad (4)$$

β is the angle between the surface of the cone and the test surface. As the parameter $\frac{E}{\sigma}$ increases, the elastic strain during indentation becomes much smaller than the strain accommodated by ductile flow; in the limit of vanishingly small elastic strain the constraint factor approaches 3.0 asymptotically.

The theory is subject to the restriction that the included angle of the indentor be greater than 120°; the material is also assumed to be isotropic and to yield according to the von Mises criterion. The theory compares favorably to VDP hardness tests done on materials with a widely varying ratio $\frac{E}{\sigma}$ if one uses an angle $\beta = 19.7°$ (see Figure 1) which is the angle corresponding to a cone displacing a volume equal to that of a Vicker's type pyramid. The actual angle in the VDP test is ~22°. Thus theory predicts and experiments agree that, for a particular geometry, the constraint factor is a function of $\frac{E}{\sigma}$ only. For these experiments, we used a slightly different empirical equation

$$\frac{H}{\sigma} = .19 + 1.6 \log \frac{E \tan \beta}{\sigma} \qquad (5)$$

designed to correct for the small offset between the data and the theoretical line (see Figure 1). In order to determine σ one

Figure 1. Correlation of the Constraint Constant (H/σ) with the Ratio of Young's Modulus to the Yield Stress (E/σ).

Correlation of the constraint constant (H/σ) with the parameter $E/\sigma \tan \beta$. $\tan \beta$ is the angle which the brale makes with the surface being indented. The elastic plastic model suggested by Johnson (1970) is given by the dashed line. Experiments using conical, spherical, and VDP indentors are shown for comparison. The solid line is the relation given in the text as Equation 5. Near the limit $E/\sigma \tan \beta \rightarrow 1.0$, the experimental data approach the elastic limit $C = 1.1$ which is the value expected for a spherical indentor in contact with a perfectly elastic solid.

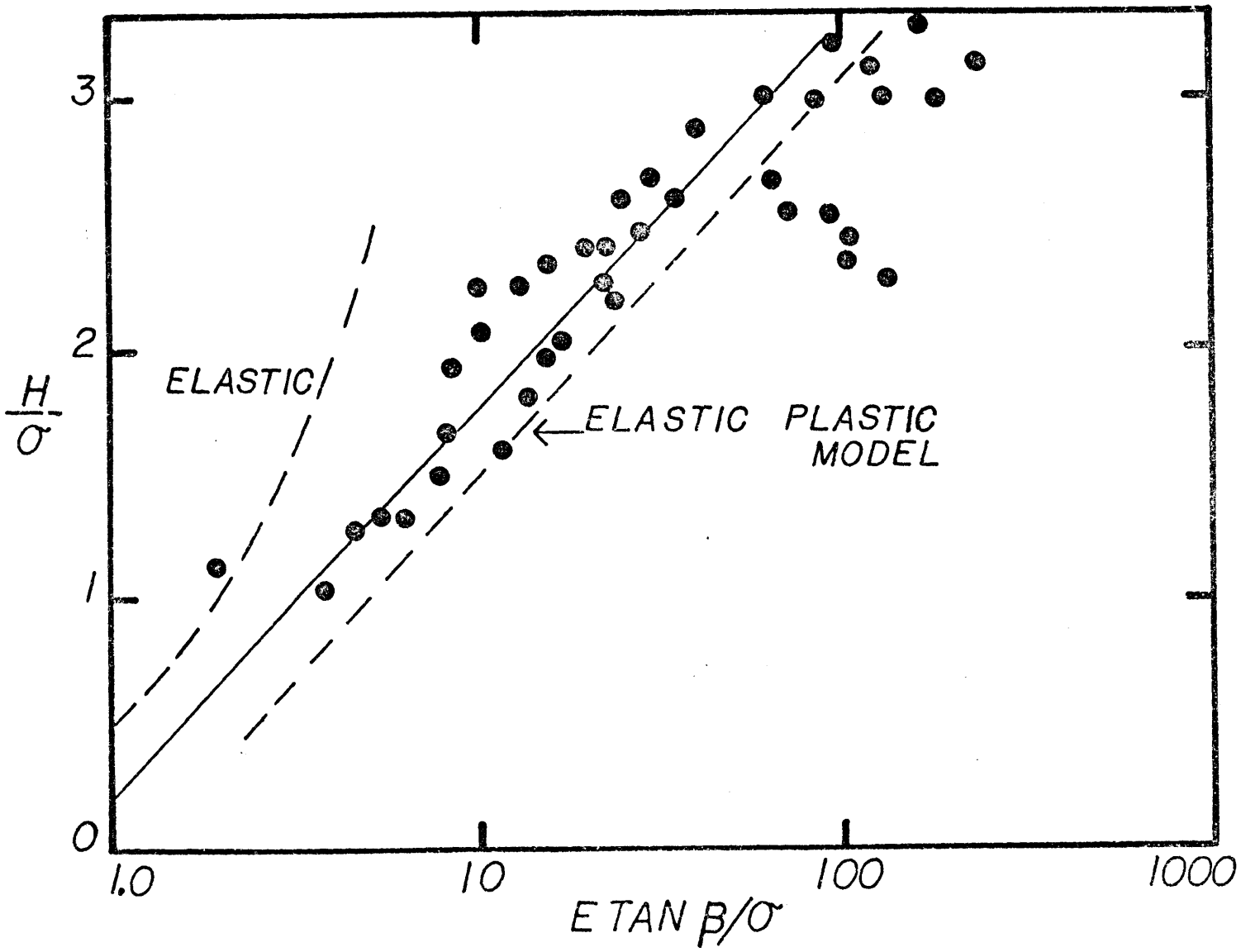
3
2
1
0
H/σ
ELASTIC
ELASTIC PLASTIC MODEL
1.0
10
100
1000
E TAN β/σ

simply needs to measure the hardness and solve equation 5 using appropriate values of the elastic moduli and the geometry of the indentor.

Thus the hardness theory is well developed for materials with isotropic yield properties. There is, however, a class of materials which exhibit markedly anisotropic yield, i.e. they show a tendency to yield on primary slip systems at much lower stresses than secondary slip systems. For this class of materials, which includes some oxides, intermetallic carbides, borides, and nitrides, and many geologic materials, the hardness sometimes appears to vary with temperature in the same fashion as the single crystal yield stress, but the constant of proportionality of hardness to yield stress on the primary slip system can be as large as 30 [Westbrook, 1957]. However, because the deformation under the indentor is nearly spherical in morphology [Johnson, 1970; Yu and Li, 1977] and probably requires secondary slip systems to operate, it is logical to assume that the Vickers hardness numbers give a measure of the stress necessary to fulfill a general yield criterion such as the Von Mises criterion [Rice, 1971]. Therefore, as suggested by Rice [1971], the single crystal hardness, taken on a surface of high perfection, and taking account of elastic strain, should give a reliable value for the ductile yielding of a polycrystalline solid.

In this paper we wish to compare polycrystalline yield data to the hardness-derived yield stresses, and further to examine the implications of this data for polycrystalline flow mechanisms for olivine. Additional information on the easy

slip system is obtained by examining the dislocation structure of the indents.

Experimental Methods for Determination of Hot Hardness

Diamond Vickers pyramid indentation

The apparatus used was a Tukon microhardness testor [Mott, 1956] with some modifications for high temperatures [Brace, 1961]. The Tukon testor mechanically loads and unloads at a fixed rate, which for this study was a few millimeters per second. The length of time of the indenting, the dwell time, was varied in order to conduct indentation creep tests, but in most of the experiments described here the diamond was in contact with the sample for approximately 15 seconds, the standard time for conventional VDP experiments. Preheated argon gas was introduced at the bottom of a coaxially wound furnace tube, exiting the furnace around a thin mica washer which formed a loose seal around the ceramic extension tube holding the diamond brale. The sample was positioned in the hottest part of the furnace by a pyrophyllite cylinder and was fastened to the cylinder with a small quantity of Sauereisen cement. The center of the cylinder was pierced by a chromel-alumel thermocouple, the junction of which was flush with the end surface of the cylinder and made thermal contact with the sample. The temperature variation over the sample volume was determined to be less than 5°, but no temperature controller was used, and so the indents were taken as the temperature slowly increased

or decreased. The temperature recorded was the temperature sensed by the thermocouple at the lower surface of the sample, which was practically constant during the 15 second period.

The brale beam was balanced before each high temperature run to an accuracy of better than 1 gram. Since the loads used for the high temperature indents were typically from 50 to 250 grams, this means an uncertainty in weight of less than 2%. The motion of the brale was measured using a direct current differential transformer, and therefore the dwell time could be measured to an accuracy of better than .5 second. Measurement of the indents was made in reflected light using a travelling Filar micrometer crosshair; the indents were quite small, so measurement was accomplished at 500 x magnification. The readings were repeatable to .4 micron, depending on the quality of the indent, i.e. whether cracks were present, or whether the brale happened to hit a minor surface flaw. As a general rule, data points were discarded if the difference between the two diagonals was >1.0μ. Since the diagonal lengths of the smallest indents routinely measured were approximately 10 μm, the asymmetry error is less than 10% and decreases as the temperature and the diagonal increase. The results of room temperature tests on olivine conducted on the apparatus described above were compared with results obtained on a second microindentation hardness tester and bound to agree within 5%.

At several times throughout the study, in order to assure uniform and accurate results, tests were performed on a calibration block of known hardness supplied by the Wilson Instrument Company. At all times the hardness values

determined agreed to within 3% of the stated value of the block.

Since hardness is sometimes a function of the load applied [McClintock and Argon, 1966], two separate crystallographic faces were indented at various loads. Between 20 and 500 grams, the hardness was independent of load to within 10%. No indent was free of cracks at temperatures <500°C, although the amount of cracking and spalling generally decreased with decreasing load and increasing temperature. Above 500°C, for the VDP points the cracking was minimal and no cracking at all was observed during the mutual indentation experiments. The effect of cracking on the hardness is discussed in the results section. Decoration of the samples by a technique devised by Kohlstedt et al. [1976] allowed the optical observation of dislocation structure around the indent.

An analysis of the dislocation pattern, often called a dislocation rosette, is presented in the discussion section.

The samples were prepared by polishing with grinding powders down to 1.0μm alumina mixed with water, to give an optical quality finish. Westbrook and Jorgenson [1968] have shown that many silicate minerals have an adsorbed layer of water which can cause anisotropy of hardness of approximately 20%, depending on the crystallographic face being indented, although certain minerals, e.g. kyanite, have anisotropies as high as 50%. They found that removing the layer by heating the samples to 300°C in dry argon reduced the anisotropy. Thus the effect of adsorbed water is expected to be reduced at higher temperatures. Table 1 gives values for the anisotropy of hardness for olivine

TABLE I

Variation of hardness with crystallographic orientation for olivine at room temperature

Plane	Average Hardness kg/mm^2	Range	No. of Indents
(100)	1015	1010-1025	5
(010)	965	935-1010	5
(001)	990	875-1045	15
$(110)_c$	990	891-1027	59

(a) $(110)_c$ denotes the plane perpendicular to the optic axis of olivine.

(b) All indents are at 50 grams load

(c) For surface preparation details see text.

at room temperature with (presumably) the adsorbed layer present. Experiments revealed that there was no experimentally significant anisotropy due to the rotation of orientation of the pyramid on a particular face; and, therefore, no attempt to control the orientation of the brale was exercised during the remainder of the experiments.

Mutual indentation hardness of olivine

For temperatures above 900°C, in oxygen fugacities necessary for the stability of iron-bearing olivine, diamond is not stable even for the short time periods (~5 to 10 minutes) used in these hardness experiments. Therefore, a mutual indentation technique similar to that of Atkins and Tabor [1966b] was used during which a mechanically polished conical point of olivine (150° apical angle) indented a polished flat olivine surface.

The furnace and deformation chamber in which the brale and surface were deformed were similar to the low stress gas deformation apparatus described by Durham et al. [1977] and Durham [1975]. Briefly described, the brale was clamped in a molybdenum anvil which hung freely guided by a leaky ball bearing race at the top of the furnace. A servo-controlled piston raised the flat to be indented until the brale and anvil were moved from their rest position, thus applying a dead weight load. The shortest time period used for the mutual indentation process was 15 seconds and ranged to as long as 5 minutes, but was most commonly 60 seconds. During a single experiment from one to three mutual indents were made at a

single temperature. After each experiment a new flat and brale were made. Thus for the two experiments done at 1070°C and 1150°C the second and subsequent indents may have been made with a brale whose shape had been altered by plastic flow.

Indentation creep tests were conducted by altering the dwell time. Similar indentation creep tests have been analyzed using either transient creep relations [Atkins et al., 1966; Atkins and Tabor, 1966b] or steady state creep relations [Sherby and Armstrong, 1971; Evans and Sykes, 1974]. The indentation creep tests are listed in Table 2d and are discussed briefly in Chapter 3.

Results

Hot hardness data for olivine

The variation of hardness with crystallographic orientation and the hot hardness data for oriented single crystals of San Carlos peridot and unoriented Twin Sisters are tabulated below (Tables 1 and 2 respectively). The mutual indents (Table 2b) were in some cases elliptical. This may have resulted from a combination of initial asymmetry of the brale, anisotropy of flow around the indent and/or flow anisotropy of the brale itself. The mutual indentation hardness was computed as

$$H = \frac{4\ W \cos \beta}{\pi d_a\ d_b} = 1.23\ \frac{W}{d_a\ d_b} \qquad (6)$$

TABLE 2: HOT HARDNESS OF OLIVINE

(a) VDP hardness of San Carlos Peridote

Average diagonal length 10^{-6}m	Temp. °C	Hardness kg/mm^2	Constraint factor	Yield stress kb*	Orientation code
9.4	27	1050	1.9	54.2	A
9.5	118	1027	2.02	49.9	A
10.0	121	927	2.02	45.0	A
10.0	121	927	2.02	45.0	A
10.0	119	927	2.02	45.0	A
10.5	277	841	2.17	38.0	A
11.0	275	766	2.17	34.6	A
10.5	280	841	2.17	38.0	A
10.8	275	795	2.17	35.9	A
11.8	420	666	2.30	28.4	A
11.5	417	701	2.30	29.9	A
11.8	412	666	2.29	28.5	A
11.5	419	701	2.30	29.9	A
11.8	500	666	2.37	27.6	A
12.0	499	644	2.37	26.6	A
12.0	504	644	2.37	26.6	A
12.8	584	566	2.45	22.7	A
12.8	587	566	2.45	22.7	A
12.3	589	613	2.45	24.5	A
13.3	640	524	2.50	20.6	A
13.5	703	509	2.56	19.5	A
14.0	705	473	2.56	18.1	A
13.8	705	487	2.56	18.7	A
13.3	705	524	2.56	20.1	A
14.2	773	460	2.56	17.6	A
16.2	773	353	2.62	13.2	A
12.0	555	644	2.62	24.1	B
12.5	554	593	2.42	24.0	B
12.3	555	613	2.92	24.84	B
12.0	555	644	2.92	26.1	B
11.0	173	766	2.07	36.2	C
10.0	168	927	2.07	43.9	C
10.6	166	825	2.07	39.1	C
11.3	237	726	2.13	33.4	C
10.8	234	795	2.13	36.6	C
11.3	229	726	2.13	33.4	C
10.8	321	795	2.20	35.4	C
11.4	317	714	2.20	31.8	C

*1 kb = 100 MPa

TABLE 2: HOT HARDNESS OF OLIVINE

(a) VDP hardness of San Carlos Peridote

(continued)

Average diagonal length 10^{-6}m	Temp. °C	Hardness kg/mm^2	Constraint factor	Yield stress kb	Orientation code
11.5	312	701	2.20	31.2	C
11.5	307	701	2.19	31.4	C
13.5	549	509	2.42	20.6	C
13.5	550	509	2.42	20.6	C
13.0	552	549	2.42	22.2	C
13.5	554	509	2.42	20.6	C
19.4	767	246	2.62	9.2	C
19.6	768	241	2.62	9.0	C
19.4	770	246	2.62	9.2	C
12.6	501	584	2.37	24.2	C
14.0	509	473	2.37	19.6	C
12.5	505	593	2.37	24.5	C

(a) All indents are at 50 grams load

(b) the orientation code letter may be interpreted from the following table:

Code letter	Angle between the normal to the plane indented and		
	100	010	001
A	45°	45°	90°
B	44°	46°	90°
C	orientation unknown (~15° from optic axis)		
D	76°	24°	78°

TABLE 2 (continued)

(b) Mutual indentation hardness of San Carlos Peridote

Axis length $10^{-6}\mu$ major	minor	Temp. °C	Load kg	Hardness kg/mm^2	Constraint factor	Yield stress kb	Corr. Temp. °K	$T^{\frac{1}{2}}$
107	57	940	.567	249	2.78	8.8	1246	35.3
107	57	1070	1.07	216	2.91	7.3	1384	37.2
107	62	1070	1.07	198	2.91	6.7	1384	37.2
96	62	1070	1.07	221	2.91	7.5	1384	37.2
74	69	1150	.562	135	3.00	4.4	1469	38.3
71	66	1150	.562	148	3.00	4.8	1469	38.3
67	62	1150	.562	166	3.00	5.4	1469	38.3
73	58	1150	.562	163	3.00	5.3	1469	38.3
83	79	1300	.283	53.1	3.00	1.7	1629	40.4
174	170	1500	.133	5.5	3.00	0.2	1845	46.0

The orientation is given as D in the table above.

(c) VDP hardness of Twin Sisters Dunite

Sample	Time secs.	Average diagonal length 10^{-6}m	Temp. °C	Load kg	Hardness kg/mm^2	Constraint factor	Yield stress kb
TS 350	27	12.3		.088	1080	1.92	55.2
TS 31-29	12	15.5	424	.100	772	2.34	33.6
-21	12	15.7	424	.100	752	2.34	32.8
-22	21	15.8	424	.100	743	2.34	32.4
-23	21	15.3	424	.100	792	2.34	34.5
-24	21	15.8	426	.100	743	2.34	32.4
-25	21	15.3	428	.100	792	2.34	34.5
TS 36-2	22	14.8	556	.088	745	2.47	30.8
-3	22	14.4	559	.088	787	2.47	32.5
-4	22	14.8	561	.088	745	2.47	30.8
-5	22	14.8	565	.088	745	2.47	30.8
TS 36-6	26	15.0	574	.088	725	2.47	29.9
-7	26	15.1	574	.088	716	2.47	29.5
-9	63	15.2	584	.088	706	2.47	29.2
-10	68	15.2	588	.088	706	2.47	29.2
TS 38-1	35	21.3	735	.100	409	2.60	21.7
-2	38	22.4	730	.100	370	2.59	19.6
-3	38	23.0	725	.100	351	2.59	18.6
-4	12	18.7	719	.100	534	2.58	21.0
-5	12	17.9	714	.100	579	2.58	22.9
-6	11	17.9	710	.100	579	2.58	22.9

The orientations of these samples are random and unknown.

TABLE 2 (continued)

(d) Indentation creep of San Carlos Peridote

Sample	Time secs	Avge diagnl length μm	Temp °C	Load kg	Hard-ness kg/mm²	Con-straint factor	Yield stress kb
DV 280 a	300.0	20.7	530	.133	576	2.43	23.2
b	300.0	20.7			576		23.2
c	60.0	20.3			598		24.2
d	60.0	20.1			610		24.6
e	60.0	20.3			598		24.2
f	60.0	20.3			598		24.2
g	60.0	20.1			610		24.0
MB6-40 2	13.8	24.6	493±4	.250	764	2.38	31.5
3	13.2	24.8			759		31.1
4	15.0	25.1			761		31.4
13	48.0	24.1			736		30.3
14	48.0	25.6			767		31.6
17	351.0	25.6			707		29.1
18	354.0	25.7			701		28.9
19	356.0	25.4			719		29.6
MB6-47 2	20.0	24.6	488±5	.250	766	2.38	31.6
3	19.2	24.6			766		31.6
4	20.0	25.0			739		30.5
7	5.4	24.6			760		31.6
8	7.2	24.7			760		31.3
9	6.0	24.5			775		31.9
10	6.0	24.5			775		31.9
12	43.2	24.9			746		30.7
14	240.0	25.6			709		29.2
15	220.0	25.3			725		29.9
19	8.4	24.7			760		31.3
23	42.0	25.0			742		30.6
24	42.0	29.6			766		31.6

The orientations of these samples are random and unknown.

where β is the indentor/specimen angle given above, and d_a and d_b are the major and minor axes of the ellipse.

For the indentation creep experiments (Table 2d), the temperature range given indicates the variation of temperature during the entire series of experiments. At 500°C, a 5° temperature variation causes 1% variation in hardness, and therefore no correction for temperature has been made. Other sources of scatter in the data are mechanical vibration of the testor during an indent, friction caused by progressive degradation of the sample surface at temperatures above 600°C, small variations in the loading speed between very long period and short period indents, deviations from the nominal load (<2%) observational errors, which are indicated by statistics to be ~4% of the hardness at 500°C, and finally errors in time determination (<4%). The scatter of the data in Tables 2a and 2b is about 10%, due to varying orientation and other experimental errors listed above, while the precision of the indentation creep experiments is higher ($\Delta H \simeq 4\%$) because each data set is for a fixed orientation and fixed load and because repeated optical measurements of each indent were made to obtain statistical averages.

In this section and the following, hardness data for several geologic and ceramic materials, including olivine, were used to determine yield stress values via Johnson's [1970] constraint factor. In order to determine the constraint factor as a function of temperature, we solved for σ in equation 5 using the following iterative method:

(a) Since C can be no larger than 3.00 [Hill, 1950], estimate σ from the measured hardness value and equation 3 using $C = 3.00$.

(b) Solve equation 5 for σ.

(c) Redetermine C using equation 3 and the hardness.

(d) Substitute into the right-hand side of equation 5 and solve again for σ.

By iteration in this fashion one soon converges to a yield value, which we call the hardness-derived yield value. The hardness and the hardness-derived yield value define a constraint factor for that temperature.

Although the iterative procedure described above could have been done at each temperature, because the constraint factor is a slowly varying monotonic function of temperature (except for quartz in the α-β phase transition region) we simply determined C for several temperatures and interpolated intermediate values (see Figure 3). The scatter caused by interpolating C was less than the experimental scatter of the hardness. Figures 2 and 3 show the temperature variation of elastic moduli of the materials discussed and the temperature variation of the constraint factor respectively. The constraint factor has been used to compute yield stress values for olivine in Tables 2a, 2b, 2c and 2d, and the results are plotted in Figure 4 along with previously published values of polycrystalline flow experiments.

Due to apparatus constraints it was advantageous to conduct the mutual indentation tests with a dwell time of 60 seconds. In order to correct the mutual indentation data from 60 second dwell time to 15 second dwell time, we assumed that the

Figure 2. The Temperature Variation of the Young's Modulus for Several Materials.

The sources of the data are given in Table 3.

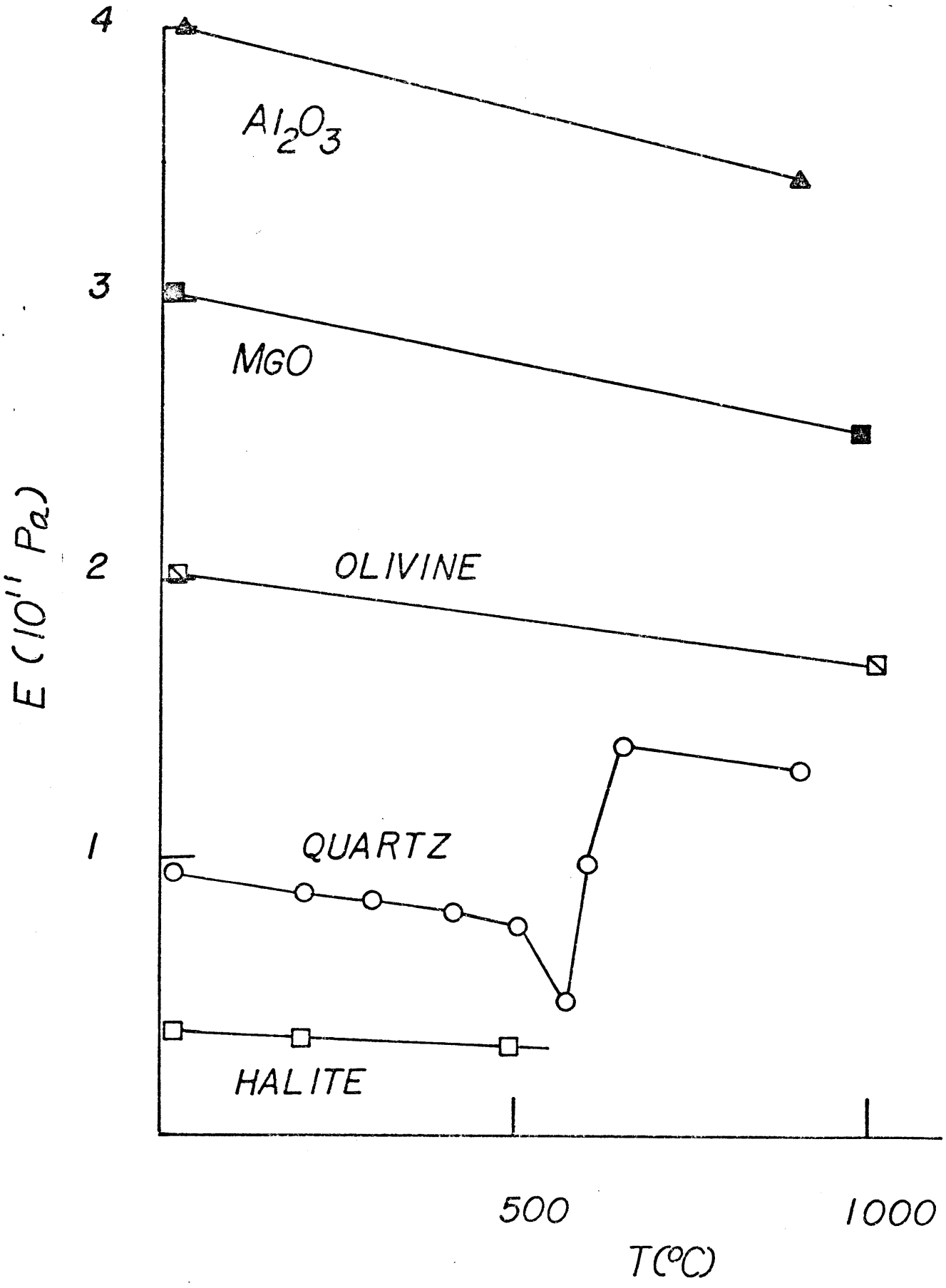
4
3
2
1
Al_2O_3
MGO
OLIVINE
QUARTZ
HALITE
E (10¹¹ Pa)
500
1000
T(°C)

TABLE 3: SOURCES OF POLYCRYSTALLINE YIELD, HOT HARDNESS AND ELASTIC CONSTANT DATA

Material	Crystal Class	Symbol	Hardness Source	Symbol	Yield Source	Elastic Constant Source
Al_2O_3	$\bar{3}$ m	K & M	Koester and Moak [1967]	H	Heuer et al. [1970a,b]	Tefft [1966]
		W	Westbrook [1966]	P	Palmour et al. [1970] (single crystal)	
				G & G	Gooch and Groves [1973a,b] (single crystal)	
				B & C	Bayer and Cooper [1967]	
MgO	m 3 m	A & T	Atkins and Tabor [1966a,b]	H	Hulse et al. [1963]	Durand [1936]
				K	Kinsland [1970]	
		W	Westbrook [1958]	P & W	Paterson and Weaver [1970]	
NaCl	m 3 m	B	Brace [1961, 1960]	H	Heard [1972]	Durand [1936]
						Swartz [1967]
Olivine	m m m	E & G	This study	B	Blacic [1972]	Graham and Barsch [1969]
				C & A	Carter and Ave'Lallemant [1970]	
				G & B	Goetze and Brace [1972]	Kamazawa and Anderson [1969]
				K & R	Kirby and Raleigh [1973]	
				P	Post [1973]	
				R & K	Raleigh and Kirby [1970]	
SiO_2	$\bar{3}$ m	B	Brace [1961]	H & C	Heard and Carter [1968]	Coe and Paterson [1969]
		W	Westbrook [1958]	T	Tullis [1971]	Zubov and Firsova [1962]

Figure 3. The Constraint Constant versus Temperature for Several Materials.

The constraint constant $C = H/\sigma$ (see Equation 5) versus temperature determined using an iterative procedure and the theory described by Johnson (1970).

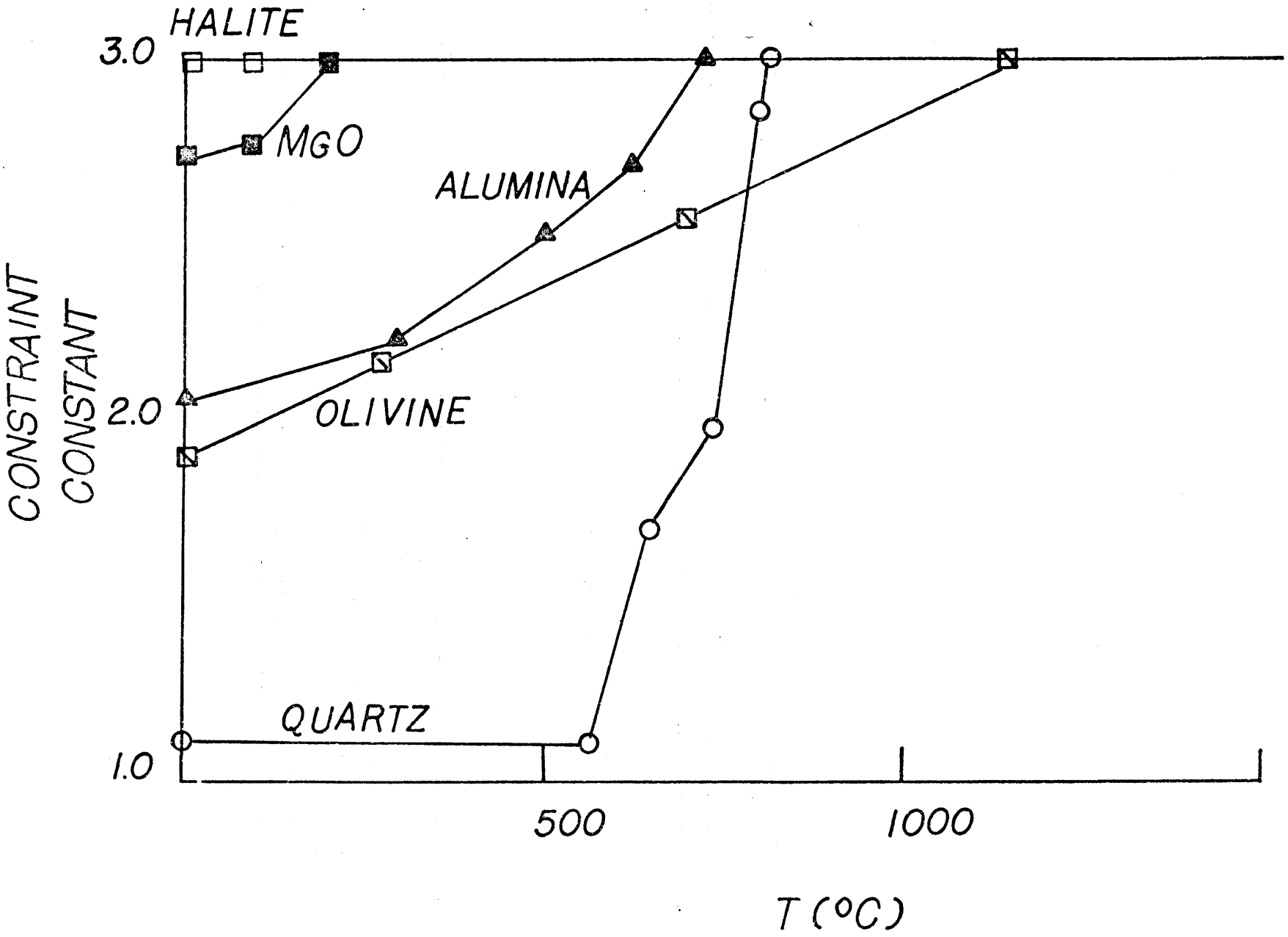
HALITE
3.0
MgO
ALUMINA
OLIVINE
2.0
CONSTRAINT
CONSTANT
QUARTZ
1.0
500
1000
T (°C)

Figure 4. The Hardness Derived-Yield Stress as a Function of Temperature for Olivine.

Shown for comparison are previously published polycrystalline yield tests conducted at strain rates of $\dot{\varepsilon} = 10^{-5\pm.5}$ and at a strain of .08 where possible. The broken lines are the best fit Peierl's stress model discussed below and an equation intended to represent the glide-climb mechanism where

$$\dot{\varepsilon} \alpha \sigma^3 \exp -\frac{125 \times 10^3 \text{ cal/mole}}{RT}$$

where R is the gas constant and T the absolute temperature.

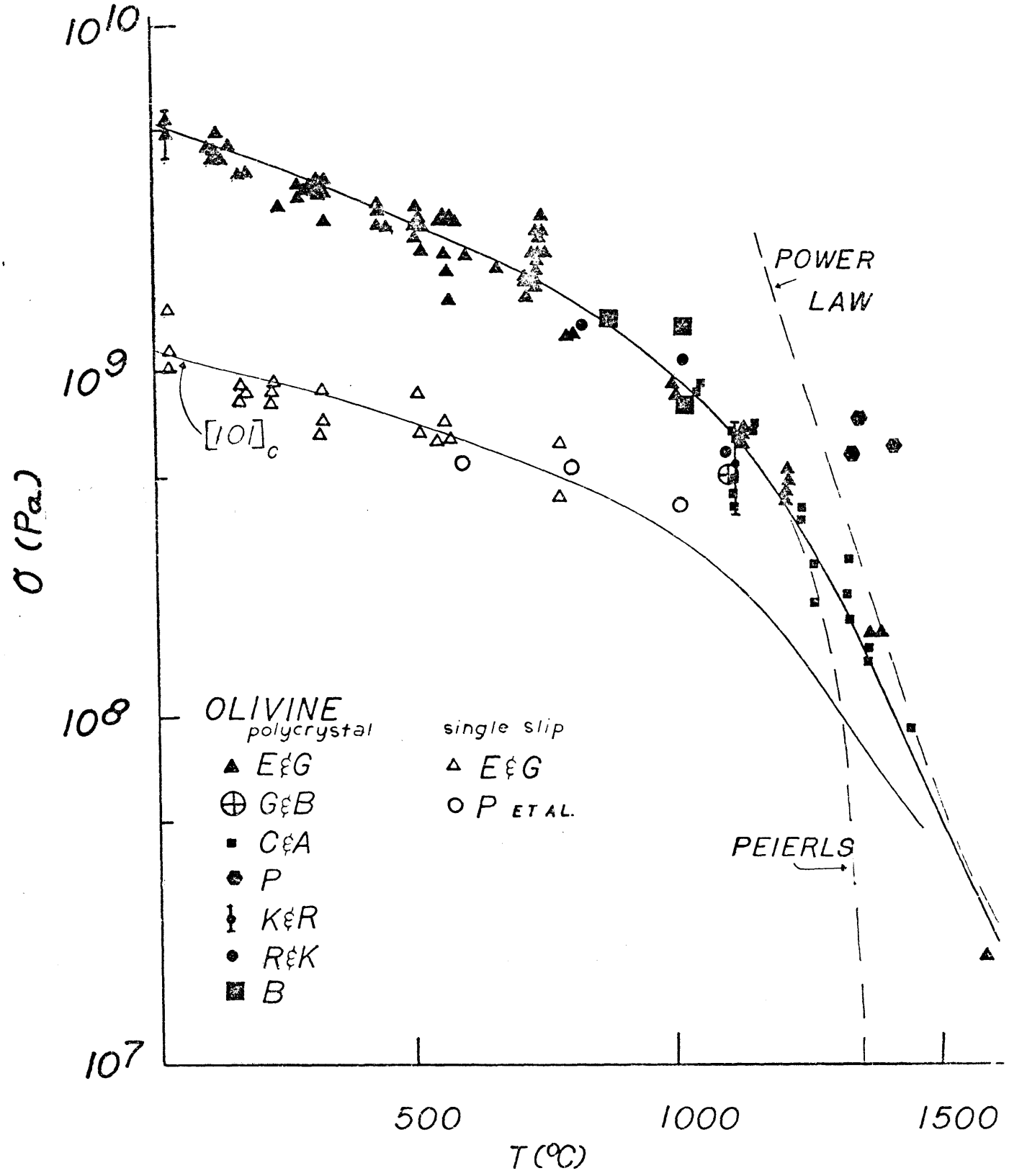
10^{10}
10^{9}
10^{8}
10^{7}
σ (Pa.)
POWER LAW
[101]c
OLIVINE
polycrystal
E&G
G&B
C&A
P
K&R
R&K
B
single slip
E&G
P ET AL.
PEIERLS
500
1000
1500
T (°C)

effective strain rate was inversely proportional to dwell time, and an approximate correction in temperature may be made by assuming the relation

$$\ell\eta \left[\frac{\dot{\varepsilon}_{corr}}{\dot{\varepsilon}_{act}}\right] = -\frac{Q_{app}}{R}\left[\frac{1}{T_{corr}} - \frac{1}{T_{act}}\right] \qquad (7)$$

where $\dot{\varepsilon}_{corr}/\dot{\varepsilon}_{act} = 60/15$, $Q_{app} \cong 125 \times 10^3$ cal/mole, and R is the gas constant. This correction is equivalent to assuming that the hardness obeys the Hargreaves equation and may amount to a slight overcorrection (cf. Atkins and Tabor [1966], equation 24 and equation 25), but the corrections determined are on the order of a few percent of the absolute temperature and so we do not regard this step as controversial.

Figures 5, 6, 7, and 8 show various images of VDP and mutual indents including decorated samples [Kohlstedt et al., 1976] which show the dislocation structure around the indentation, called the dislocation rosette.

For indentations below ~1200°C at all orientations, the glide loops in the rosette and, hence, the primary slip system [Groves and Fine, 1964] are observed to lie on the {110} plane agreeing with Phakey et al. [1972], Durham [1975], Durham et al. [1977], and others. Above 1300°C, the rosettes do not show loops on distinct planes, indicating presumably that climb and cross glide velocities are competitive with glide velocities.

Dislocation rosettes about indentations have been utilized by many studies, among them, Groves and Fine [1964] and Hopkins et al. [1973]. Hopkins et al. [1973] showed that the rosette

Figure 5. SEM Micrograph of a VDP Indent in Olivine

A VDP indent made at room temperature and imaged in backscattered electrons. Notice the median cracks extending from the sides of the indent. The length of the diagonal as measured in reflected light is 13.4 μm. The indent appears to be asymmetrical because it is viewed at an angle of 36° from the vertical.

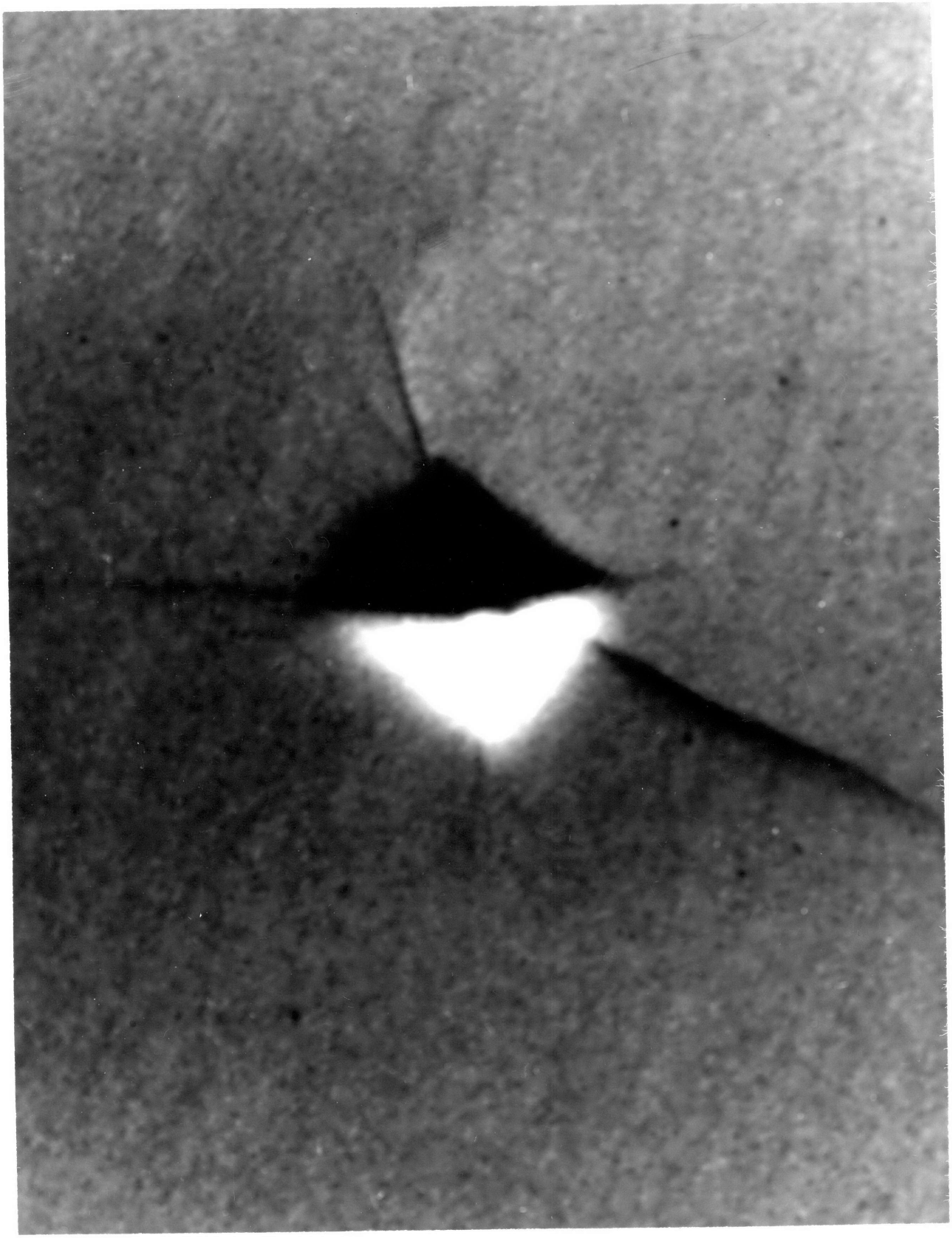

Figure 6. Dislocation Rosette of a VDP Indent in Olivine

A 700°C VDP indent viewed in transmitted light under an oil immersion lens at 1000x. The indent has been decorated by heating in air according to Kohlstedt et al. [1976]. The plane of the picture is $(110)_c$; the rosette sprigs and the dislocation loops point along the [001] direction. The field of view is approximately 150 μ.

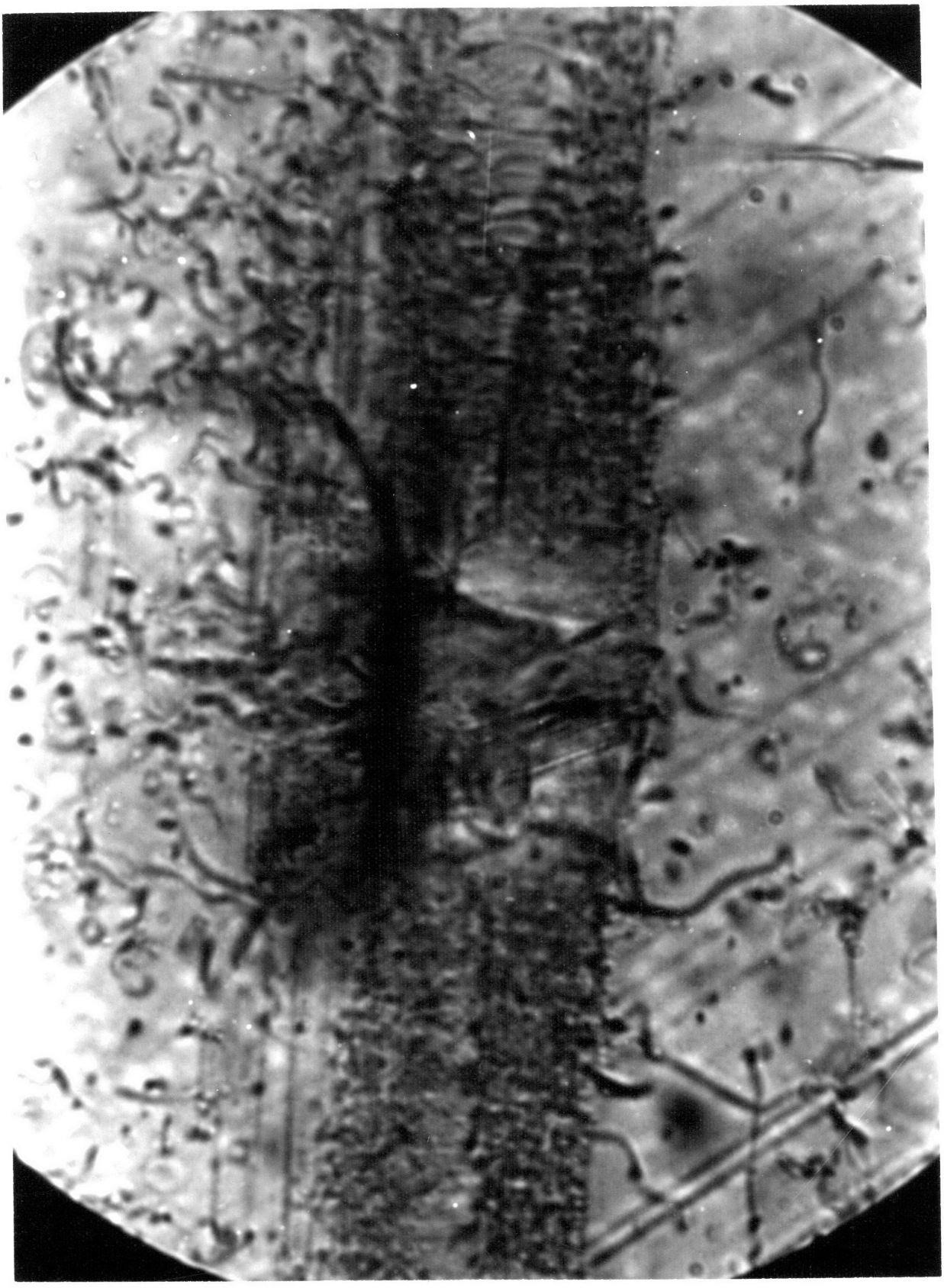

Figure 7. Optical Micrograph of a Mutual Indent in Olivine

An 1150°C mutual indent taken in reflected light. The indent has been decorated and the resulting surface degradation is clearly evident. The major semiaxis of the ellipse is 71 μm.

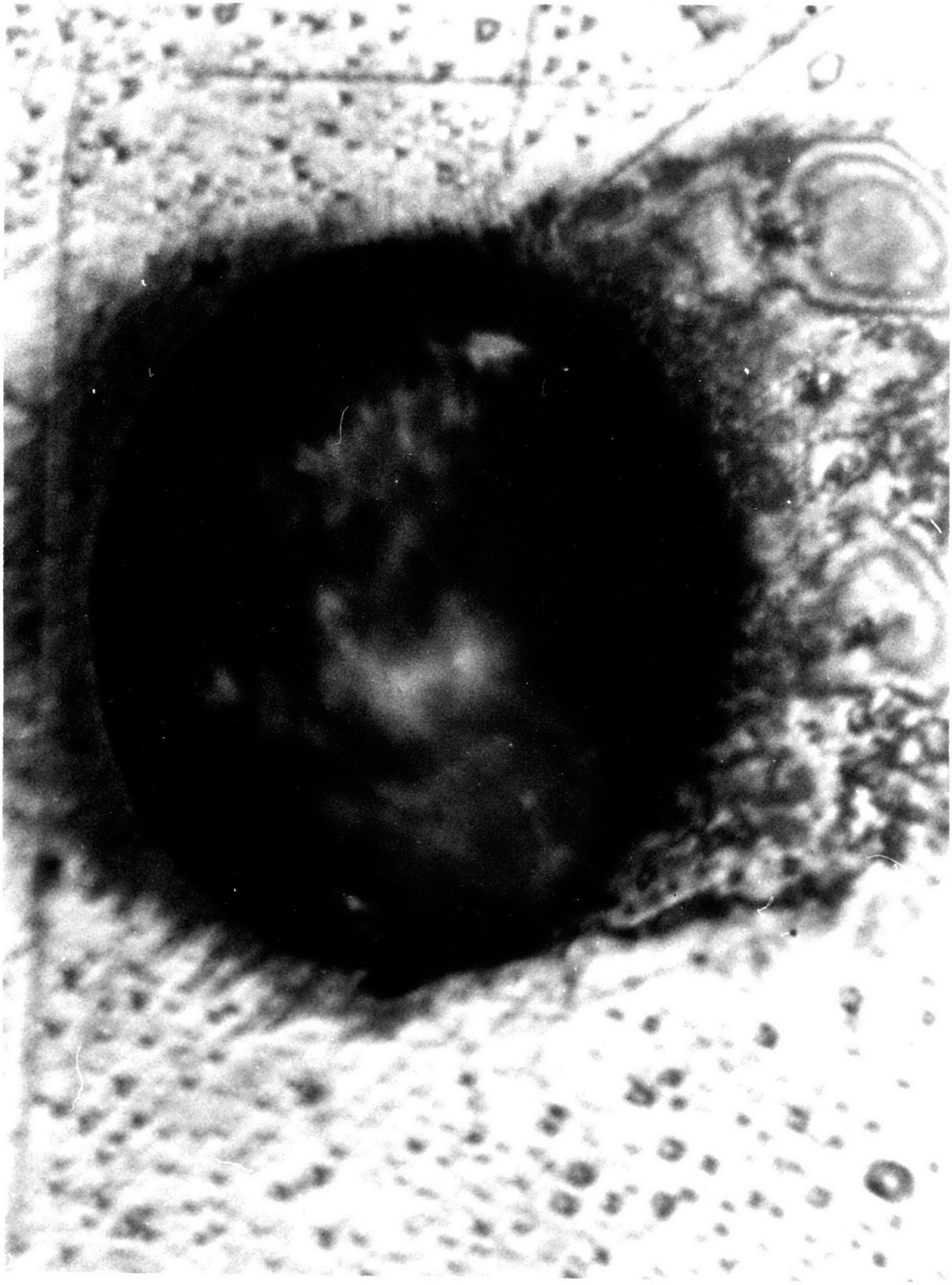

Figure 8. Dislocation Rosette of a Mutual Indent in Olivine

The same indent in transmitted light showing the dislocation rosette surrounding the indent. Notice that the dislocations are no longer simple rectilinear loops confined to a single glide plane as in Figure 6. The "woolly" appearance is presumably due to the contribution of climb and cross glide.

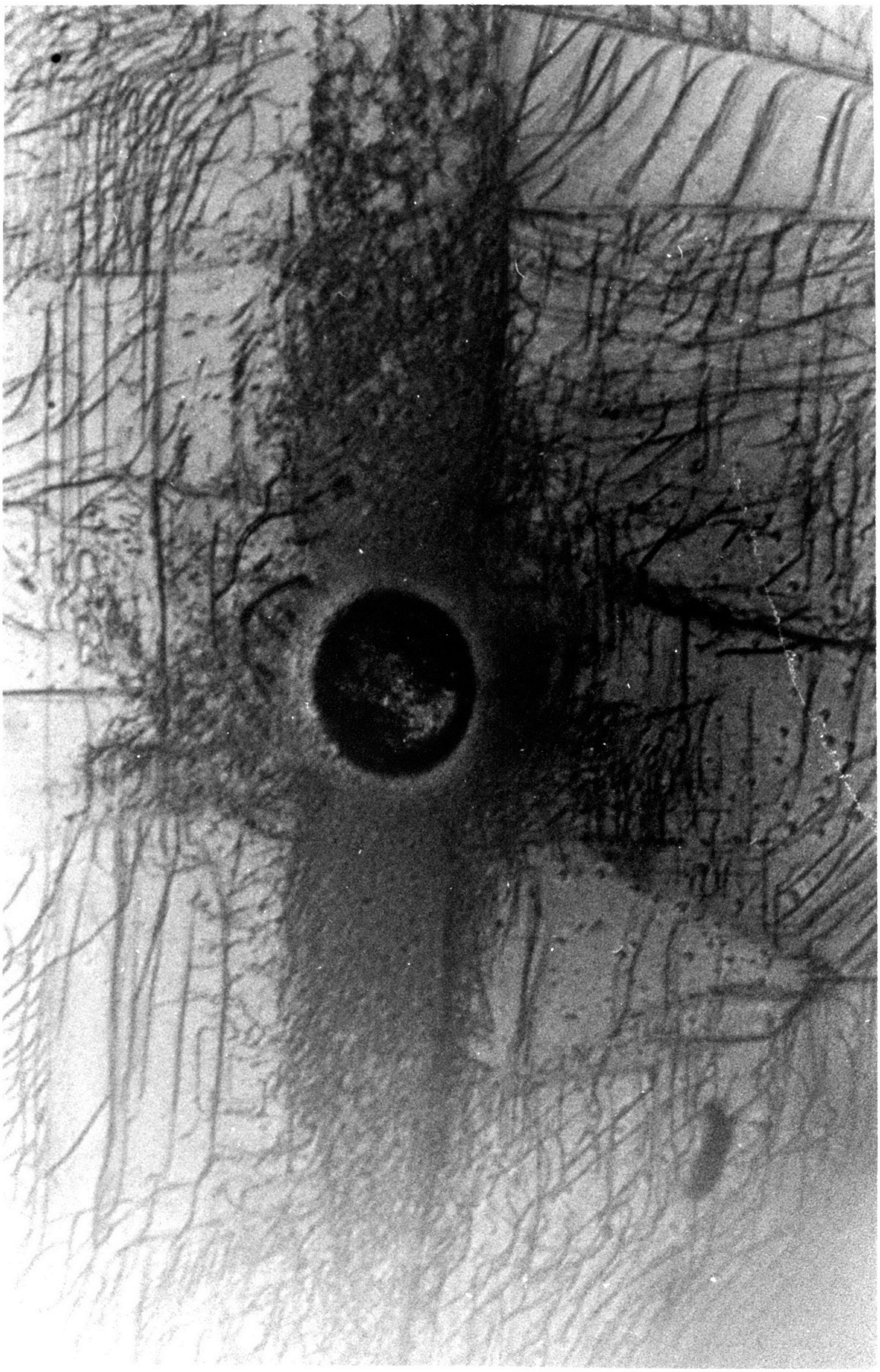

length (L) is inversely proportional to the yield stress of the primary slip system for KCl crystals with varying impurities. One may determine the constant of proportionality between $\frac{1}{L}$ and yield stress at one temperature and then use the variation of rosette length to determine the variation of yield stress with temperature. The yield stress for the {110} system at 800°C as determined by Phakey et al. [1972] was used to scale the relation below:

$$\sigma_{\{110\}}(T) = \frac{L_{800}}{L_T} \sigma_{800} \qquad (8)$$

where L_{800} is the rosette length at 800°C, σ_{800} is the critical resolved shear stress given by Phakey et al. [1972] for 800°C (~.27 GPa) and L_T is the rosette length at a given temperature T, and $\sigma_{\{110\}}(T)$ is the critical resolved shear stress for the {110} system at some temperature. Table 4 contains the observed L_T values and the computed critical resolved shear stresses over the temperature range 160°C-780°C. Single crystal data for the several slip systems of olivine are compared in Figure 14 and discussed below.

Discussion

Hardness vs. polycrystalline yield of olivine and several other geologic and ceramic materials

In this paper we wish to present new evidence that hardness may be used to determine polycrystalline yield stress. In order to compare hardness-derived yield stresses to yield

TABLE 4: AVERAGE ROSETTE LENGTH AND COMPUTED RESOLVED SHEAR STRESS FOR {110} SYSTEM AS A FUNCTION OF TEMPERATURE

Sample	Temp °C	L_T (10^{-6}m)	$\sigma_{\{110\}}$ kbar*
10 AB5-8	172	26	7.2
9	168	26	7.2
10	166	24	7.8
10 AB4-1	207	32	5.9
2	209	30	6.3
3	211	32	5.9
10 FB5-5	237	28	6.7
6	234	28	6.7
7	229	28	6.7
3	312	28	6.7
1	317	33	5.7
2	321	33	5.7
10 AB4-4	360	32	5.9
5	363	36	5.2
6	367	34	5.5
10 AB3-1	549	45	4.2
2	550	42	4.5
3	552	43	4.4
4	554	45	4.2
10 AB2-1	767	75	2.5
2	768	70	2.7
3	780	71	2.6
4	781	71	2.6

* 1 kb = 100 MPa

stresses of purely ductile flow as determined by polycrystalline creep tests, one must exclude those polycrystalline creep tests done under conditions where brittle failure is present. The brittle-ductile transition is a subject of current research [Tullis and Yund, 1977], and many aspects of this complex deformation mode (or modes) remain unexplored. One method to detect the presence of brittle failure is to measure the effect of confining pressure on the yield stress, since increasing confining pressure enhances ductility [Handin et al., 1967; Paterson and Weaver, 1970; Tullis and Yund, 1977; and others]. Thus far the transition region has been studied in detail for only a few rocks, e.g. Solenhofen limestone [Heard, 1960], limestone, dolomite, and glass [Handin et al., 1967] and Westerly granite [Tullis and Yund, 1977]. Tullis and Yund [1977] found that the transition from dominantly microcracking to dominantly ductile behavior occurred at about 300°-400° for strain rates of $\sim 10^{6} s^{-1}$, but some microcracking must persist to higher temperatures since the experiments of Heard and Carter [1968] on Simpson orthoquartzite show substantial pressure sensitivity of yield stress up to at least 600°C for similar strain rates. Likewise, for polycrystalline MgO at temperatures of at least 800°C ($\dot{\varepsilon} = 10^{-3} s^{-1}$, Paterson and Weaver, 1970] and Solenhofen limestone at room temperature ($\dot{\varepsilon} = 10^{-4} s^{-1}$, Handin et al., 1967], confining pressure approximately equal to the differential stress are needed to suppress fracture. For these materials deforming by different mechanisms, particularly such low stress high temperature mechanisms as grain boundary sliding or Nabarro-Herring or

Coble creep, or for other materials the confining pressure to suppress fracture may not need to be so large.

For the comparison of hardness and fully ductile flow, as a rule of thumb we have selected only those polycrystalline creep tests conducted under confining pressures at least as large as the differential stress. Since such confining pressures are necessary for fully ductile flow in MgO [Paterson and Weaver, 1970] and in quartz [Heard and Carter, 1968] when the yield stress is greater than several kilobars, it is not unreasonable to expect a similar situation to obtain for olivine and Al_2O_3. We have therefore adopted that criterion as defining experiments performed in the fully ductile region. Experiments performed under confining pressures insufficient to suppress brittle failure would be expected to exhibit yield stresses smaller than the fully ductile polycrystalline yield stresses and by inference also less than the hardness-determined yield stress.

An additional piece of information needed to compare yield stress from polycrystalline creep tests and hardness-derived yield stresses: namely, to which strain rate should one compare a hardness test with a particular dwell time (t). Atkins et al. [1966b] have correlated hardness in indentation creep tests to the parameter $(t^{\frac{1}{3}}-t_o^{\frac{1}{3}})$; however, their derivations and experiments and subsequent experimental results [T. Evans and Sykes, 1973] conflict as to whether the deformation is controlled

by transient [Atkins et al., 1966b] or steady state [T. Evans and Sykes, 1973] processes. Furthermore, the finite time of loading and other processes, most notably cracking during the indenting process (see discussion of cracking below) may further shorten the effective dwell time. We may empirically determine the effective strain rate in much the same way that Tabor [1956] determined the effective strain for a VDP indent. In Figure 9a data from polycrystalline creep tests of Maryland diabase [Y. Caristan, unpublished manuscript] conducted at .5 GPa confining pressure and at 990°C are compared to Knoop hardness experiments of Brace [1960] on the same diabase. For this rock at these conditions the effective strain rate for a 15-second Knoop indentation test is found empirically to be $10^{-5.0 \pm .5} s^{-1}$.

Figure 9b is a similar determination of an effective hardness strain rate for olivine using the flow law of Kohlstedt et al. [1976] and the mutual indentation data of Table 2b. It is interesting to note that except for one anomalously low data point the effective hardness strain rate is approximately constant even though some experiments (T < 1200°C) are in the power law breakdown region.

In Figure 4, the polycrystalline yield data, at strain rates of $10^{-4} \lesssim \dot{\varepsilon} \lesssim 10^{-5} s^{-1}$ (for sources see Table 3), are

Figure 9. Determination of an Effective Strain Rate for the Hardness Test.

9a: Frederick Diabase

The solid line is from the data of Y. Caristan (personal communication) for the creep of Frederick, Maryland diabase for various strain rates at a confining pressure of .5 GPa (argon) and 990°C. The hardness derived-yield stress as determined by polycrystalline indentation on the same material by Brace (1961) corresponds to a strain rate of $10^{-5.3\pm.3}$. Gas deformation apparatus experiments (Caristan, unpublished) are circles. The large triangle is the hardness experiment of Brace (1961).

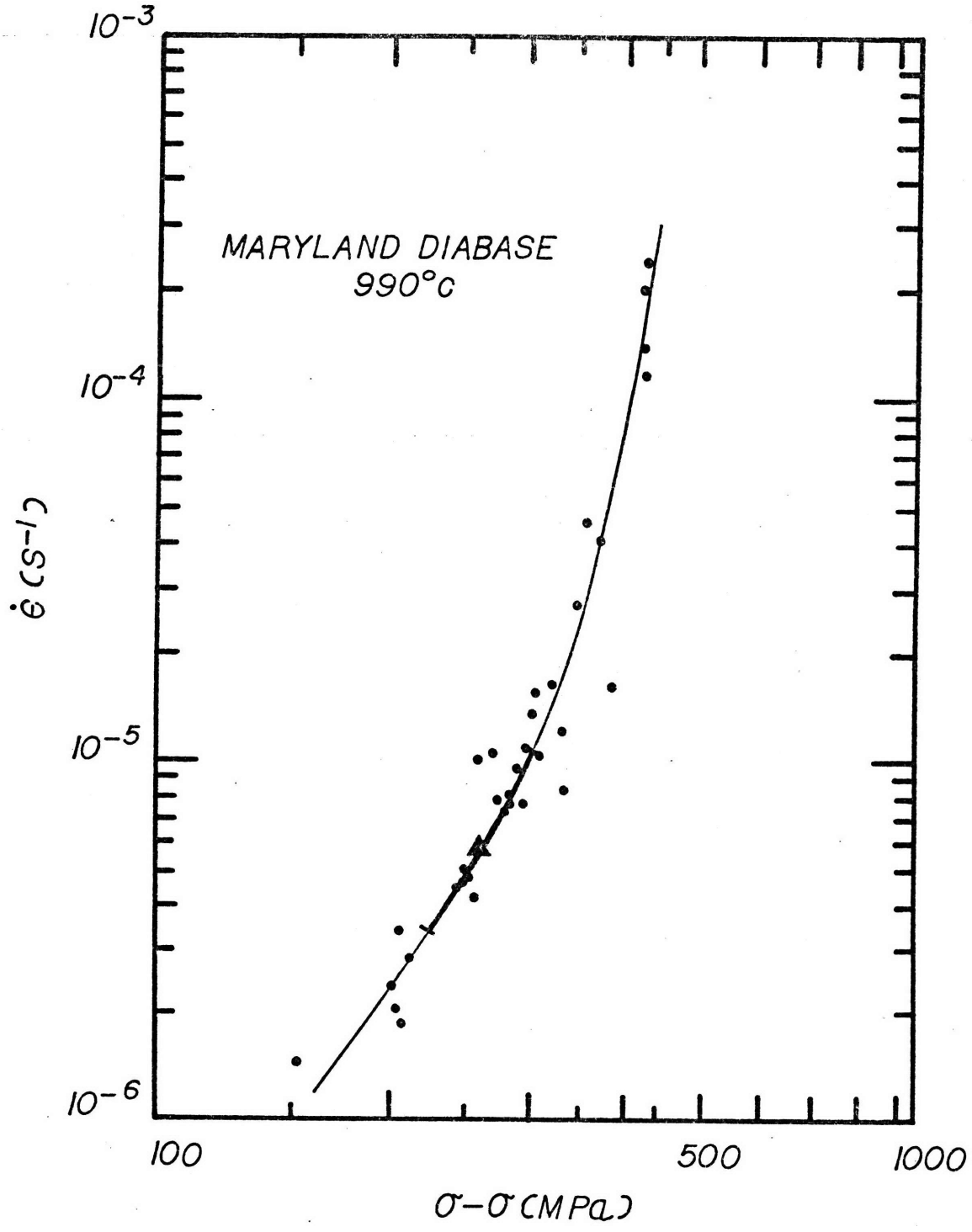
MARYLAND DIABASE
990°C
10^{-3}
10^{-4}
10^{-5}
10^{-6}
$\dot{\varepsilon}$ (s^{-1})
100
500
1000
$\sigma - \sigma$ (MPa)

9b: Olivine

A similar determination of the effective strain rate of indentation for olivine. The mutual indentation hardness-yield stresses are compared to the flow law of Kohlstedt et al. (1976). The squares are intended to indicate uncertainties in yield stress and temperature. With the exception of one anomalously low data point, the effective strain rates are $10^{-5\pm.5}$.

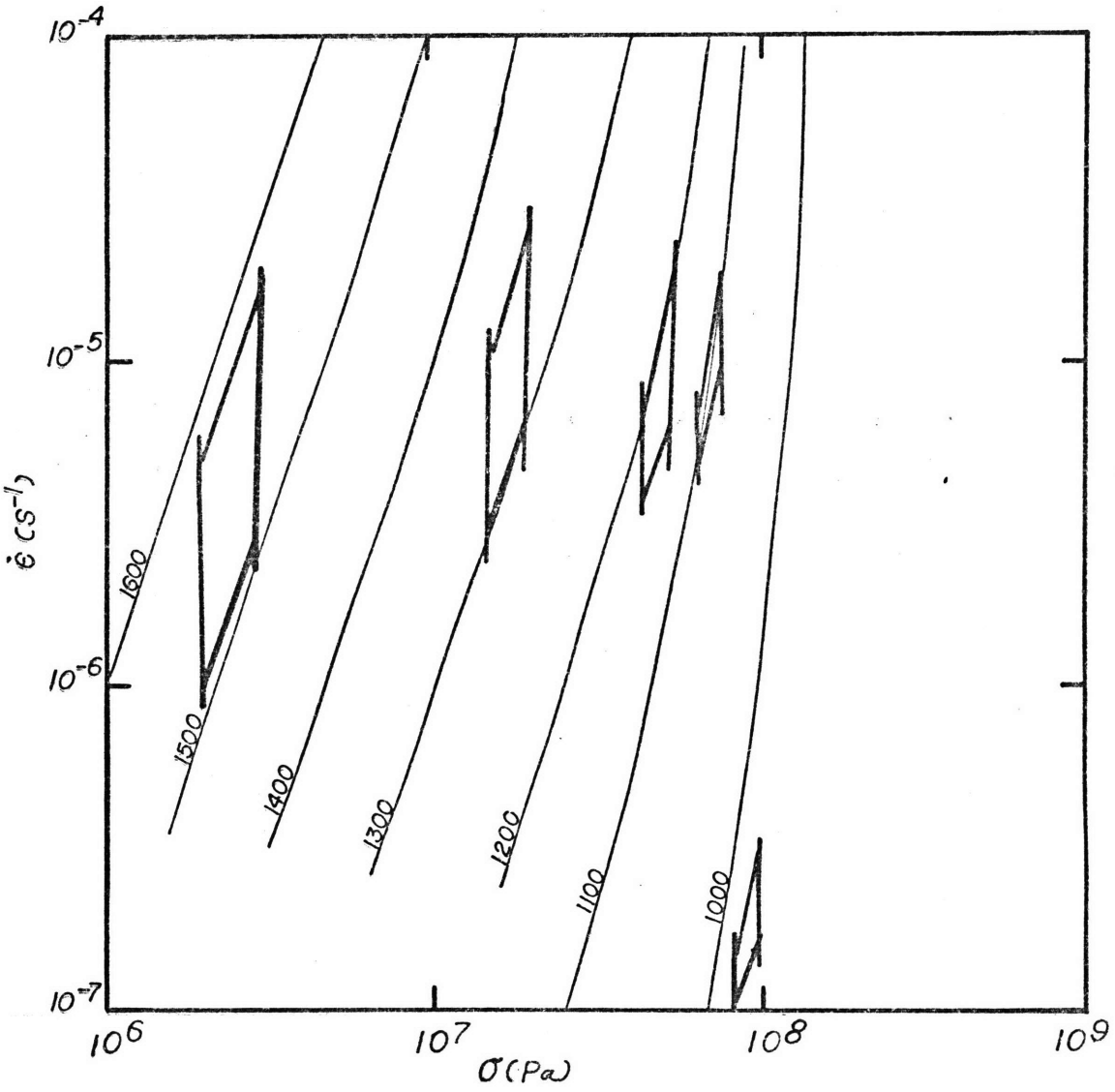
10^{-4}
10^{-5}
10^{-6}
10^{-7}
$\dot{\epsilon}\ (s^{-1})$
1600
1500
1400
1300
1200
1100
1000
10^6
10^7
10^8
10^9
σ (Pa)

compared with the hardness-derived yield values for olivine (see Table 2). The agreement is good over the entire range of temperature where both data sets exist. Similar curves are shown for MgO (Figure 10), Al_2O_3 (Figure 11), quartz (Figure 12), and NaCl (Figure 13) (the sources of the data are also given in Table 4).

For magnesium oxide, the comparison is straightforward (Figure 10). Data from Paterson and Weaver [1970] are systematically high, indicating that the strain rate used ($10^{-3}sec^{-1}$) is faster than the effective strain rate corresponding to the 15 sec VDP indenting process. Likewise, the data for alumina also correlate well despite the fact that five separate data sets are used. Not plotted on this graph is an anomalously low yield point from a compression test reported by Heuer et al. [1971] in which a "foam structure" was observed among larger grains of alumina.

The large changes in the elastic moduli of quartz caused by the α-β phase transition [Coe and Paterson, 1969] cause the constraint factor to vary widely. Additionally, because of the presence of large hydrostatic confining pressures, it is probable that the material in the immediate vicinity of the indentor does not undergo the α-β transition. This can be verified using a simple estimate of the hydrostatic pressure of the indentation process ($\sim\frac{2}{3}H$ [Tabor, 1972]), and the pressure sensitivity of the phase transition (~26 °/100 MPa [Coe and Paterson, 1969]). However, the elastic hinterland probably has undergone the transition and, in fact, because nonhydrostatic stresses perturb the α-β transition, the presence of large tensile

Figures 10-13. Comparison of Hardness Derived-Yield Stress and Polycrystalline Yield Stress for MgO, Al_2O_3, Quartz, and Halite.

A comparison of hot hardness and bulk polycrystalline yield experiments at high confining pressure for MgO (Figure 10), Al_2O_3 (Figure 11), quartz (Figure 12), and NaCl (Figure 13). The data sources are given in Table 3. The agreement between hardness derived values and polycrystalline values is good for all materials except NaCl. This discrepancy between hardness and bulk yield is probably due to grain size effects in the hardness measurements (see text). The broken curve sketched in Figure 11 is the best fit Peierls model given in Table 5 and explained in the text.

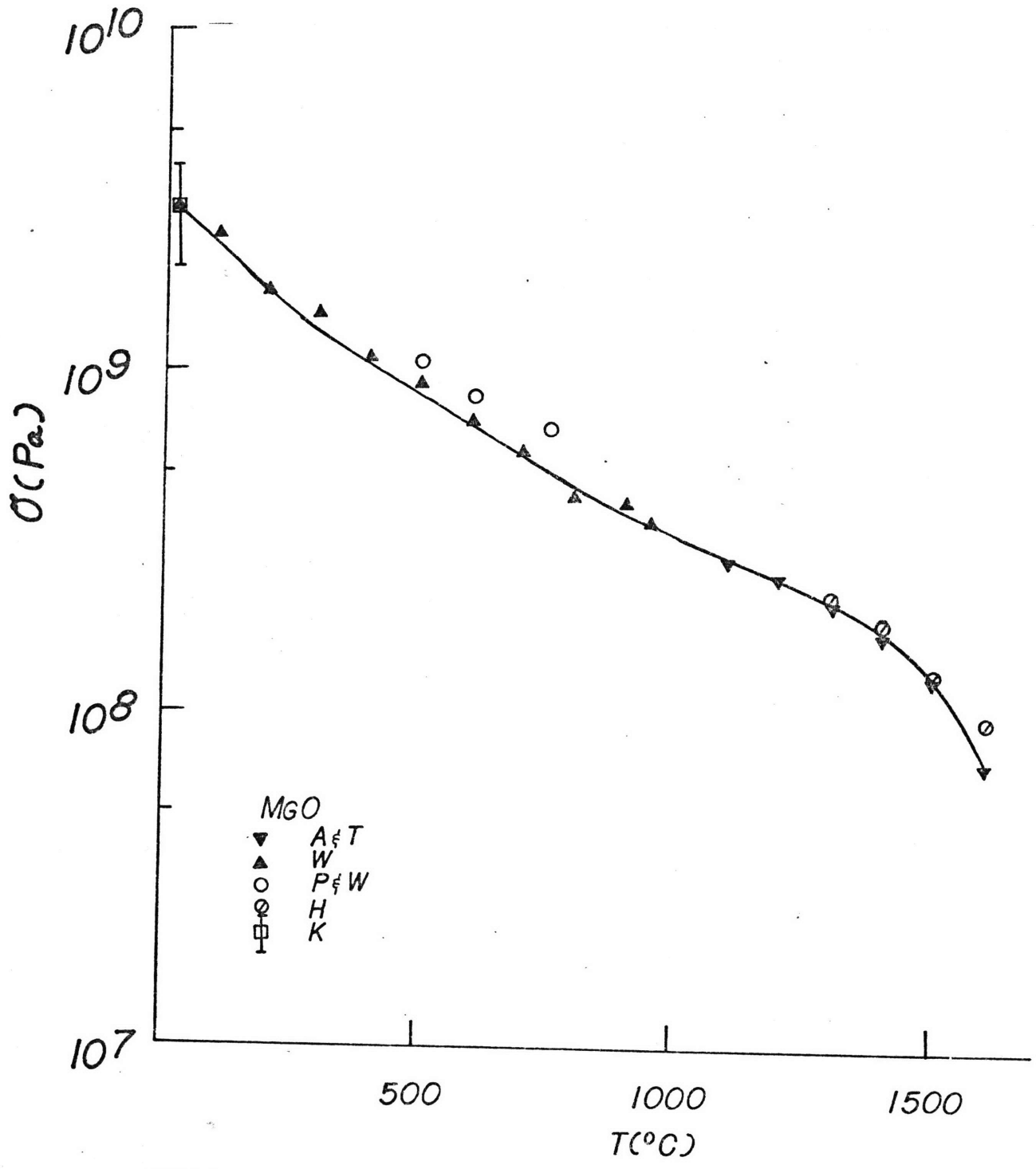
10^{10}
10^{9}
10^{8}
10^{7}
σ(Pa)
MgO
A & T
W
P & W
H
K
500
1000
1500
T(°C)

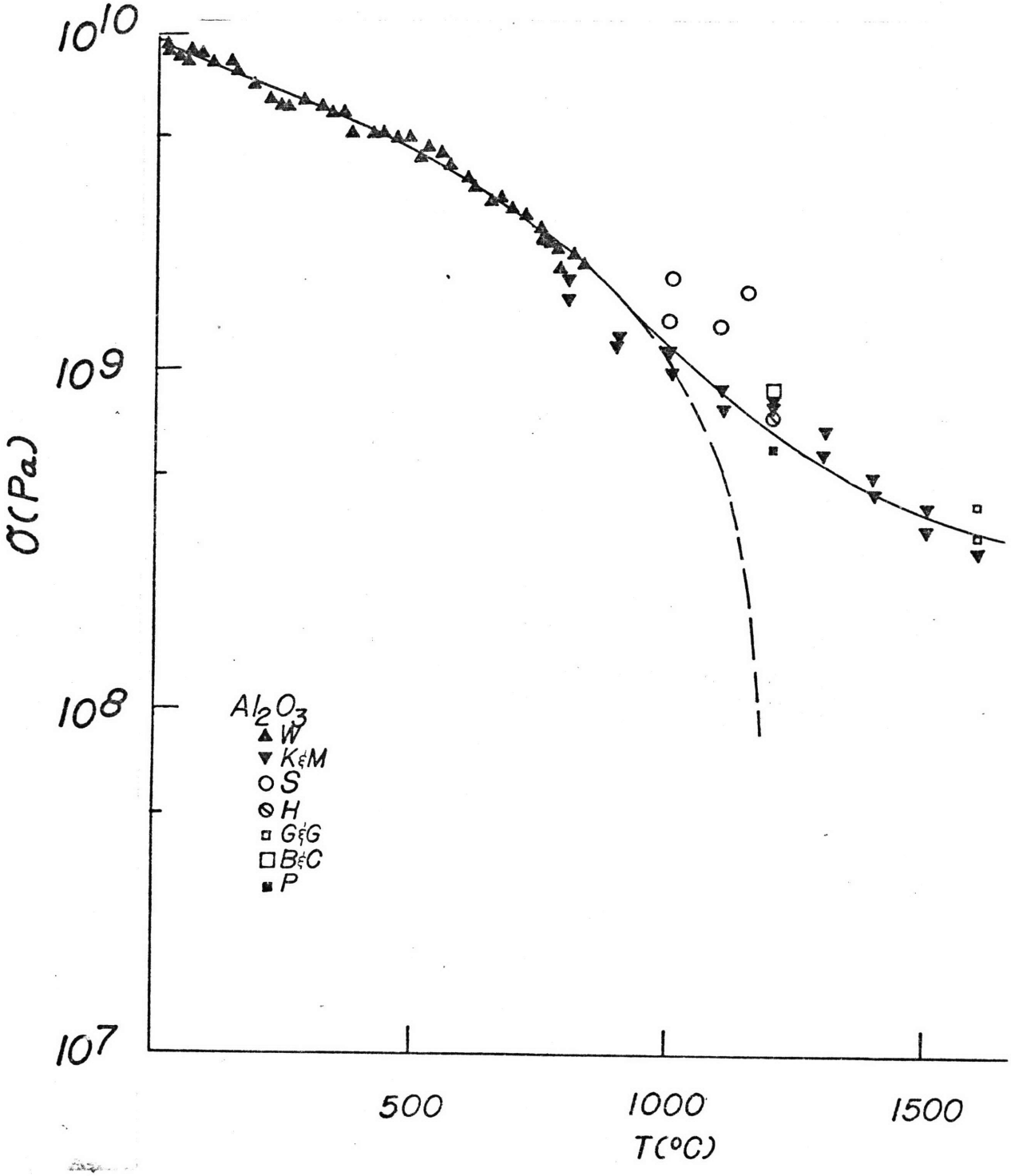
10^{10}
10^{9}
10^{8}
10^{7}
σ(Pa)
Al_2O_3
W
K&M
S
H
G&G
B&C
P
500
1000
1500
T(°C)

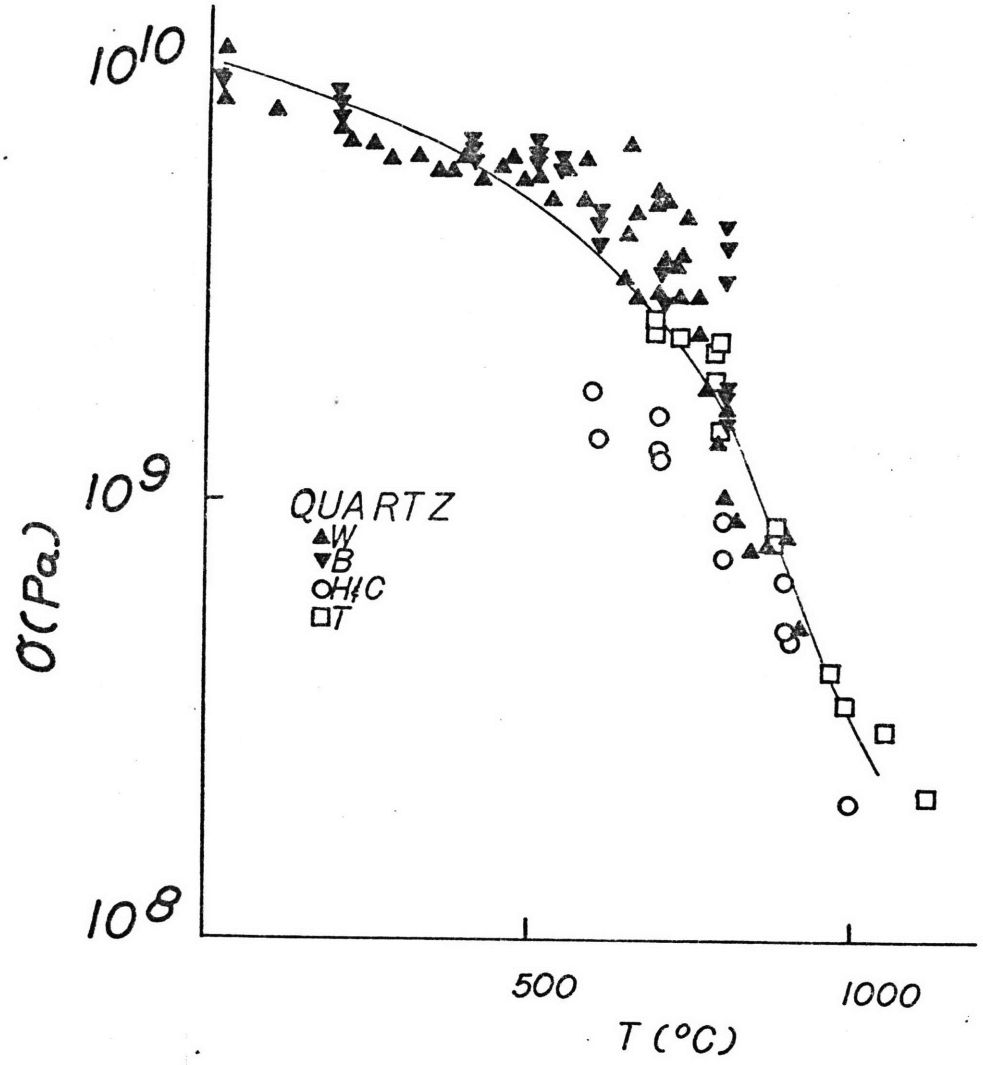
10^{10}
10^{9}
10^{8}
σ(Pa.)
QUARTZ
W
B
H&C
T
500
1000
T (°C)

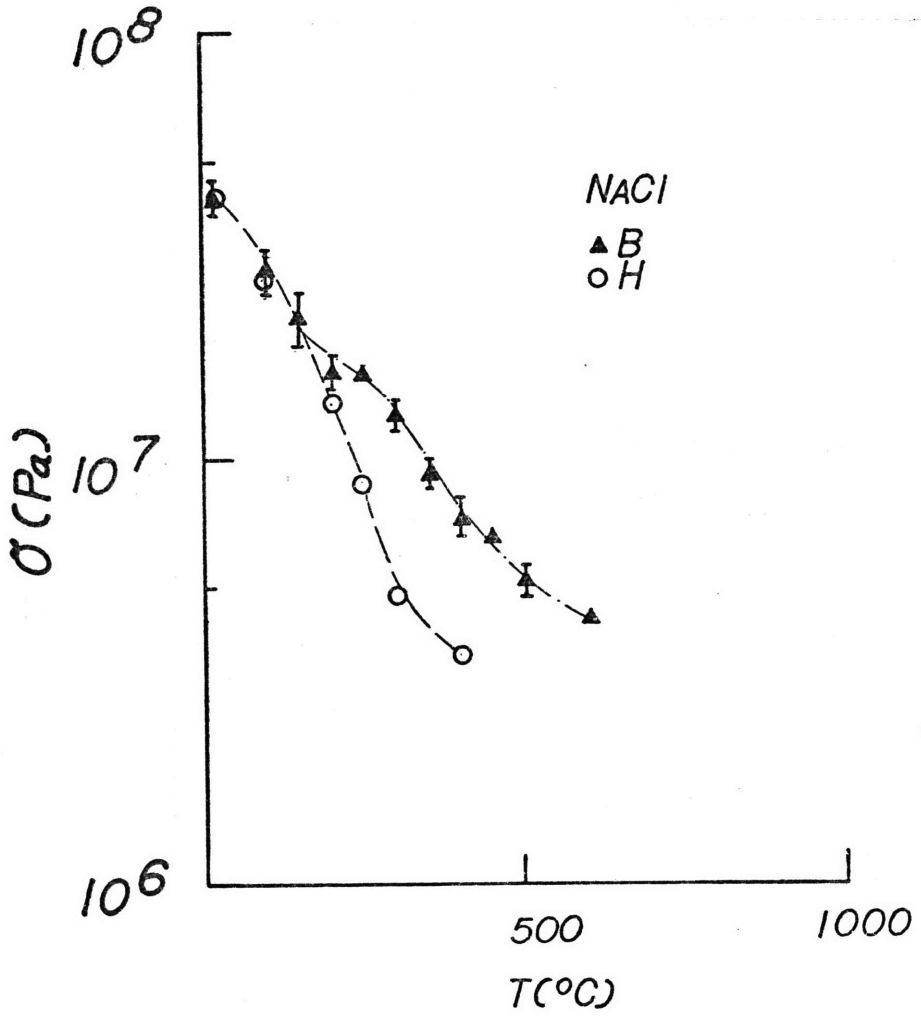
10^8
10^7
10^6
σ(Pa)
NACl
▲B
○H
500
1000
T(°C)

stresses in the indentor stress field probably causes the transition temperature in some regions in the far stress field to be below 573°C, the value at zero stress. It is for this reason that scatter in the quartz hardness data becomes more pronounced above 400°C. In the case of quartz, the Johnson theory probably represents an oversimplification of the facts, in that it assumes a homogenous isotropic elastic hinterland, whereas the true state is an anisotropic solid composed of two phases. However, despite these difficulties the agreement of the data sets is good. The comparison between Westbrook's [1958] data and Brace's [1961, 1960] data is not entirely straightforward, however, since the former used a synthetic quartz crystal while the latter indented a Herkimer diamond. The hydroxyl impurity content of neither is known, but presumably the natural quartz contains a much smaller amount. Secondly, the two indentor types differed: Brace using a Knoop, Westbrook a Vickers diamond pyramid. Knoop hardness is generally higher than VDP hardness, due to the different constraint factor [McClintock and Argon, 1966], although for quartz Westbrook [1958] states that the reverse may be true. Further complicating the comparison, the hardness of the $\{10\bar{1}0\}$ plane used in Westbrook's experiments is ~10% harder than the $\{10\bar{1}1\}$ utilized by Brace [1963] at lower temperatures (<200-300°C).

For halite (Figure 13) there is a systematic difference between hardness and yield, hardness being larger. This is probably due to the fact that Brace [1961, 1963] indented a fine-grained polycrystal, the indent spanning at least 10 grains. A grain size dependence of yield stress, the Hall-Petch effect,

is known to cause strengthening of fine-grained materials deforming by dislocation glide [see, for example, Hirth and Lothe, Chap. 21, 1968]. Brace [1963] also presents data on the grain size dependence of hardness at room temperature for halite, presumably due to the same effect.

Cracking during the indentation process

If cracking during polycrystalline creep tests lowers the yield stress measured, what effect does cracking have during the hardness test? Lawn and Swain [1975] and Swain and Hagen [1976] have studied the formation of cracks around indentations of various glasses at room temperatures, and, although they observe the formation of a median crack during loading, they describe the cracking process as an adjunct to the plastic deformation processes. As was noted above, it is possible that the effective strain rate could be lowered by cracking, perhaps by causing stress release near the region of plastic flow controlling the indentation process. It should be noted that the effective strain rate determined from mutual indents in olivine with no cracking is the same as in VDP indents in diabase with cracking. Also, it was noted that cracks frequently intersected individual dislocation loops, indicating that dislocation motion occurred prior to the cracking process.

This was true both for cracks which emanated from the corners of the indentations, called median cracks [Swain and Lawn, 1976] or for spalls, called radial or lateral cracks, which appear either directly upon unloading or after the test has been completed. Because of the relationship of the dislocation rosettes and cracks observed in this study, the

good agreement between polycrystalline yield experiments and hot hardness experiments described above, and the consistency of results of VDP experiments with mutual indentation experiments done at temperatures >1000°C where no cracking was present, we infer that hardness measurements reflect ductile properties and that the adjunct brittle properties are not rate-controlling.

Rosette length as an indication of lattice friction(Peierl's) stress on the primary glide system

The relation of the length of the dislocation rosette and the lattice friction stress on this slip system may be understood by analogy to a dislocation pile-up [see Hirth and Lothe, 1968, Chap. 21]. Neglecting dislocations in the intense zone of deformation, the last dislocation in the rosette is repelled by the interaction force of the other dislocations in the pile-up. Resisting the motion of the end dislocation away from the indent is the Peierls' or lattice friction stress, analogous to the applied stress of the pile-up theory. The indent itself, surrounded by the intense deformation zone, plays the role of the pile-up obstacle. The problem of the position of the individual dislocations in a pile-up was solved analytically by Eshelby et al. [1951] and the length of the pile-up (L) can be expressed as follows:

$$L = \frac{\mu N b}{\pi(1-\nu)\ \sigma_a} \quad \text{[Hirth and Lothe, 1968, p. 705, 21-33]} \tag{9}$$

where ν is Poisson's ratio, μ is the shear modulus, b is the magnitude of the Burger's vector, σ_a is the applied stress,

in this case, the lattice friction stress, and N is the number of dislocations in the pile-up. Thus, the pile-up analogy suggests an explanation for the inverse relationship of L and σ_a. Using Equation 9 and values appropriate to olivine and Figure 6 (N = 908), we estimate the lattice friction stress to be 3.0 kb. To be sure, the indentation rosette is not completely analogous to the Eshelby et al. [1951] theory since the rosette is not contained on a single plane but is blunted by spreading of the dislocations upon several different {110} planes. Furthermore, the rosette is composed of loops dissected by the free surface, while Eshelby et al.'s theory is for straight, infinitely long dislocations. Additionally we have neglected the interaction with dislocations in the hemispherical intense deformation zone directly under the indentor, and, finally we presume that the lattice friction stress is fixed regardless of dislocation velocity in order to compare it to Phakey et al.'s [1972] yield point.

However, it is probable that dislocation interactions cause the rosette to form, since an estimate of the elastic stresses generated by the indentor alone show them to be 1-2 orders of magnitude too small to have caused the outer dislocations to move [see Timoshenko and Goodier, 1970, for a discussion of the elastic stress field under a point force]. A more convincing estimate of the dislocation interaction stress may be obtained in the following: If the lead dislocation, i.e. the dislocation in the rosette furthest away from the indent, is being pushed outward from the indent by interaction of self-stress fields of the other dislocations in the rosette, then motion of the

lead dislocation is resisted only by the lattice friction stress. If the self-stress contributions at the lead dislocation are summed up using the expression for the self-stress field [e.g. Hirth and Lothe, 1968, equation 3-42] and the relative positions of the dislocations for the 908 dislocations visible in Figure 6, then the corresponding value of σ_f is approximately 2.7 kb.

These calculations are highly simplified, but their agreement with the experimental data is encouraging. Furthermore, Hopkins et al. [1973] have experimentally verified the inverse relationship between yield stress on the primary system and the rosette length and therefore we feel that one may use this rather quick and easy method to estimate yield stress with some confidence.

Comparison of single crystal and polycrystalline flow stresses for olivine

Comparisons between hardness-derived yield stresses and critical resolved shear stresses (CRSS) for slip on a particular glide system have shown that the ratio of the yield stress to the CRSS on the primary glide system may be as high as 30 [Westbrook, 1958]. We emphasize here that the data support the contention that hardness-derived yield stresses are characteristic of polycrystalline flow, so that single crystal CRSS are expected in general to be less than or equal to the polycrystalline yield stress. Furthermore, even though the Von Mises criterion states that five independent slip systems

must be activated within polycrystalline grains if homogeneous and pore-free deformation is to be achieved [Von Mises, 1928; Groves and Kelly, 1963], fewer slip systems may be required for nonhomogeneous deformation [Hutchinson, as quoted by Ashby and Verrall, 1977].

Several theories exist to explain the relationship of the yield of polycrystalline aggregates and single crystal slip properties [Lin and Ito, 1966; Hutchinson, 1975; and others], but to our knowledge no theory exists to explain pore-free flow of a material with only three independent slip systems. A fuller discussion of the relationship of single crystal and polycrystalline flow properties is outside the scope of this paper, but for a review of the flow properties of olivine, including single and polycrystalline data and the data in this paper, consult Goetze [1978].

In Figure 14 we compare the single crystal flow stress obtained from the rosette analysis to other published single crystal data.

The high stress deformation regime of olivine as inferred from hardness

Stocker and Ashby [1973] suggest that the appropriate high stress mechanism for olivine is thermally activated glide and use the Dorn and Rajnak [1964] line tension kink model to construct their deformation map. Durham et al.[1977] (Figure 14) have summarized the experimental constraints on both the low stress (high temperature) region, called (A), thought to involve

Figure 14. Comparison of Polycrystalline and Single Crystal Yield Stresses of Olivine.

The creep strength of three single crystal orientations and the trend of the polycrystalline data determined from Figure 4. The orientation $[110]_c$ indicates that the largest principal stress direction (σ_1) is on the (001) plane, and 45° between the <100> and <010> directions, $[011]_c$ and $[101]_c$ are similar. The data are collected from Table 4, Phakey et al. (1972) and Durham (1975). In particular, the data from Table 4 determine the $[101]_c$ curve from 775°C to room temperature. (------)

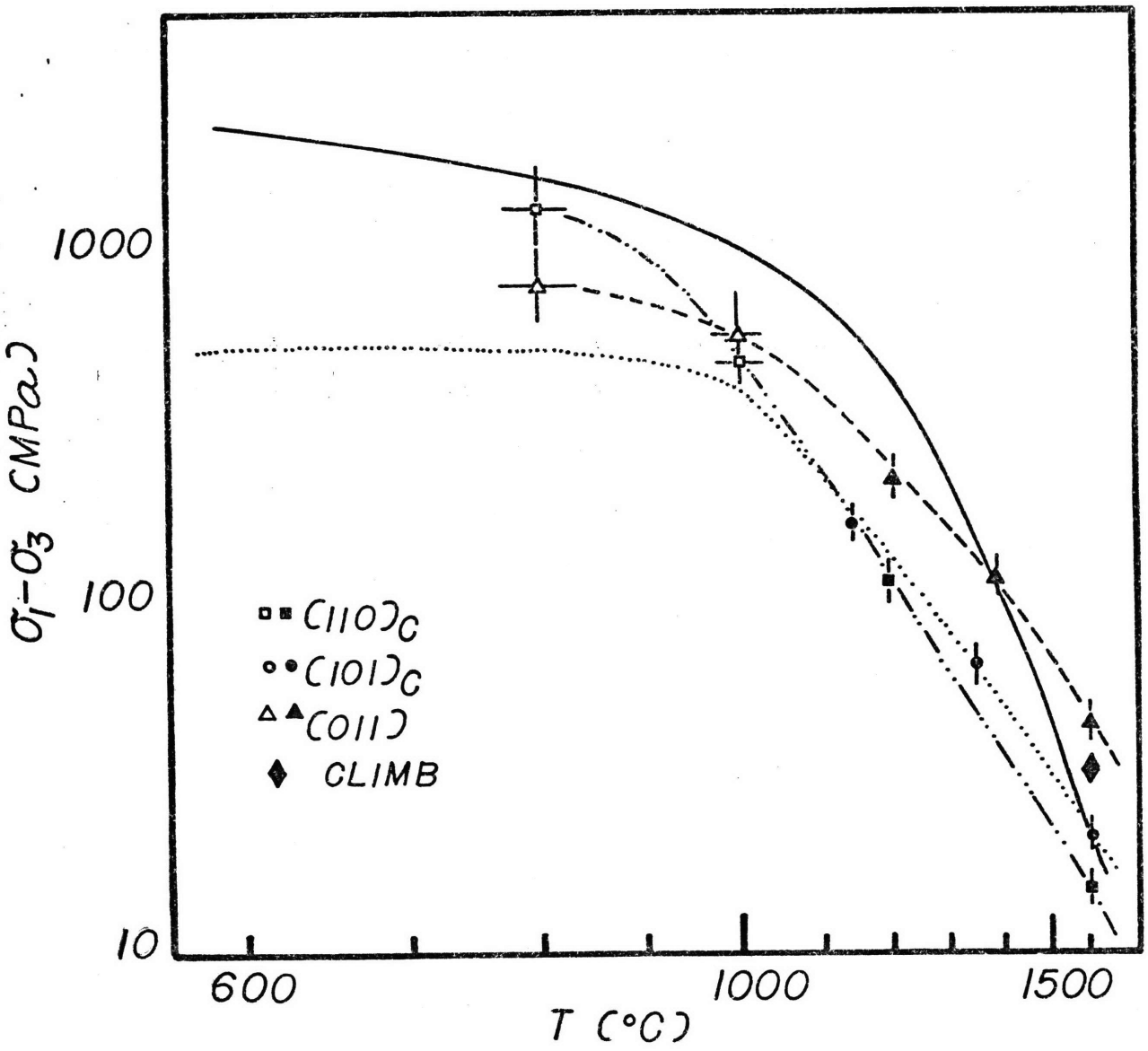
1000
100
10
$\sigma_1-\sigma_3$ (MPa)
600
1000
1500
T (°C)
(110)c
(101)c
(011)
CLIMB

glide, cross slip, and climb mechanisms, and the high stress (low temperature) region, called (B), which may possibly be glide-controlled, and the reader is referred to that paper for a discussion of the abundant experimental evidence supporting this division. Because of the experimental difficulties in achieving the very high stresses necessary for yield in region (B), the identity of the dislocation mechanism in this region has proven elusive. The hardness-derived data is unique in that it spans a stress range heretofore unachieved. Observation of the dislocation pattern about the indentations serves to further illustrate the transitions between regions (A) and (B). Low temperature (<1100°C) indents (e.g. Figure 6) are surrounded by rosettes composed of rectilinear glide loops confined to well-defined {110} glide planes. By contrast, higher temperature (>1300°C) indents (e.g. Figure 8) are surrounded by diffuse patterns of dislocations which are not restricted to discrete crystallographic planes. These observations, in concert with many other similar observations [e.g. Phakey et al., 1972; Durham et al., 1977] suggest the presence of strong crystalline control of deformation (i.e. a Peierls force) in region (B).

Several models, listed in a review by Kocks et al. [1975], have been proposed for the glide-limited Peierls' stress region; they differ slightly in the form of the stress, temperature, strain rate relation, depending primarily on the form of the activation energy barrier being surmounted as the dislocation changes position. However, a common

feature of all is that the activation free energy (ΔG) is assumed to be a function of stress in contrast to the mechanism usually assumed (primarily on empirical grounds) for the low stress, power law region. The Dorn-Rajnak line tension mechanism may be expressed in the form

$$\dot{\varepsilon} = \dot{\varepsilon}_o \exp - \frac{\Delta G(\sigma)}{RT} \tag{10}$$

where $\Delta G(\sigma) = F_o[1 - \frac{\sigma}{\sigma_p}]^2$ [Kocks et al., 1975, p. 137; Dorn and Rajnak, 1969]

$\dot{\varepsilon}_o$ is a pre-exponential factor assumed to be constant, F_o is an activation free energy, R, the gas constant, T. the absolute temperature, and σ_p, the differential stress necessary to deform the material at 0°K. The data are compared against this theory in Figure 15 by noticing that for constant strain rate, i.e., constant dwell time, and assuming that the temperature and stress dependence of $\dot{\varepsilon}_o$, if any, is small, Equation 10 implies that

$$\sigma = \sigma_p - m\, T^{\frac{1}{2}} \tag{11}$$

where $m = \sigma_p[\frac{R\ell n(\dot{\varepsilon}_o/\dot{\varepsilon})}{\Delta F_o}]^{\frac{1}{2}}$

For comparison, bounding curves computed for different barrier geometries [see Kocks et al., 1972, Chap. 34] are also plotted. Since the low stress region $T^{\frac{1}{2}} \gtrsim 35(°K)^{\frac{1}{2}}$ includes a change of mechanism to the power law, one cannot judge the applicability of barrier assumptions in this region. However, the high stress region, $T^{\frac{1}{2}} > 25(°K)^{\frac{1}{2}}$, seems to argue

against an activation energy of the form, $\Delta G = F_o \left(1 - \frac{\sigma}{\sigma_p}\right)$. Included among the models with this form of activation energy is the high applied-stress approximation of the flow law

$$\dot{\epsilon} = \dot{\epsilon}_o \exp - \frac{F_o}{RT} \sinh \frac{2V_o(\sigma-\sigma_o)}{KT} \quad \text{[Kocks et al., 1975, Chaps. 34 and 35]} \qquad (12)$$

$\dot{\epsilon}_o$, V_o and σ_o are material constants for the glide process. Poirier and Vergobbi [1977] have suggested that the yield data in the low stress region (A) can be explained by a cross slip controlled creep mechanism, with linear stress dependence of the activation energy, rather than a diffusion controlled climb mechanism. The hardness experiments do not offer any additional information on the low stress region. We re-emphasize that no information is obtained on any pre-exponential stress dependence of strain rate (which would of course be more important proportionally in the low stress region), that only "flat-topped" barrier geometries such as Equation 12 are excluded, and that the other geometries represent the data equally well. But, since Equation 10 is the simplest mathematically, and because the equations representing the various barrier geometries agree over their applicable temperature range, even when extrapolated to $\dot{\epsilon} = 10^{-15}$ sec, we prefer to use Equation 10.

The functional form (Equation 10) also well represents the data for alumina (Figure 16), as well as data for several spinel structure compounds [Dekker and Rieck, 1974], but is contraindicated for magnesia (Figure 17) and halite (Figure 18). A summary of the best fit parameters derived, using Equations

Figures 15-18. Yield Stress versus (Temperature)$^{1/2}$ for Olivine, Al_2O_3, MgO, Quartz and Halite.

A plot of differential yield stress versus (temperature)$^{1/2}$ for olivine (Figure 15) shown to emphasize agreement or disagreement with various barrier geometries of the thermally activated glide processes summarized by Kocks et al. (1975). The solid lines represent different stress dependence of the activation free energy as suggested by theoretical considerations, where Equation 10 of the text and the relation

$$\Delta G(\sigma) = G_o\{1-(\frac{\sigma}{\sigma_p})^P\}^q$$

are used. Theoretically, P and q are constrained to the values of $0 < P \leq 1$ and $1 \leq q \leq x$. (See Kocks et al. (1975) for a complete discussion.) Similar plots are shown for Al_2O_3 (Figure 16), MgO (Figure 17), and NaCl (Figure 18). In Figure 15 the bounding curves, P=1, Q=1, and P=1/2, Q=2/3 are light and the curve for P=1, Q=2 is heavy.

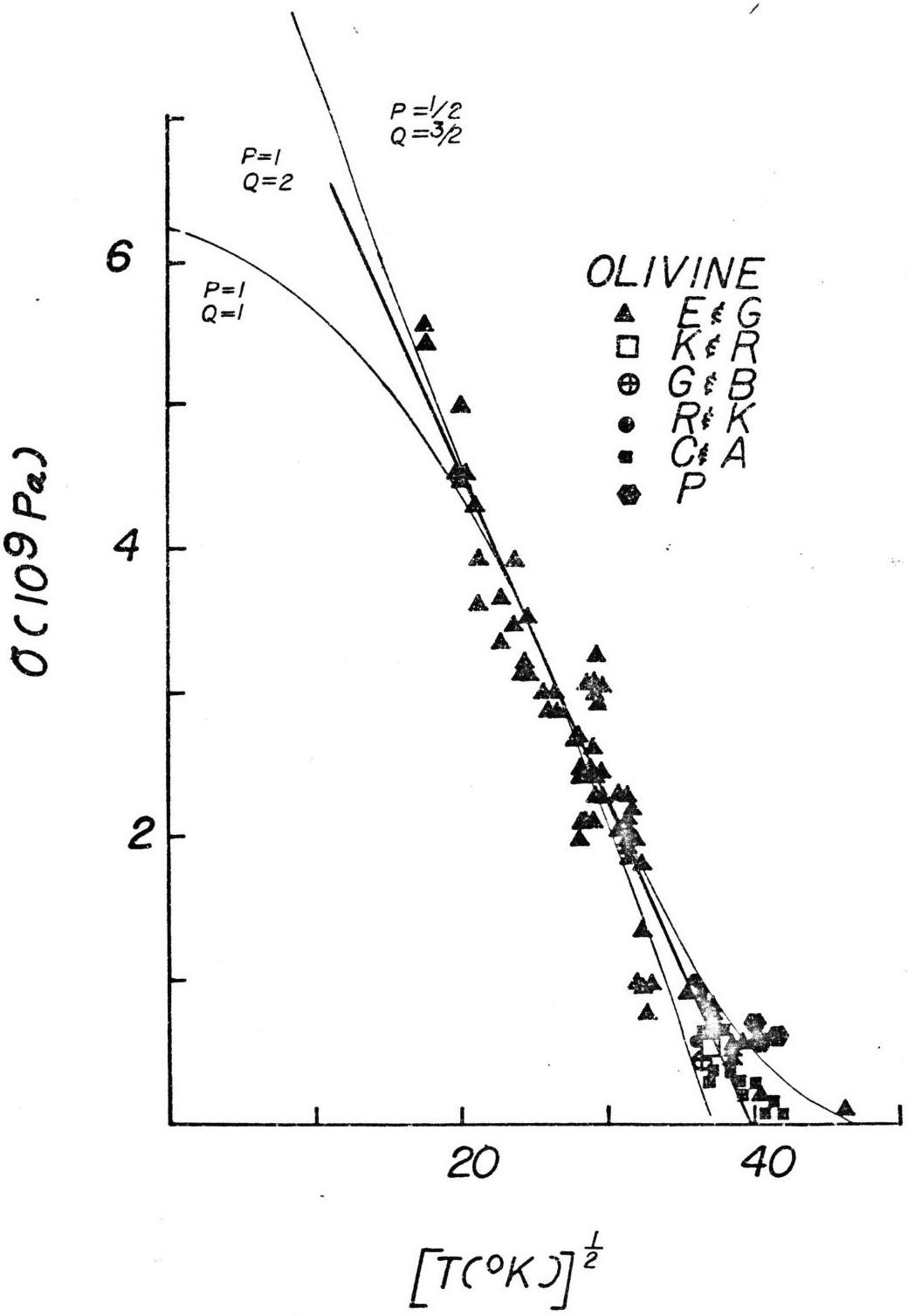
P = 1/2
Q = 3/2
P=1
Q=2
P=1
Q=1
OLIVINE
E & G
K & R
G & B
R & K
C & A
P
6
4
2
20
40
σ (10⁹ Pa)
[T(°K)]^½

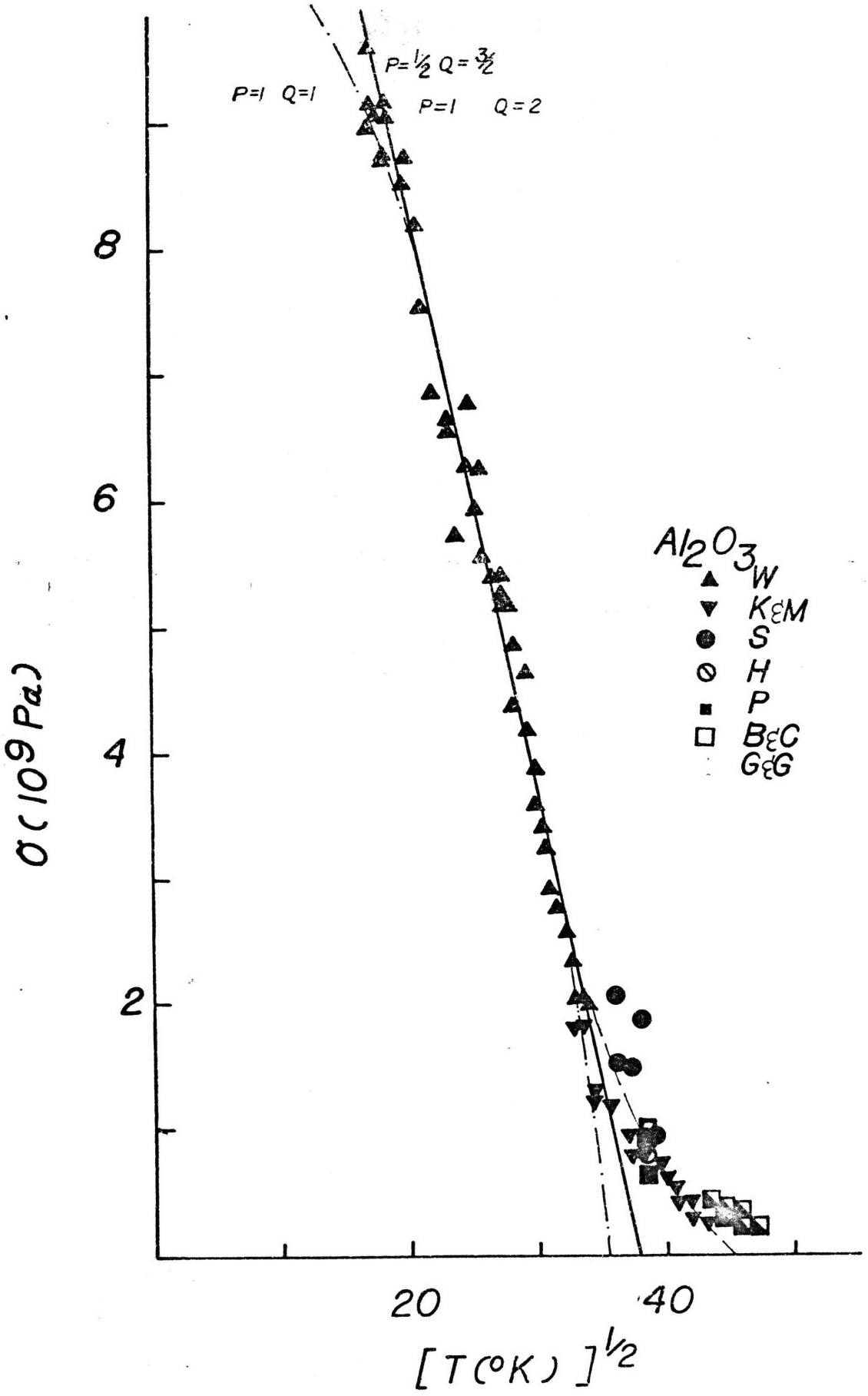
P=1 Q=1
P=½ Q=3/2
P=1 Q=2
8
6
4
2
σ(10⁹ Pa)
20
40
[T(°K)]^½
Al2O3
W
KεM
S
H
P
BεC
GεG

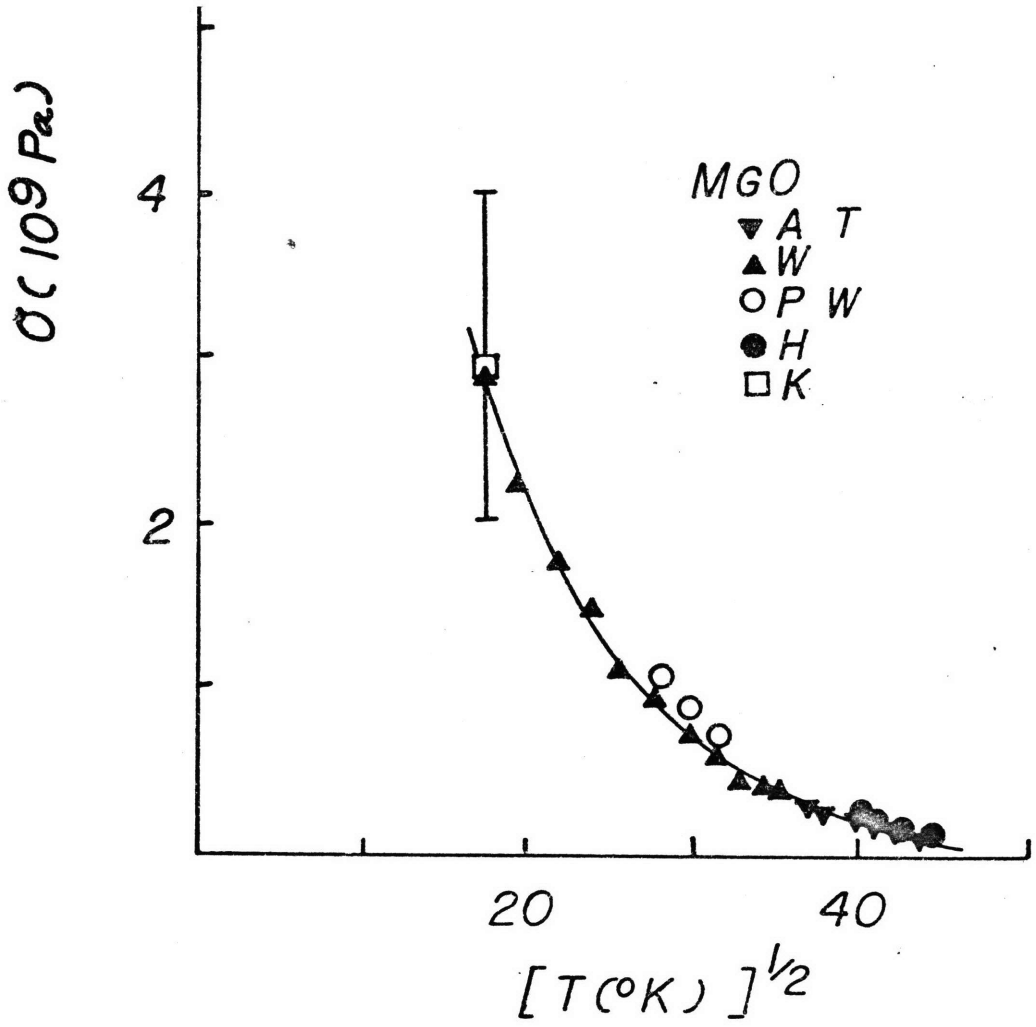
MGO
A T
W
P W
H
K
4
2
20
40
[T(°K)]^1/2

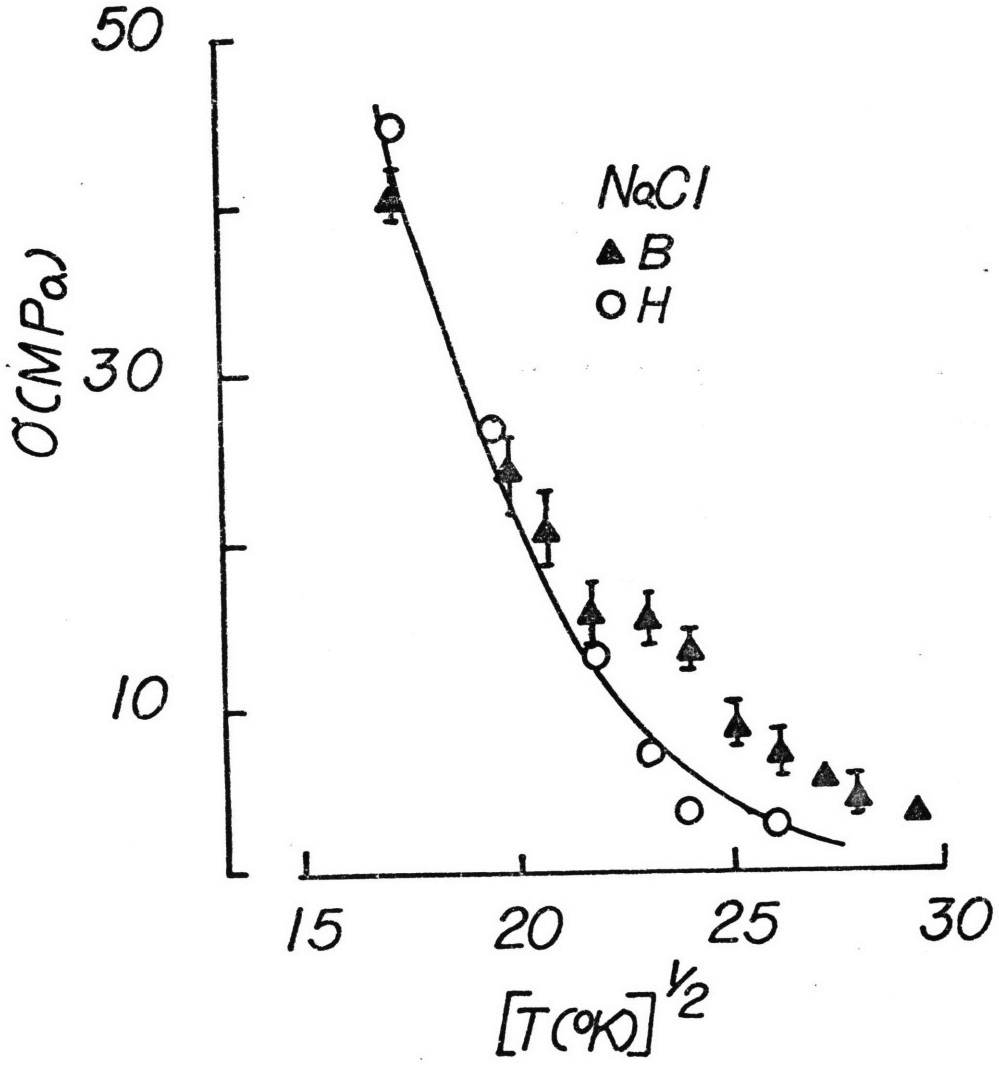
50
30
10
σ(MPa)
NaCl
B
H
15
20
25
30
[T(°K)]^1/2

10 and 11 and the data from Tables 2a, b, c, and d, is given in Table 5. If, in addition, one uses stress relaxation data from experiments on dunite at 800°C conducted by Kirby and Raleigh [1970], Equation 11 may be solved for F_o.

Finally, we feel that the present experimental scatter in the quartz data is too severe to draw conclusions on the applicability of the Peierls mechanism in the high stress region.

Summary and Conclusions

(1) The hot hardness of olivine from room temperature to 1500°C is as presented in Table 2 and Figure 4.

(2) A literature review and the new data for olivine give further confirmation to the relationship of hardness and yield stress proposed by Rice [1971], to wit: single crystal hardness data may be reduced, using Johnson's [1970] theory for the constraint factor, to give the polycrystalline yield stress (a) at 8% strain, (b) with no grain-size effects, such as Hall-Petch hardening, Coble creep, or grain boundary sliding, (c) at confining pressure high enough to cause suppression of cracking during the polycrystalline tests, (d) at a strain rate which, for the materials studied here, seems empirically to be about $10^{-5}sec^{-1}$ for a 15 second indent.

(3) The yield stress data obtained from the hardness measurements on olivine indicate agreement with models

for thermally activated glide with a non-linear stress-dependent activation free energy. Al_2O_3 also shows good agreement with such models, but MgO and NaCl do not.

TABLE 5: VALUE OF CONSTANTS m, σ_p IN EQUATION 11 FOR Al_2O_3, OLIVINE, AND QUARTZ

Material	$m[\frac{kb}{(°K)^{\frac{1}{2}}}]$	σ_p [kb]	Remarks
Al_2O_3	4.67 ± .1	175 ± 5	
Olivine	2.31 ± .09	90.5 ± 3	Stress relaxation tests at 800°C [Raleigh and Kirby, 1970] indicate an activation ethalpy of F = 120 ± 40 kcal.
Si O_2	5.6	200	Not a least squares fit because of scatter in data

REFERENCES

ASTM, ASTM Standards, 3, 30-38, 39-52, 1961.

Atkins, A.G., A. Silverio, and D. Tabor, Indentation hardness and the creep of solids, J. Inst. Met., 94, 369-378, 1966.

Atkins, A.G., and D. Tabor, The plastic deformation of crossed cylinders and wedges, J. Inst. Met., 94, 107-115, 1966a.

Atkins, A.G., and D. Tabor, Hardness and deformation properties of solids at very high temperatures, Proc., Roy. Soc. A, 292, 441-459, 1966b.

Bayer, P.D., and R.E. Cooper, A new slip system in sapphire, J. Mater. Sci., 2, 301, 1967.

Blacic, J.D., Effect of water on the experimental deformation of olivine, in Flow and Fracture of Rocks, ed. by H.C. Heard, I.Y. Borg, N.L. Carter, and C.B. Raleigh, Amer. Geophys. Un. Monograph #16, 109-115, 1972.

Brace, W.F., Behavior of rock salt, limestone, and anhydrite during indentation, J. Geophys. Res., 65, 1773-1788, 1960.

Brace, W.F., Experimental study of the indentation of rocks and minerals, Final Report, NSF Grant G-4647, Oct. 1, 1961, 81 pp.

Brace, W.F., Behavior of quartz during indentation, J. Geol., 71, 581-595, 1963.

Brace, W.F., Indentation hardness of minerals and rocks, N. Jahrbuch f. Mineralogie Monatshefte 9-11, 257-269, 1964.

Carter, N.L., and H.G. Ave'Lallemant, High temperature flow of dunite and peridotite, Geol. Soc. Amer. Bull., 81, 2181-2202, 1970.

Coe, R.S., and M.S. Paterson, The α-β inversion in quartz: A coherent phase transition under nonhydrostatic stress, J. Geophys. Res., 74, 4921-4948, 1969.

Darolia, R., and T.F. Archbold, Plastic deformation of polycrystalline zirconium carbide, J. Mater. Sci., 11, 283-290, 1970.

Dekker, E.H.L., and G.D. Rieck, Microhardness investigations on manganese aliminate spinels, J. Mater. Sci., 9, 1839-1846, 1974.

Dorn, J.E., and S. Rajnak, Nucleation of kink pairs and the Peierls' mechanism of plastic deformation, Trans. AIME, 230, 1052-1074, 1964.

Durand, M.A., The temperature variation of the elastic moduli of NaCl, KCl, MgO, Phys. Rev., 50, 449-455, 1936.

Durham, W.B., Plastic flow of single crystal olivine, PhD thesis, Massachusetts Inst. of Technology, Cambridge, 1975.

Durham, W.B., and C. Goetze, Plastic flow of oriented single crystals of olivine, Part I: Mechanical data, J. Geophys. Res., in press, 1977.

Durham, W.B., C. Goetze, and B. Blake, Plastic flow of oriented single crystals of olivine, Part II: Observations and interpretations of the dislocation structures, J. Geophys. Res., 82, 5755-5770, 1977.

Eshelby, J.D., F.C. Frank, and F.R.N. Nabarro, The equilibrium of linear arrays of dislocations, Phil. Mag., 42, 351-364, 1951.

Evans, T., and J. Sykes, Indentation hardness of two types of diamond in the temperature range 1500°C to 1850°C, Phil. Mag., 29, 135-147, 1974.

Goetze, C., The mechanisms of creep in olivine, Phil. Trans. Roy. Soc. London, 288, 99-119, 1978.

Goetze, C., and W.F. Brace, Laboratory observations of high temperature rheology of rocks, Tectonophysics, 13, 583-600, 1972.

Gooch, D.J., and G.W. Groves, the Creep of sapphire filaments with orientations close to the axis, J. Mater. Sci., 8, 1238-1246, 1973a.

Gooch, D.J., and G.W. Groves, Non-basal slip in sapphire, Phil. Mag., 28, 623-637, 1973.

Graham, E.K., and G.R. Barsch, Elastic constants of single crystal forsterite as a function of temperature and pressure, J. Geophys. Res., 74, 5949-5960, 1969.

Groves, G.W., and M.E. Fine, Solid solution and precipitation hardening in Mg-Fe-O alloys, J. Appl. Phys., 35, 3587-3593, 1964.

Groves, A., and G.W. Kelly, Crystallography and Crystal Defects, Addison-Wesley Publ. Co., Reading, Mass., 422 pp., 1970.

Handin, J., H.C. Heard, and J.N. Magouirk, Effects of the intermediate principal stress on the failure of limestone, dolomite, and glass at different temperatures and strain rates, J. Geophys. Res., 72, 611-640, 1967.

Heard, H.C., Steady state flow in polycrystalline halite at pressure of 2 kilobars, in Flow and Fracture of Rocks, ed. by H.C. Heard, I.Y. Borg, N.L. Carter, and C.B. Raleigh, Amer. Geophys. Un. Monograph #16, 191-210, 1972.

Heard, H.C., and N.L. Carter, Experimentally induced "natural" intragranular flow in quartz and quartzite, Amer. J. Sci., 266, 1-41, 1968.

Heuer, A.A., R.F. Firestone, J.D. Snow, and J.D. Tullis, Non-basal slip in aluminum oxide, in 2nd Intnl. Conf. on the Strength of Metals and Alloys, ASM, p. 1165, 1970.

Heuer, A.H., R.F. Firestone, J.D. Snow, and J.D. Tullis, Non-basal slip in alumina at high temperatures and pressures, in Ceramics in Severe Environments, Mater. Sci. Res., Vol. 5, ed. by W.W. Kriegel and H. Palmour III, Plenum Press, New York, p. 331, 1971.

Hill, R., The Mathematical Theory of Plasticity, Clarendon Press, Oxford, 1950.

Hirth, J.P., and J. Lothe, Theory of Dislocations, McGraw-Hill, New York, 780 pp., 1968.

Hopkins, J.R., J.A. Miller, and J.J. Martin, Flow stress, Vickers hardness and wing size for KCl and KCl:KBr, Phys. St. S., A, 19, 591-595, 1973.

Hulse, C.O., S.M. Copley, and J.A. Pask, Effect of crystal orientation on plastic deformation of magnesium oxide, J. Amer. Ceram. Soc., 46, 317-323, 1963.

Hutchinson, J.W., Bounds and self-consistent estimates for creep of polycrystalline materials, Report of Div. of Eng. and App. Phys., DEAP S-13, Harvard Univ., Cambridge, Mass. June 1975, 37 pp.

Johnson, K.L., The correlation of indentation experiments, J. Mech. Phys. Solids, 18, 115-126, 1970.

Kinsland, G.L., Yield strength under confining pressures to 300 kb in the diamond anvil cell, PhD thesis, Univ. of Rochester, New York, 1974.

Kirby, S.H., and C.B. Raleigh, Mechanisms of high-temperature, solid state flow in minerals and ceramics and their bearing on creep behavior of the mantle, Tectonophysics, 19, 165-194, 1973.

Kocks, W.F., A.S. Argon, and M.F. Ashby, Thermodynamics and kinetics of slip in Progress in Materials Science, Vol. 19, Pergamon Press, New York, p. 291, 1975.

Koester, R.D., and D.P. Moak, Hot hardness of selected borides, oxides, and carbides to 1500°C, J. Amer. Ceram. Soc., 50, 290-296, 1967.

Kohlstedt, D.L., C. Goetze, and W.B. Durham, Experimental deformation of single crystal olivine with application to flow in the mantle, in The Physics and Chemistry of Minerals and Rocks (ed. R.G.J.Strens), pp. 35-49, John Wiley, London, 1976.

Kohlstedt, D.L., C. Goetze, W.B. Durham, and J. Vander Sande, A new technique for decorating dislocations in olivine, Science, 191, 1045-1046, 1976.

Kohlstedt, D.L., and C. Goetze, Low stress high temperature creep in single crystal olivine, J. Geophys. Res., 79, 2045-2051, 1974.

Kumazawa, M., and O.L. Anderson, Elastic moduli, pressure derivatives, and temperature derivatives of single crystal olivine and single crystal forsterite, J. Geophys. Res., 74, 5961-5972, 1969.

Lawn, B.R., and M.V. Swain, Microfracture beneath point indentations in brittle solids, J. Mater. Sci., 10, 112-122, 1975.

Liepold, M.H., and T.H. Nielsen, Mechanical properties of hot-pressed ZrC tested to 2600°C, J. Amer. Ceram. Soc., 47, 419, 1964.

Lin, T.H., and M. Ito, Theoretical plastic stress-strain relationship of a polycrystal and the comparisons with the Von Mises and the Tresca plasticity theories, Int. J. Engng. Sci., 4, 543-561, 1966.

McClintock, F., and A.S. Argon, Mechanical Behavior of Materials, Addison-Wesley, Reading, Mass., 770 pp., 1966.

von Mises, R., Mechanik der Plastichen Formänderung von Kristallen, Z. angew. Math. Mech., 8, 161-185, 1928.

Mott, B.W., Microindentation Hardness Testing, Butterworth, London, 272 pp., 1956.

Palmour, H., III, W.W. Kriegel, P.F. Becker, and M.L. Huckabee, Grain boundary sliding in alumina bicrystals, Prog. Rept. No. ORO-3328-17, Contract At(40-1)33328, 1970.

Paterson, M.S., and C.W. Weaver, Deformation of polycrystalline MgO under pressure, J. Amer. Ceram. Soc., 53, 463-471, 1970.

Phakey, P., G. Dollinger, and J. Christie, Transmission electron microscopy of experimentally deformed olivine crystals, in Flow and Fracture of Rocks, ed. by H.C. Heard, I.Y. Borg, N.L. Carter, and C.B. Raleigh, Amer. Geophys. Un. Monograph #16, pp. 117-138, 1972.

Poirier, J.P., and B. Vergobbi, Splitting of dislocations in olivine, cross-slip controlled creep, and mantle rheology, in press, 1977.

Post, R.L., Jr., High temperature creep of Mt. Burnet dunite, PhD thesis (Geophysics), Univ. of California, Los Angeles, 1973.

Raleigh, C.B., and S.H. Kirby, Creep in the upper mantle, Mineral Soc. Amer. Spec. Pap. 3, 113-121, 1970.

Rice, R.W., The compressive strength of ceramics, in Ceramics in Severe Environments, Mater. Sci. Res., Vol. 5, ed. by W.W. Kriegel and H. Palmour III, Plenum Press, New York, pp. 195-229, 1971.

Sherby, O.D., and P.E. Armstrong, Prediction of activation energies for creep and self-diffusion from hot hardness data, Met. Trans., 2, 3479-3484, 1971.

Swain, M.V., and J.T. Hagen, Indentation plasticity and ensuing fracture of glass, J. Phys. D., Appl. Phys., 9, 2201-2214, 1976.

Swartz, K.D., Anharmonicity in sodium chloride, J. Acoust. Soc. Amer., 41, 1083-1092, 1967.

Tabor, D., The Hardness of Metals, Oxford Univ. Press, London, 1951.

Tabor, D., The physical meaning of indentation and scratch hardness, Brit. J. Appl. Phys., 7, 159-166, 1956.

Tabor, D., The hardness of solids, Rev. Phys. Tech., 1, 145-179, 1970.

Tefft, W.E., Elastic constants of synthetic single crystal corundum, J. Res. Nat. Bur. Stand., 70A, 277-280, 1966.

Timoshenko, S.P., and J.N. Goodier, Theory of Elasticity, 3rd Edition, Chap. 4, Sec. 3, McGraw-Hill, New York, 1970.

Tullis, J., Preferred orientations in experimentally deformed quartzites, PhD thesis, Univ. of California, Los Angeles, 344 pp., 1971.

Tullis, J., and R.A. Yund, Experimental deformation of dry Westerly granite, J. Geophys. Res., 82, 5705-5718, 1977.

Westbrook, J.H., Microhardness testing at high temperature, ASTM Proc., 57, 873-897, 1957.

Westbrook, J.H., Temperature dependence of strength and brittleness of some quartz structures, J. Amer. Ceram. Soc., 41, 433-440, 1958.

Westbrook, J.H., The temperature dependence of hardness of some common oxides, Rev. Hautes Temper. Refract., 3, 47-57, 1966.

Westbrook, J.H., and P.J. Jorgenson, Effects of water desorption on indentation microhardness anisotropy in minerals, Amer. Mineral., 53, 1899-1909, 1968.

Yu, F.C., and J.C.M. Li, Impression creep of LiF single crystals, Phil. Mag., 36, 811-825, 1977.

Zubov, V.G., and Firsova, M.M., The elastic properties of quartz near the α-β transition, Sov. Phys.-Cryst., 7, 374-375 (trans.), 1962.

CHAPTER II

THE VARIATION OF THE HARDNESS OF QUARTZ AS A FUNCTION OF TEMPERATURE AND IMPURITY CONTENT AND ITS IMPLICATION FOR POLYCRYSTALLINE YIELD STRESS

Abstract. Comparative hardness tests are well established as a means of determining relative mechanical effects of annealing or compositional variations in solid-solution series or isostructural compounds. In this chapter, the hardness technique is used to compare the relative strength of quartz with structural hydroxyl impurities. Even though the samples measured span the range of structural hydroxyl impurity contents which are expected to be found for reasonable geologic conditions, no impurity weakening was discovered. In order to see if high pressure would induce weakening that is associated with the gel hydroxyl impurity commonly found in synthetic quartz, two samples were annealed at 1.5 GPa in the presence of water for two days at 800°C. When the samples were subsequently tested by the hardness method in dry argon up to 500°C, the strengths were within the 30% of the hardness of natural quartz at the same temperature. Heating quartz in anhydrous environments for periods of several hours at temperatures above 600°C seems to harden the crystals. The cause of the hardening is not yet known.

The hardness data may be reduced to hardness derived yield stresses. The data thus obtained agree well with previously published natural polycrystals. The fully ductile yield strength of quartz is indicated to rise well above 5 GPa at temperatures below 500°C, reaching values near or above 10 GPa at room temperature.

Room temperature hardness phenomena such as form anisotropy, directional anisotropy and adsorbed water layer effects correlate with other studies of surficial and mechanical properties and are consistent with the idea that the hardness properties are controlled by fully ductile flow.

Introduction

Many field observations strongly suggest that quartz may be deformed ductily during tectonic events. Despite many attempts quartz resisted laboratory efforts to produce detectable ductile flow until the experiments of Griggs and others (1960). A vigorous scientific effort has ensued in an attempt to describe the natural deformation of this important mineral. (See Carter, 1976 or Nicolas and Poirier, 1976 for reviews.) Despite this prodigious effort by many workers, many questions remain unanswered.

In particular, one troubling inconsistency was that the stresses necessary for ductile flow as inferred from laboratory examinations were much higher than those which were estimated to be operating in the earth. This paradox was apparently resolved by the discovery that synthetic crystals were much weaker at given strain rates and temperatures than natural crystals (Griggs and Blacic, 1964; Griggs, 1967). Natural single crystal quartz deformed in the presence of dehydrating talc at 15 kb confining pressure and 800°C was also observed to deform at low stresses. These discoveries sparked an intensive investigation of the mechanical properties of synthetic quartz single crystals (Griggs, 1967; 1974; Heard and Carter, 1968; Baeta and Ashbee, 1969a and b; 1970a and b, 1973; McLaren et al., 1970; Blacic, 1971, 1975; Hobbs et al., 1972; Ardell et al., 1973; Balderman, 1974; Kirby, 1975, 1977; Morrison et al., 1976; and McCormick, 1976; among

others). Beginning slightly prior to and continuing concurrently with the discovery of the so-called hydrolytic weakening phenomena was a burgeoning literature concerning trace impurities in quartz. (For a review of the early literature, see Frondel, 1962; Cohen, 1954, 1956, 1958, 1959, 1960; or Dennen, 1965 . Among the impurities discovered residing in the quartz structure was hydrogen (Kats and Haven, 1960; Kats, 1961; 1962; Brunner et al., 1961; Bambauer, 1961; Bambauer et al., 1961a,b, 1962; Haven and Kats, 1962) and this was widely interpreted as indicating that hydrolytic weakening mechanisms were operative in the earth. The influence of the impurities other than hydrogen on the mechanical properties has been neglected except for a single investigation using indentation hardness testing (Nadeau, 1970).

The Nadeau (1970) study and the several previous studies of hot hardness of quartz (Westbrook, 1958, 1966; Brace, 1961) have been overlooked by workers examining the ductility of quartz. It is one of the purposes of this paper to compare these hardness studies as well as new hardness experiments on quartz to the results obtained using uniaxial and triaxial compressive apparatus. It will be seen that not only can the two types of test be related, but also that the incorporation of the hardness data into the body of yield data on quartz allows some interesting conclusions to be drawn.

Hardness tests have been widely used in the metallurgical and ceramics literature to investigate the flow properties of

even quite strcng materials (see McClintock and Argon, 1966; or Tabor, 1970 for reviews). Rice (1970) has suggested that single crystal hardness tests may be used to predict polycrystalline flow stress. In a previous paper, Evans and Goetze (1978) have presented experimental evidence that the hardness test can be used to relate the indentation hardness and yield stresses using the theory of Johnson (1970). Regardless of the exact relation of hardness to yield stress, the use of hardness as a relative measure of ductility is well documented. Thus a second purpose of this paper is to compare the hardness, and by inference, the yield stress, of several natural crystals of widely differing natural impurity states.

Yield Studies of Quartz

The first unequivocal evidence of experimentally produced plastic flow was given by Carter et al. (1961) using a simple squeezer. The results of those experiments and other experiments conducted in a cubic anvil apparatus are discussed in Carter et al. (1964a,b). Experiments were done both on polycrystalline material and single crystals allowing Carter et al. (1964b) to analyze slip tracings on the polished faces of the single crystal and to identify a basal slip system. Christie et al. (1964) used a piston and cylinder device to deform single crystals at room temperature and 2.7 GPa confining pressure using bismuth as the confining

medium. Analysis of the deformed specimens revealed ruptures which appeared to be crystallographically controlled. Thin zones of optically isotropic material which coated the rupture surface and some small crystals of coesite were detected. Christie et al. (1964) suggested that slip along the rupture planes caused brittle fractures to form which were then propagated to complete the rupture. The stress to rupture, that is, the maximum principal stress difference (σ_1-σ_3) depended on the orientation, varying between ~4.2-4.3 GPa when σ_1 was perpendicular to the r(11$\bar{2}$1), z(01$\bar{1}$1), or m(10$\bar{1}$0) planes and 4.6 GPa when σ_1 was perpendicular to the c(0001) plane.

The disparity between the observed natural ductility and intransigence of quartz in the laboratory was apparently resolved when Griggs and Blacic (1965) discovered a phenomenon which has come to be called hydrolytic weakening. Griggs and Blacic (1964; see also Griggs, 1967) were able to deform synthetic hydrothermally grown crystals at much lower stresses than natural crystals deformed in dry environments. They also made the observation that natural crystals were weakened when deformed in an environment (950°C, 1.5 GPa confining pressure) which was rendered hydrous by the presence of dehydrating talc. This discovery sparked a large number of studies of the properties of synthetic crystals. Only a brief summary of a few of the more important points is given here; for a more complete review, particularly concerning

the controversy over the development and use of deformation lamellae, please see Carter (1967) or Nicolas and Poirier (1976). A comparison of data available for single crystal experiments for both natural and synthetic crystals is given in Figure 1, and the data sources and a few pertinent experimental details are given in Table 1.

(1) For low strains (ε < 10-15%, and at temperatures between 300-800°C, synthetic quartz crystals compressed in directions which activate the basal and unit prism slip systems (see below for a listing of slip systems in natural and synthetic quartz) are much weaker than natural crystals (Griggs and Blacic, 1965; and many others).

(2) The stress-strain curves are often found to be sigmoidal in shape (Baeta and Ashbee, 1970a; Hobbs et al., 1972) having a yield point, a stage of low work hardening, and a stage of greater work hardening (Hobbs et al., 1972; Morrison-Smith et al., 1976).

(3) Synthetic crystals contain grown-in inclusions which are one or more of the following: a solid second phase, being perhaps acmite (Morrison-Smith et al., 1976); a colloidal suspension of water, silica and/or sodium hydroxide, possibly ordered in some fashion (Kirby, 1975; McCormick, 1976); water in gaseous or liquid phases probably with some dissolved compounds (observed in crystal X_o by McCormick, 1976).

(4) Bubbles containing liquid water are produced in many deformation experiments (Kirby, 1975; McCormick, 1976;

Figure 1. Single Crystal Yield Data for Synthetic Quartz: Yield Stress versus Temperature.

The yield stress is plotted for experiments at strain rates of 10^{-5} $.5s^{-1}$ for strain of .08 (when possible). The orientation of each crystal is given near the end of each data curve along with the hydroxyl content in $H/10^6$ Si. For the sources, symbols, and experimental details see Table 1.

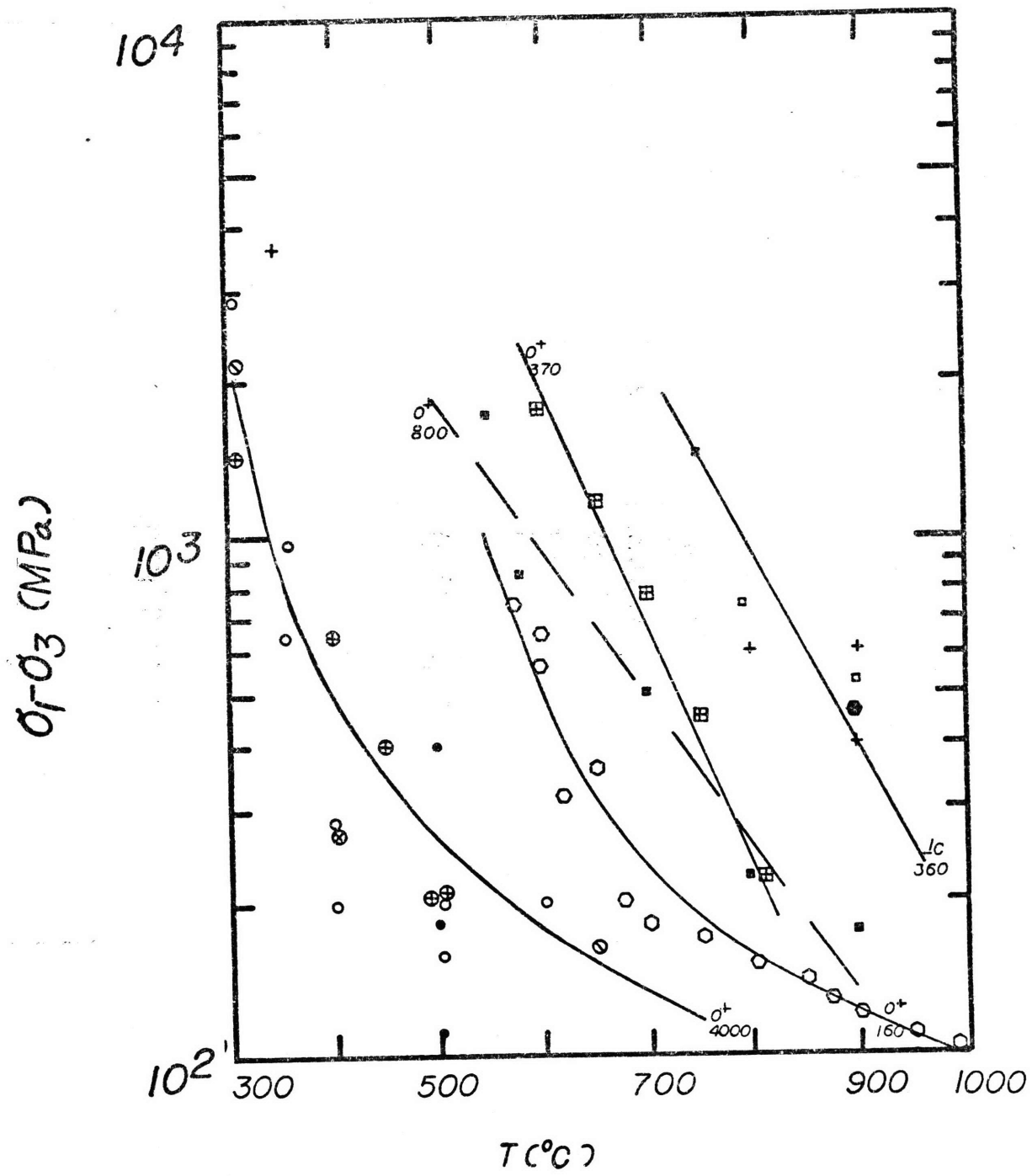
10^4
10^3
10^2
$\sigma_f - \sigma_3$ (MPa)
300
500
700
900
1000
T (°C)
0+ 800
0+ 870
0+ 4000
0+ 160
IC 360

TABLE 1. SYNTHETIC SINGLE CRYSTAL YIELD STUDIES

	Temperature (°C)	Orientation	Strain Rate (s^{-1})	Max. Strain	Symbol
Balderman (1974)	250-500	o^+	$7x10^{-3}$ - $5x10^{-8}$	~.10	⊕
Blacic (1971)	300-600	o^+	10^{-5}	.06-.10	o
Heard and Carter (1968)	500-1020	o^+	10^{-4} - 10^{-6}	~.08	▣
Hobbs (1968)	350-900	Various	$8x10^{-6}$	.60	+
Hobbs et al. (1972)	400-900	o^+	10^{-5} 10^{-5} 10^{-5}	.12	▣ ▣ □
Baeta and Ashby (1970)	600-100 900	o^+ c	10^{-3}-10^{-5}	.35	○ ●
Kirby (1975)	400-616	o^+	10^{-4}-10^{-7}	~.08	⊙
McCormick (1976)	400-555	o^+	$7x10^{-3}$ - $6x10^{-7}$	.05	●
Morrison-Smith et al. (1976)	475-900	$\perp r$	10^{-5}	.20	■

NOTE: o^+ orientation is 45° from <0001> and $<1\bar{2}10>$.

Morrison-Smith et al., 1976). The bubbles are mobile in experiments at high confining pressure and temperature and commonly are found at triple nodes of dislocations (McCormick, 1976; Morrison-Smith et al., 1976). It is not known whether the water which forms the precipitated bubbles migrates through the bulk lattice or along the dislocation cores. A substantial fraction of the hydroxyl which is present in the synthetic crystal resides in the form of inclusions (Kirby, 1975; see also Chernov and Khadzi, 1968 and the following section on impurities).

(5) Crystals in which the bubbles have been precipitated are much stronger (Jones, 1975; Kekulawala et al., 1978).

(6) Although most crystals have been deformed in an orientation which exerts maximum resolved shear stress on the basal and unit prism slip systems (Griggs and Blacic, 1965; Heard and Carter, 1968; Kirby, 1975; McCormick, 1976) several studies have been done to discover the effect of orientation (Baeta and Ashbee, 1969; Hobbs et al., 1972); those crystals deformed with $\sigma_1 \perp$ to the basal plane are strongest.

(7) Inhomogeneity in water content causes an inhomogeneity in dislocation generation which is frequently, but not always, found to occur near the grown-in inclusions (Morrison-Smith et al., 1976).

(8) Climb and recovery processes including recrystallization are competitive with glide and dislocation generation at strain rate = 10^{-5}/s and 800°C (Baeta and Ashbee, 1973) and

there is a suggestion that climb and other recovery processes are active at temperatures as low as 550°C to 600°C (Morrison-Smith et al., 1976; Baeta and Ashbee, 1973).

(9) At lower temperatures (<650°-750°C) most of the strain is taken up building dense tangles of dislocations which may become visible as optical lamellae or deformation bands (Christie et al., 1973; Morrison-Smith et al., 1976). The tangles spread to other portions of the crystal, sometimes dividing the crystal into zones which contain dislocations of primarily one slip system (Morrison-Smith et al., 1976) but which may form intersecting tangles which involve two slip systems (Baeta and Ashbee, 1973).

(10) Recrystallization takes place on a very fine scale in the experiments when there are dense tangles of dislocations and water is present but much higher temperatures are required for completely dry systems (Hobbs, 1968).

(11) There have been several attempts to determine activation parameters such as apparent activation enthalpy and the exponent of strain rate ($\dot{\varepsilon}$) sensitivity (n) in an expression such as

$$\dot{\varepsilon} = A\sigma^n \exp - \frac{Q}{RT} \qquad \text{(Eq. 1)}$$

(Baeta and Ashbee, 1969b; Balderman, 1974; Griggs, 1974)

σ is the yield stress.

A is an empirical constant but which may actually be a function of temperature, microstructure or other variables.

n is an empirical "constant" which strictly applies only in the limits of stress, temperature, strain rate, pressure,...space in which it was determined.

R is the gas constant.

T is the absolute temperature (K).

However these efforts are cast in severe doubt due to the observed complexity in generation of dislocations around the inclusions and their subsequent entanglement in complex tangles of dislocations as well as the uncertain effect of precipitating water (Kirby, 1975; McCormick, 1976; Morrison-Smith, 1976).

(12) Recent experiments by Kirby et al. (1977) and Kirby (1975, 1977) show that the generation of dislocations depends on the hydroxyl content but that the velocity of the dislocations (V_{dis}) can be represented by an Arhennius type equation which contains an apparent activation enthalpy which does not depend on the water content:

$$V_{dis} = V_o \exp -\frac{\Delta H}{RT} \qquad \text{(Eq. 2)}$$

where ΔH = 40 5 kcal/mole;

V_o = some constant which may depend on the concentration of hydroxyl.

(13) The slip systems which are found to operate in both synthetic and natural quartz are listed below in Table 3. The basal (0001) slip systems and the unit prism $\{1\bar{1}00\}$ slip systems have approximately the same apparent activation enthalpy (Baeta and Ashbee, 1970b) and yield stress at 800°C (Baeta and Ashbee, 1969; Hobbs et al., 1972; Morrison-Smith,

Table 3: Slip Systems Observed in Quartz by TEM

Plane	Burger's vector	Source
--	$1/3\langle 2\bar{1}\bar{1}0\rangle$	McCormick (1976)
$(2\bar{1}\bar{1}0)$	[0001]	" "
--	$1/3\langle 2\bar{1}\bar{1}3\rangle$	" "
(0001)	$\langle 2\bar{1}\bar{1}0\rangle$	Morrison-Smith et al. (1976)
$\{10\bar{1}0\}$	$\langle\bar{1}2\bar{1}3\rangle$	" " " " "
$\{10\bar{1}0\}$	<0001>	" " " " "
$\{10\bar{1}0\}$	$\langle\bar{1}2\bar{1}0\rangle$	" " " " "
$\{2\bar{1}\bar{1}0\}$	[0001]	" " " " "
$\{10\bar{1}2\}$	$\langle\bar{1}2\bar{1}0\rangle$	Baeta and Ashbee (1973)
{1013}	$\langle\bar{1}2\bar{1}0\rangle$	" " " "
plus all of the above		" " " "

1976) but which of these systems operate under given conditions may be affected by hydroxyl content (Blacic, 1975).

Concurrently with the intensive effort which was being lavished on synthetic crystals, a much more modest effort was being expended on natural single crystals and natural polycrystalline experiments. Griggs and Blacic (1964; see also Griggs, 1967) deformed natural single crystals in the o^+ orientation, which develops high shear stresses on the basal and prism planes. Subsequent TEM observations (McLaren and Phakey, 1967) revealed no dislocations in the experiments deformed below 600°C; glassy fracture zones similar to those described by Christie et al. (1964) were observed as well as

twinning according to the Brazil law. At somewhat higher temperatures, 600°-750°C, many basal dislocations were observed in addition to the basal faults.

Heard and Carter (1968) performed a series of experiments on natural and synthetic crystals and a natural polycrystal, the Simpson orthoquartzite. Subsequently a reanalysis of the Simpson experiments, and a new set of experiments on the Canyon Creek orthoquartzite which was deformed at 1.0 GPa confining pressure under hydrous conditions, was published by Parrish et al. (1976). Heard and Carter (1968) observed optical deformation lamellae in their suite of samples and attempted to define the operating slip systems from these observations. Although in some cases lamellae may indicate the predominant slip system operating (Carter, 1976; Twiss, 1974) they need not necessarily form parallel to slip planes (Christie and Ardell, 1974; Ardell et al., 1976). Heard and Carter (1968) do not identify recrystallization as occurring, nor do the photographs in their report evidence recrystallization to any significant degree. By contrast the experiments of Parrish et al. (1976) on the Canyon Creek orthoquartzite are replete with recrystallization fabrics. A previous study of the Canyon Creek rock (Ave' Lallement and Carter, 1970) had shown that recrystallization occurred at temperatures above the dehydration of the talc confining medium but not below it. The rocks were strong when deformed at the same temperature when no water (and

also no recrystallization) were present. Tullis (1972) and Tullis et al. (1973) deformed samples of the Simpson and Canyon Creek quartzites and, in addition, a Black Hills quartzite in order to investigate the development of fabric with strain. Many experiments were conducted using talc confining medium but in some experiments above the dehydration temperature AlSiMag 222, boron nitride or salt were used. Similar observations were made concerning recrystallization, and in addition they note that below 800°C, there was no recrystallization even for quite large strains. The deformation was very inhomogeneous, and some grains oriented with the (0001) axis parallel to the greatest principal compressive stress survived the deformation relatively unstrained. Figure 2 contains a comparison of the polycrystalline data; the sources of the data and some of the pertinent experimental details are listed in Table 2.

A recent set of experiments conducted by Kekulawala et al. (1978) are particularly interesting in that they failed to discover any significant hydrolytic weakening in natural single crystals except for amethyst at confining pressures of 300 MPa. It may be possible to reconcile these results with Griggs and Blacic (1964) if the weakened state is more easily attainable under the higher confining pressure used by the latter (1.5 GPa). However, at present, this question is unresolved.

Figure 2. Previous Natural Single and Polycrystalline Yield Studies: Yield Stress versus Temperature.

The yield stress was taken at .08 strain where possible and at a strain rate of $10^{-5\pm.5}$. For data sources, symbols and experimental details see Table 2.

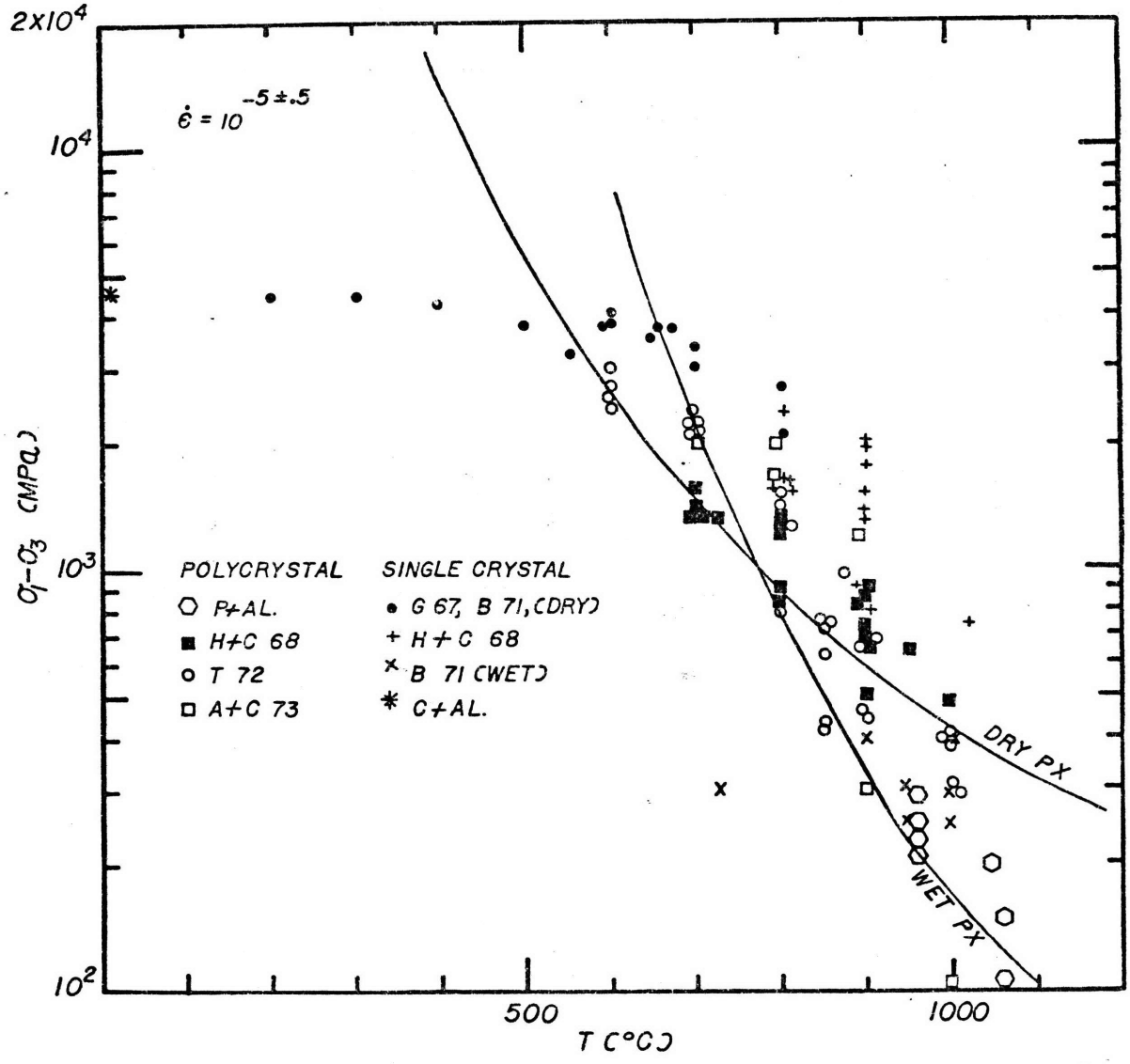
2x10^4
10^4
10^3
10^2
σ1-σ3 (MPa)
ε̇ = 10^-5±.5
POLYCRYSTAL
P+AL.
H+C 68
T 72
A+C 73
SINGLE CRYSTAL
G 67, B 71, (DRY)
H+C 68
B 71 (WET)
C+AL.
DRY PX
WET PX
500
1000
T (°C)

TABLE 2. NATURAL SINGLE AND POLYCRYSTAL YIELD STUDIES

Reference	Temperature (°C)	Orientation & Type	Strain Rate (s^{-1})	Maximum Strain	Confining Pressure (GPa)	Symbol
Heard and Carter (1968)	500-1000	Simpson Orthoquartzite; polycrystal	10^{-3}-10^{-7}	~.10	Argon 1.0-.6	■
Ave'lallement and Carter (1973)	600-1050	Canyon Creek; polycrystal	$.8x10^{-5}$	.10	Talc 2.0-.4	□
Tullis (1972	400-1100	Simpson, Canyon Creek, Black Hills; polycrystals	10^{-5}-10^{-7}	up to .60	Talc Alsimag Halite	○
Parrish et al. (1976)	860-1160	Canyon Creek; polycrystal	10^{-4}-$10^{-6.4}$	~.15	Talc 1.0	⬡
Griggs (1967), Blacic (1971)	200-750	Single crystal O^+	$.8x10^{-5}$	.08-.10	1.5 GPa	●
Heard and Carter (1968)	500-1000	Single crystal O^+	10^{-3}-10^{-7}	~.10	Argon 1.0-.6	+
Blacic (1971)	700-1000	Single crystal O^+	10^{-5}	~.08	Talc 1.5-.6 GPa	×
Christie et al. (1964)	23	Single crystal; various	$3x10^{-4}$	Rupture	Bismuth 2.7-3.0	✳

Room Temperature Hardness Studies of Quartz

Early room temperature studies of indentation hardness quartz were primarily aimed at the use of hardness as a diagnostic tool (Winchell, 1945) or as a device to study the deformation mechanisms including fracture in quartz single crystals (Mügge, 1898). These studies and others of a similar nature are reviewed extensively by Brace (1961, 1963, 1964). Brace's (1961, 1963) detailed explanation of the morphology of Knoop indentations (Winchell, 1945; McClintock and Argon, 1966), using a replication technique observed by SEM, revealed markings on the facets of the indentations which he likened to slip tracings observed in halite and metals (Figure 3a). Brace suggested that these might in fact be evidence of plastic flow on these planes. He also examined the patterns of cracks about the indentations (Figure 3c) and the actual shape of the indent itself, which was found to depart from the shape of the indentor, particularly, in that the ratio of the diagonals was 10:1 instead of 7:1 (Figure 3d) and the sides of the indentation were slightly concave outward. These painstaking observations are pertinent in the correlation of hardness and yield properties and are discussed below.

Comparison of results of room temperature tests led to the discovery that hardness varied as a function of the crystallographic face being tested (Winchell, 1945; Brace, 1961, 1963). A second sort of anisotropy of hardness exists

Figure 3a. Knoop Indentation Morphology.

High resolution scanning electron micrograph of a replica of a Knoop microhardness indentation in quartz made by Brace (1961). The arrow shows the direction of shadowing of the replica. The orientation of the crystal axes with respect to the long axis of the indentation are the same as the relative orientation of the diagram shown in Figure 3b. In the inset is shown a scale length for 1 μm. (From Brace, 1961)

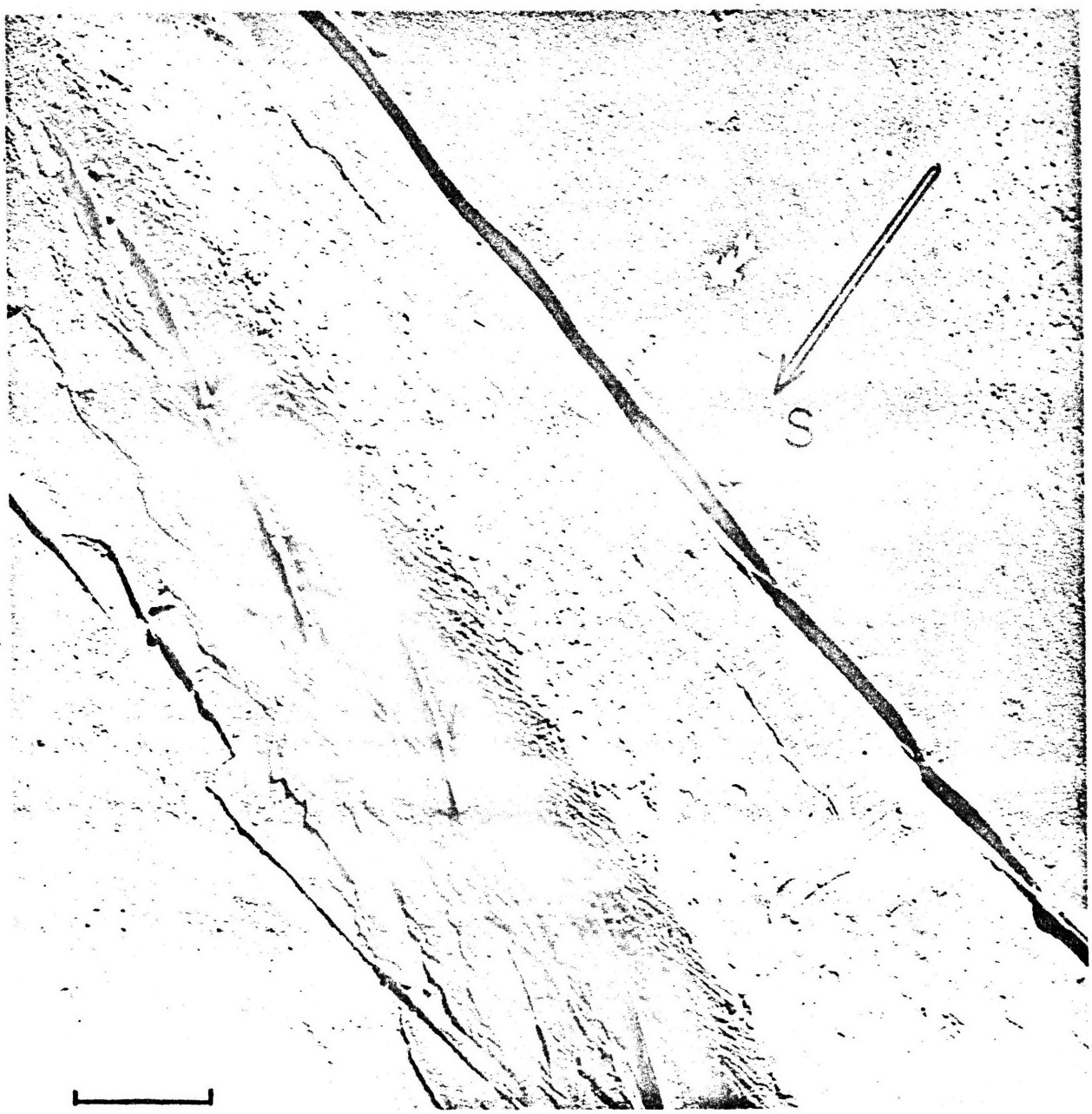
S

Figure 3b. Crystallographic Orientation of Figure 3a.

The trace which several important crystal planes make on the plane of the shaded facet of the indentation is shown. The symbols and their corresponding planes are:

M unit prism $\{1\bar{1}00\}$

A secondary prism $\{2\bar{1}\bar{1}0\}$

R + rhombohedral $\{10\bar{1}1\}$

Z - rhombohedral $\{01\bar{1}1\}$

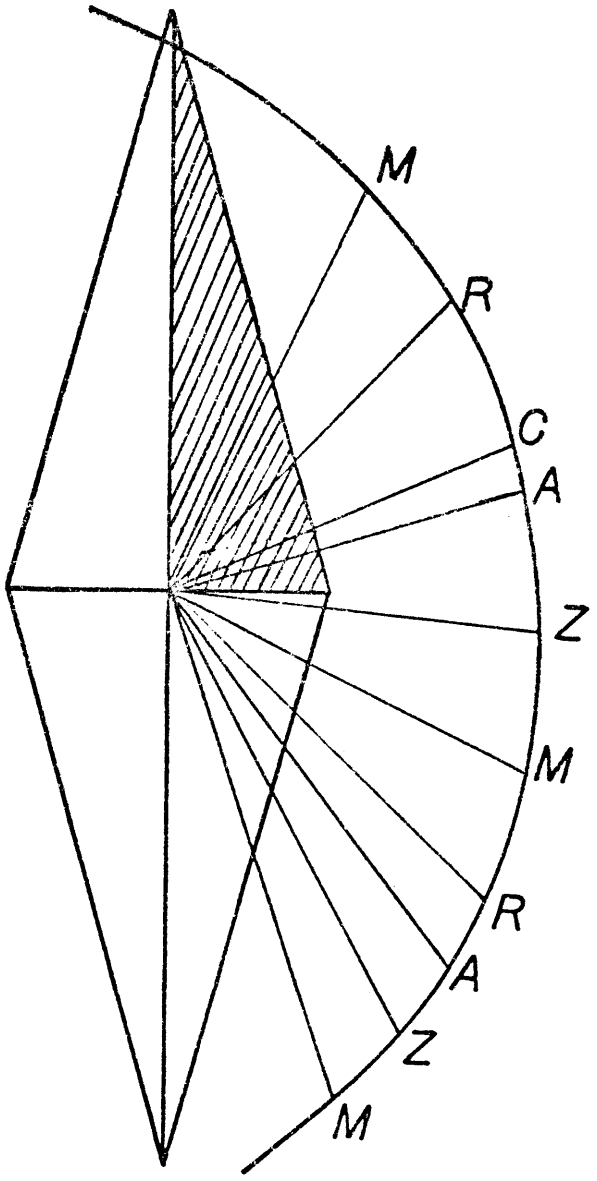
M
R
C
A
Z
M
R
A
Z
M

Figure 3c. Cross Section of Knoop Indentation.

A scale drawing of a Knoop indentation on the + rhombohedral face of quartz (from Brace, 1961, 1963). The ring cracks shown often form upon unloading or shortly after unloading. In addition, there may be median cracks which extend parallel to the trace of $z\{1\bar{1}01\}$ planes into the crystal half-space.

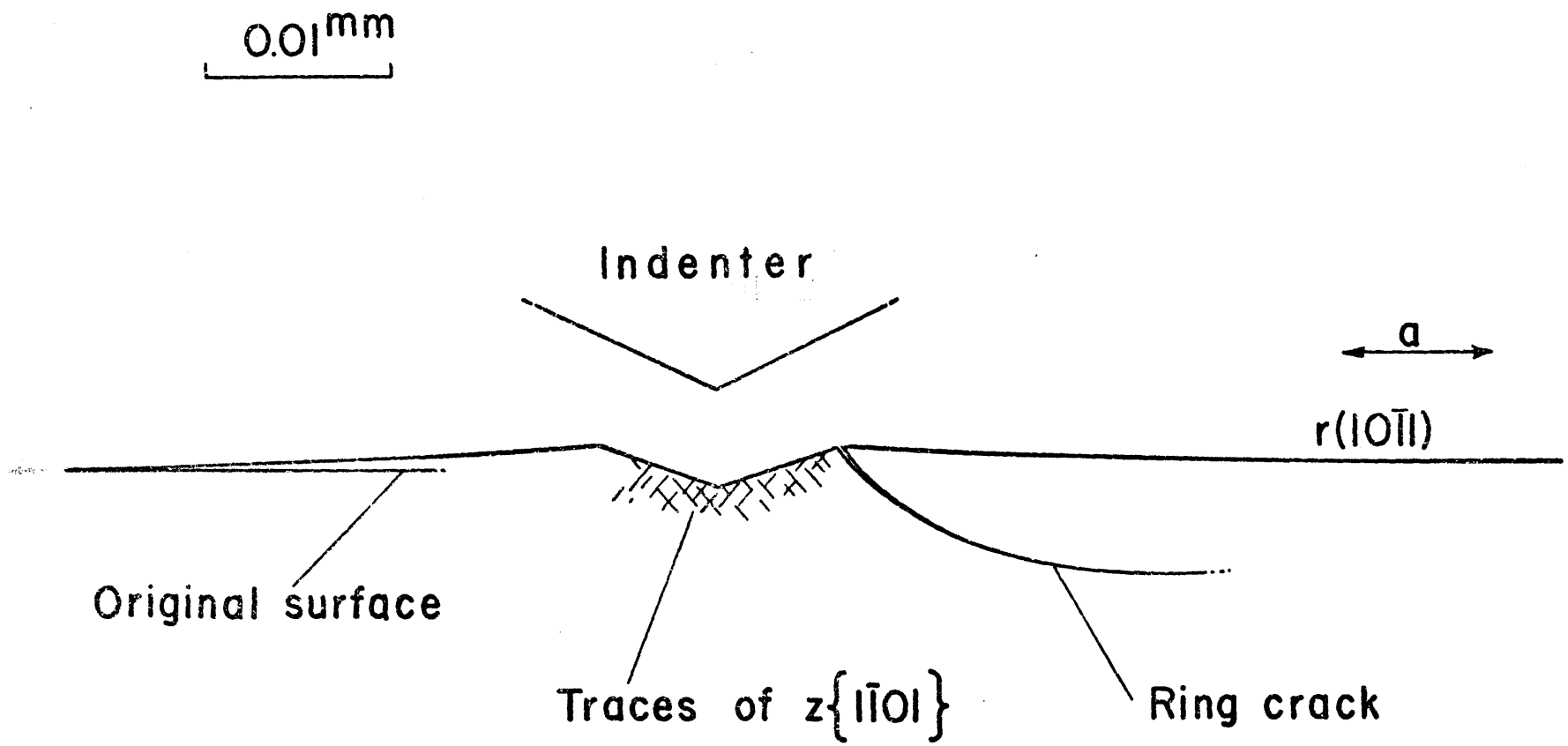
0.01 mm
Indenter
a
r(10$\bar{1}$1)
Original surface
Traces of z{1$\bar{1}$01}
Ring crack

Figure 3d. An Idealized Knoop Indent for Quartz.

The birefringent zone is an upwarped area which may be observed optically. The indentation departs from the ideal shape, the ratio of the long axis to the short axis being 10:1 instead of the ideal ratio 7:1. The illustration is taken from Brace (1961, 1963).

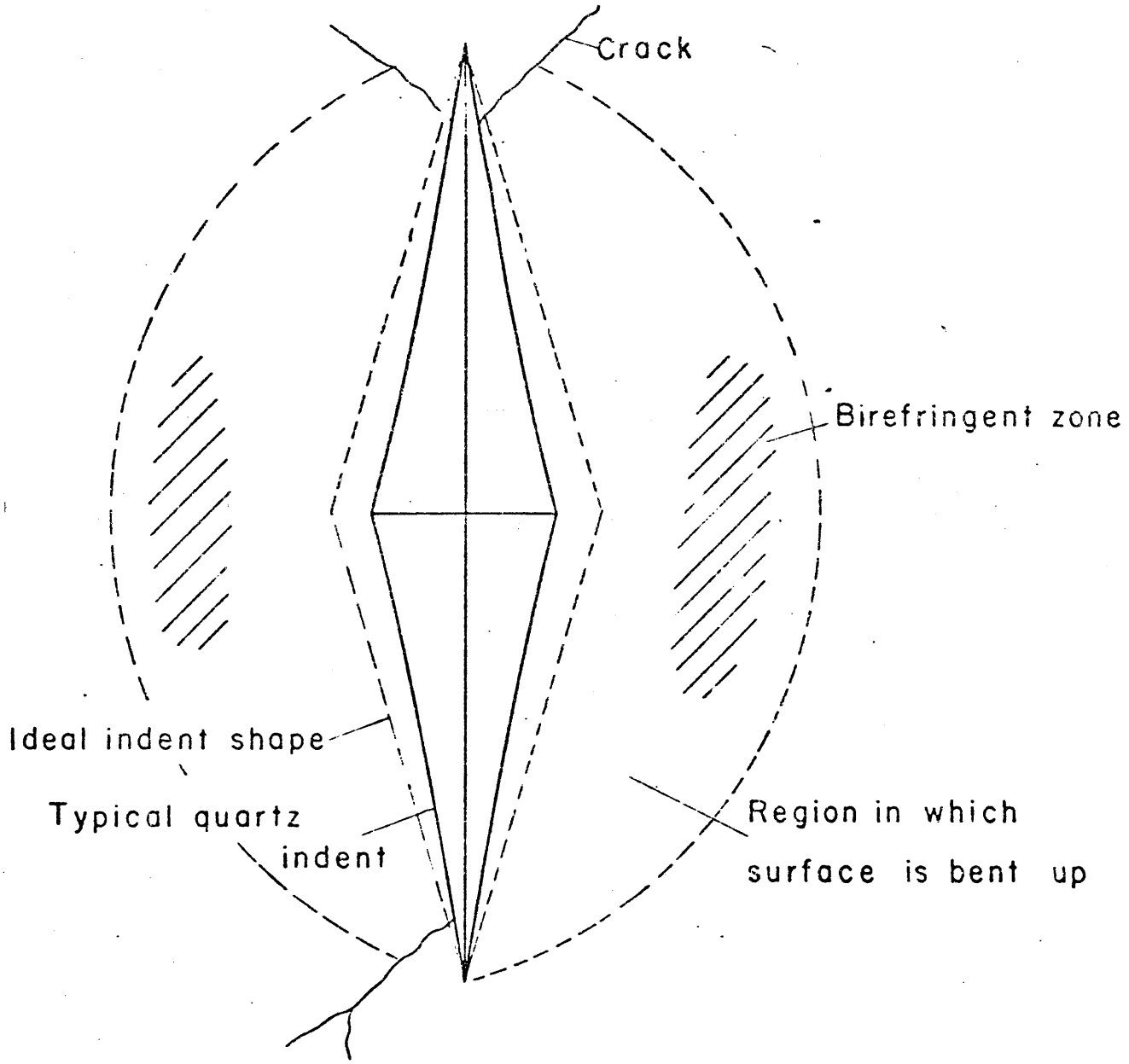
Crack
Birefringent zone
Ideal indent shape
Typical quartz indent
Region in which surface is bent up

when using the Knoop geometry: the hardness has been found to vary as a function of the crystallographic direction of the long axis of the Knoop brale in the plane of the crystal form being indented. These two types of anisotropy of hardness will be called form anisotropy and directional anisotropy respectively. Because of the relative symmetry of the Vicker's brale, Vicker's diamond pyramid (VDP) hardness usually does not show directional anisotropy (Westbrook and Jorgenson, 1968). Form anisotropy, when it exists, is shown by all brale geometries (Mott, 1956). Form anisotropy and its relationship to minerals is discussed first, followed by a presentation of directional anisotropy theories.

The form anisotropy of hardness of nonmetallic compounds was initially attributed to intrinsic mechanical differences. (See Table 4 for the form anisotropy of quartz.) However, Westbrook and Jorgenson (1968) have shown that the form anisotropy disappears when absorbed water is removed by heating to approximately 350°C for several hours and the material is subsequently tested in scrupulously anhydrous conditions. Tests have shown that water is the causative agent during testing in laboratory environments and not other common gases in the environment including H_2, N_2, and CO_2. The hardness of crystals from which water has been desorbed is found to approach a common value which is greater than the hardness in the presence of the adsorbed layer. This softening effect may be suppressed by increasing the load during

TABLE 4. FORM ANISOTROPY OF ROOM TEMPERATURE HARDNESS OF QUARTZ

Source	Crystal	Form: Hardness in kg/mm^2 (0001)	{10$\bar{1}$1}	{01$\bar{1}$1}	{10$\bar{1}$0}	Cond.
Westbrook & Jorgenson (1968)	Natural		935	1020	870	VDP 50g
	Desorbed natural		1240	1245	1140	VDP 50g
Winchell (1945)			653-748	674-748	834-902	KHN 100g
Taylor (1949)		1103			1260	VDP 50g
Brace (1961)	Natural		1000-870	950-890	1100-950	KHN 100g
	Synthetic #705		870 40			" "
	#704		795 45			" "
	#690-1		810 60			" "
	#690-2		750 30			" "
	#WE		790 50			" "
	#HQ		790 20			" "
Nadeau (1970)	Natural Brazilian	1100				
	Same crystal annealed	1300				
	Hydrogen doped	850				
Westbrook (1950, 1966)	Synthetic	900	1050			
This study	Herkimer diamond				727-658	KHN 300g
	Herkimer diamond	1220			990-850	" 100g
	U.Q.	1240	(not oriented)		1225	VDP "
	C105	1290				" "
	HBQ275	1170				" "
	HBQ338	1310				" "
	R H Hoffman (syn.)	1280				" "
	HBQ329 (annealed)	1120				" "
	HBQ275 (annealed in P_{H_2O} = 15 kbar)	1100				" "

Notes: (1) VDP signifies Vickers diamond pyramid hardness while KHN signifies the Knoop hardness test.
(2) The crystals used in this study are described in the Experimental Section.

indentation. When the indentor penetration is on the order of 3 μm in InSb the weakening cannot be observed (Hanneman and Westbrook, 1968). Desorbed crystals are observed to weaken in a time period of several days for laboratory humidities or several minutes if immersed in water. In most cases the magnitude of the weakening ($H_{dry}-H_{wet}/H_{dry}$) is about .25 for materials of geologic interest. Etching of the indentations frequently reveals a characteristic pattern of dislocations around the indentation (the dislocation rosette). These rosettes have been used to assess the apparent increase in dislocation mobility with the adsorbed layer present (Hanneman and Westbrook, 1968). Three mechanisms are presented as being likely to be responsible for the weakening effect:

(1) Adsorbate-point defect dislocation interactions.

(2) Adsorbate alteration of surface bond strengths.

(3) Release of friction between the brale and the test material.

No new evidence is presented in this study which bears on the selection of one of these mechanisms, but the information gained about the relative adsorption of water to the crystal surfaces of quartz appears to mesh with information obtained in synthetic quartz impurity studies. However, it should be noted that the surface water weakening persists to temperatures as low as -70°C so that strongly thermally activated processes are unlikely (Westbrook and Jorgensen, 1965).

Directional anisotropy was discovered during the original development of the Knoop hardness test (Knoop et al.,

1939; Winchell, 1945; Thibault and Nyquist, 1947). Several attempts to understand the nature of the anisotropy have been made (Daniels and Dunn, 1949; Feng and Elbaum, 1958; Garfinkle and Garlick, 1968; Brooks et al., 1971). Brookes et al. (1971) were able to explain the form of the hardness anisotropy curve for calcium fluoride, aluminum oxide, lithium fluoride and magnesium oxide using a modification of the earlier theories. Subsequently anisotropy of hardness in niobium carbide (Morgan and Lewis, 1974) and titanium carbide (Hannink et al., 1972) were explained using the Brookes et al. (1971) theory. In brief, Knoop hardness anisotropy results from the activation of preferred slip systems which allow the accommodation of strain elements required by the geometry of the brale. Thus a crystal would appear to be least hard when the indentor orientation was such that it resulted in the greatest resolved shear stress on the preferred slip system and that it also allowed rotation of the crystal during plastic deformation such as to displace material to the crystal surface. This is to say, if the axis of rotation of the primary slip system is codirectional with the zone of an indentor facet and the surface being indented, the slip system will be preferentially activated. [Although VDP hardness tests sometimes show phenomena called barrelling and pincushioning (see Figure 4; and Tabor, 1966), one cause of which may be directional anisotropy of flow, the effect is not large enough to cause the magnitude of the VDP hardness

Figure 4. Barreling and Pincushion Shapes.

Vicker's diamond pyramid indentations may depart from the shape of the brale by exhibiting barreling (A) or pincushioning (B). The concavity or convexity of the indentation sides is thought to result either from work hardening constraints or anisotropy of yield stress (Tabor, 1970). An additional factor may be large changes in the elastic modules as a function of direction. Brace (1961, 1963) has observed that indentations in quartz are typically pincushioned shape (B) although the reason or combination of reasons for this shape is unknown. The amount of pincushioning has been greatly exaggerated for purpose of illustration.

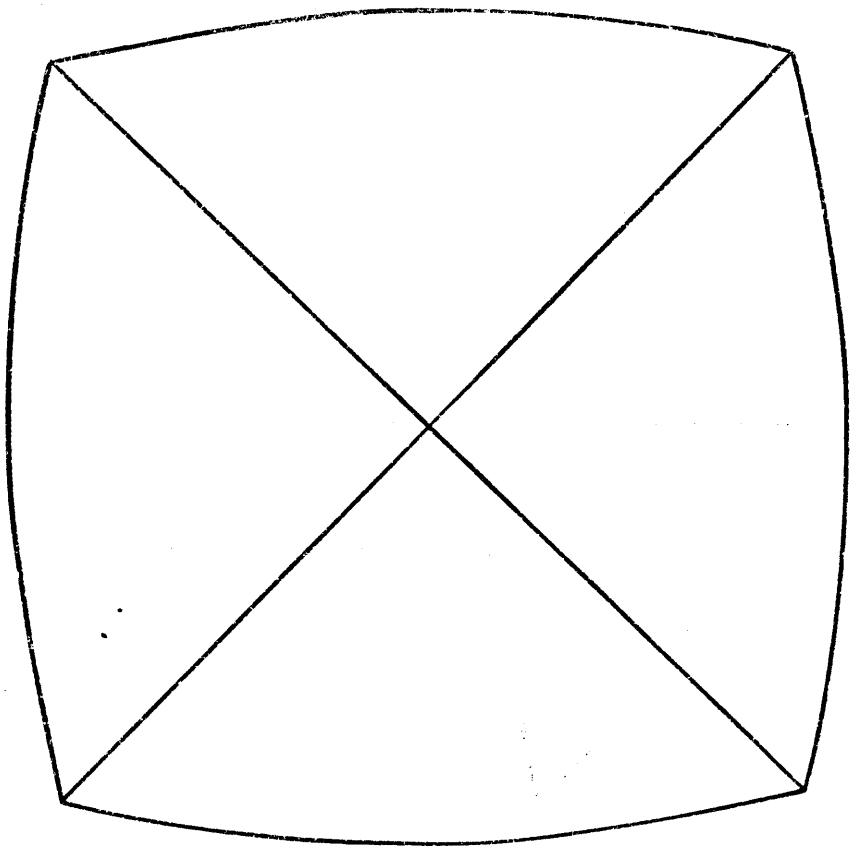

(A)

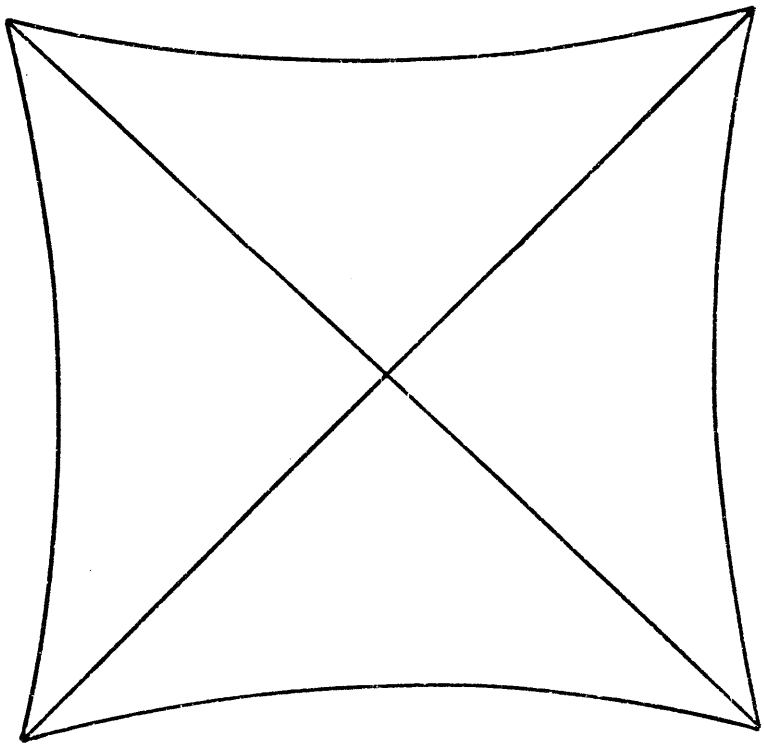

(B)

Figure 5. Directional Anisotropy Factor (τ) for a Knoop Indentation on the {1011} Face of Quartz.

Shown are the directional anisotropy factors (τ) calculated using the theory of Brook et al. (1971) for the (0001)<11$\bar{2}$0>, (11$\bar{2}$0)<0001> and the {1$\bar{1}$00}<11$\bar{2}$0> slip systems in quartz. The angle (θ) measures the angle between the long axis of the indentation and the <11$\bar{2}$0> direction. Since τ is proportional to the mean of the critical resolved shear stresses developed by the four facets of the indentor, large τ implies lessening hardness.

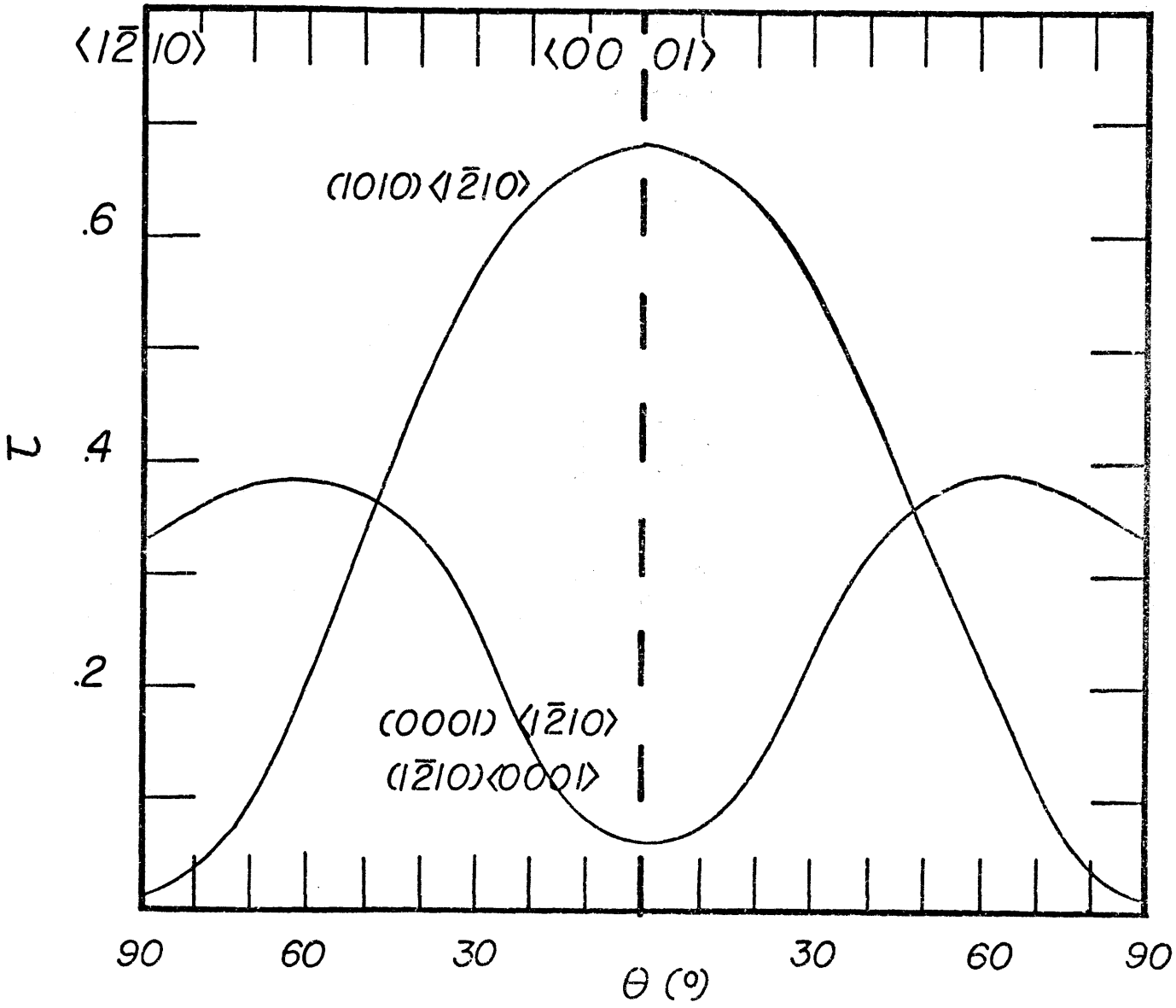
⟨12̄10⟩
⟨0001⟩
(1010)⟨12̄10⟩
(0001)⟨12̄10⟩
(12̄10)⟨0001⟩
.6
.4
.2
I
90
60
30
30
60
90
θ (°)

to be a function of direction in quartz.] For each slip system on a given facet, one may write an equation of the form:

$$\tau = \cos \lambda \cos \phi \frac{1}{2}(\cos \psi + \sin \gamma)$$

The angles are as follows:

λ is the angle between the stress axis (line of steepest descent on the facet) and the slip direction.

ψ is the angle between the rotation axis of the slip system and the zone of the facet and the test surface.

γ is the angle between the zone of the facet and the test surface and the slip direction.

ϕ is the angle between the stress axis and the normal to the slip plane.

τ is proportional to the resolved shear stress on the slip plane generated by the particular indentor facet. The mean of the values of τ for the primary slip system for the four facets gives an indication of the relative magnitude of the hardness. Thus those orientations of the brale which generate the largest mean of resolved shear stresses on the primary system will be the weakest. Figure 5 shows the directional anisotropy factor (τ) vs. or orientation curve for indentation on the $(1\bar{1}00)$ plane of quartz for the slip systems $(0001)\langle 1\bar{2}10\rangle$ $\{1\bar{2}10\}\langle 0001\rangle$ and $\{1\bar{1}00\}\langle 1\bar{2}10\rangle$ as computed by the expression given above (Brookes et al., 1971). By matching the form of the τ versus orientation curves for possible slip systems to that

observed experimentally, one can potentially identify the primary slip system. Thus Knoop hardness can be used as a quick method to identify slip systems in minerals for which they are not known.

Previous Hot Hardness Studies

The temperature dependence of hardness of quartz has been examined by several authors (Fig. 6): Westbrook (1958, 1966) used a VDP brale on the basal and prism planes of synthetic crystals up to approximately 900°C. Brace (1961) used both VDP and Knoop geometries in the temperature range 23° 800°C, on rhombohedral planes of natural single crystals and the Knoop geometry on a quartzite where the indentation spanned many grains. Nadeau (1970) determined the VDP hardness of a natural Brazilian crystal as received and after being doped electrolytically with lithium and hydrogen impurities up to temperatures of about 900°C.

Some interesting comparisons and conclusions may be made by considering the aggregated data. Firstly, Westbrook (1958) suggested that the break in the trend of his data near the α-β transition point (573°C) was caused by the difference in deformation characteristics of those two phases. However, the data of Brace (1961) and Nadeau (1970) do not show this effect even though Nadeau exercised special care to observe the discontinuity. Secondly, the effect of impurities may be qualitatively assessed from the hardness-temperature curve.

Figure 6. Hardness versus Temperature for Quartz.

Shown are the collected hardness data from Nadeau (N, 1970), Westbrook (W, 1958, 1966), Brace (B, 1961) and this study (see Appendix B and the Results section). The small scale bar near the ordinate axis shows the probable magnitude of error for the points from this study. The heavier line is an attempt to indicate the trend of the aggregated data.

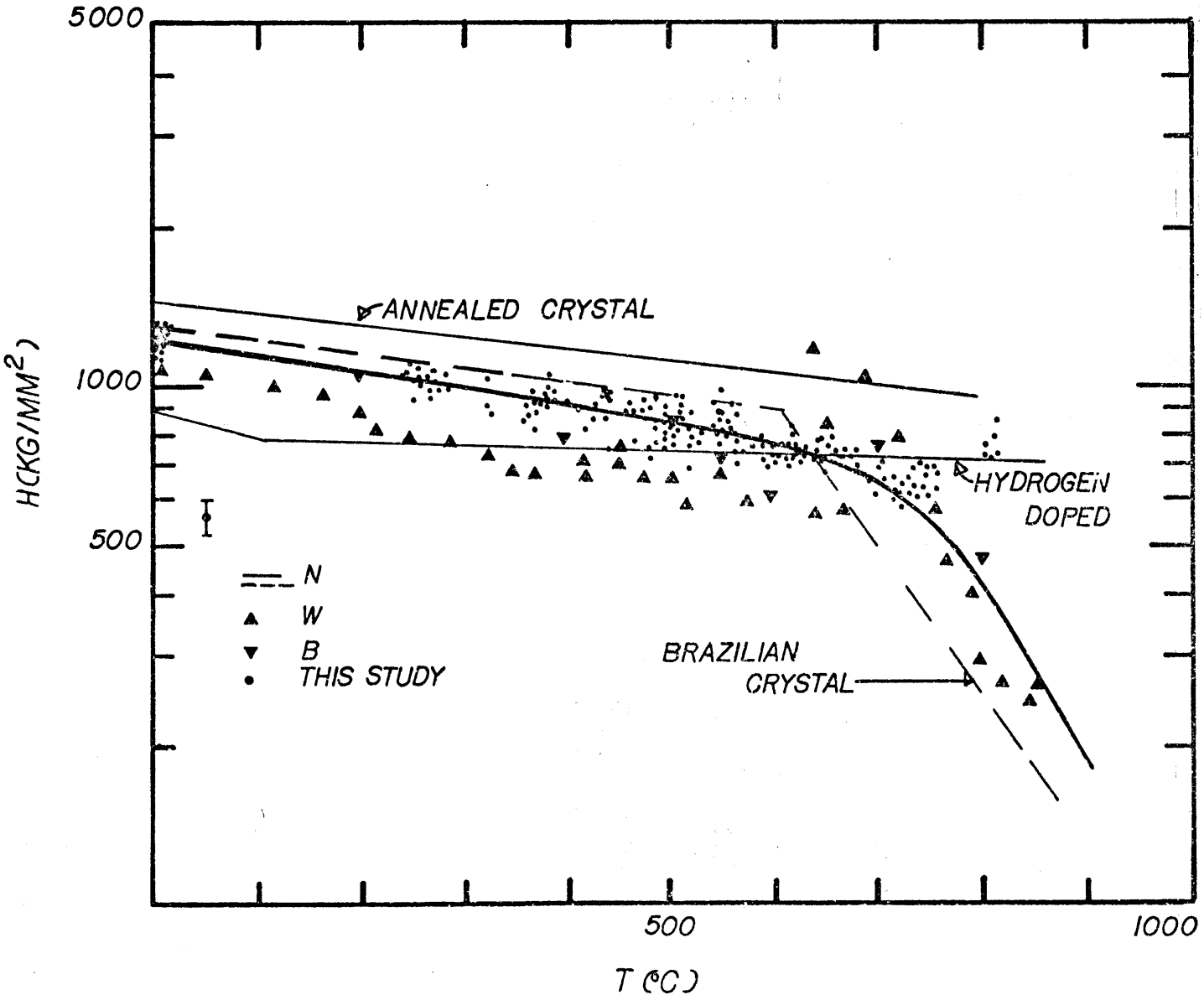
5000
1000
500
H(KG/MM²)
ANNEALED CRYSTAL
HYDROGEN
DOPED
N
W
B
THIS STUDY
BRAZILIAN
CRYSTAL
500
1000
T (°C)

Brace indented a natural hydrothermal crystal from Herkimer County, New York while Westbrook indented synthetic crystals. The impurity content of neither is known, but as will be discussed in some length in a following section, the synthetic crystal might be expected to contain much larger amount of hydrogen impurity. Yet, the hardness of Westbrook's crystals was only slightly less than the Herkimer diamond hardness from Brace. The natural Brazilian crystal tested in the "as-received" condition by Nadeau (1970) was comparable in hardness to Herkimer diamond at temperatures less than 500°C but was weaker at higher temperatures. In order to vary the content Nadeau (1970) electrolytically injected alkali and hydrogen ions into the natural crystal after annealing it at 1400°C for 24 hours. Annealing strengthened the crystals while injecting hydrogen appeared to lower the annealed curve by a factor of approximately 30%. Electrolytic injection of lithium caused only slight weakening at temperatures up to 550°C but caused rapid weakening (as compared to the annealed curve) at higher temperatures. Both the impurity state of the natural crystal as received, as well as the doped impurity states were unstable upon heating to 800°C. Additionally, material around the lithium doped crystals was observed to have undergone alteration to a phase which was unstable to laboratory conditions.

A second indication of the importance of the impurity state to the mechanical properties was shown by Brace (1961).

Shown in Figure 7 are the Knoop hardness numbers of different growth regions of a synthetic quartz. Since the impurities are known to exhibit zonal specificity in synthetic quartzes (Cohen and Hodge, 1958), Brace subsequently irradiated the crystal to develop the color centers due to aluminum impurities and measured the darkening of the growth zones (Cohen, 1960; see also the following impurity discussion). There was a general correlation between darkening after irradiation and the hardness: those growth zones which darkened most were weakest.

Thus hardness studies have shown that alkali impurities as well as hydrogen impurities can affect the mechanical strength of quartz. One aim of this study is to further investigate the relationship of mechanical properties and impurity states which can be expected to occur in natural geologic settings. In the following section, I review previous studies of the impurity state of quartz in some detail in order to point out some differences between natural quartz and synthetically grown quartz, and to outline the natural impurity states which have been investigated thus far.

The Impurity Content of Quartz

The primary impurity elements in quartz are (in no particular order) Li, Na, Al, H, Ti, Fe, Mg, Ge, K, Co, Ca, Ag and sometimes B and Mn (Frondel, 1962; Cohen and Hodge, 1958). A great deal of interest has centered around the role of

Figure 7. Hardness versus Impurity Content of a Synthetic Crystal (after Brace, 1961).

Indentation hardness tests were made in different growth zones of a synthetic crystal slab. After hardness testing the crystal was irradiated to develop the color centers of the quartz (see dicussion of impurities). There is a rough correlation of impurity content with decreasing strength (after Brace, 1961, 1963).

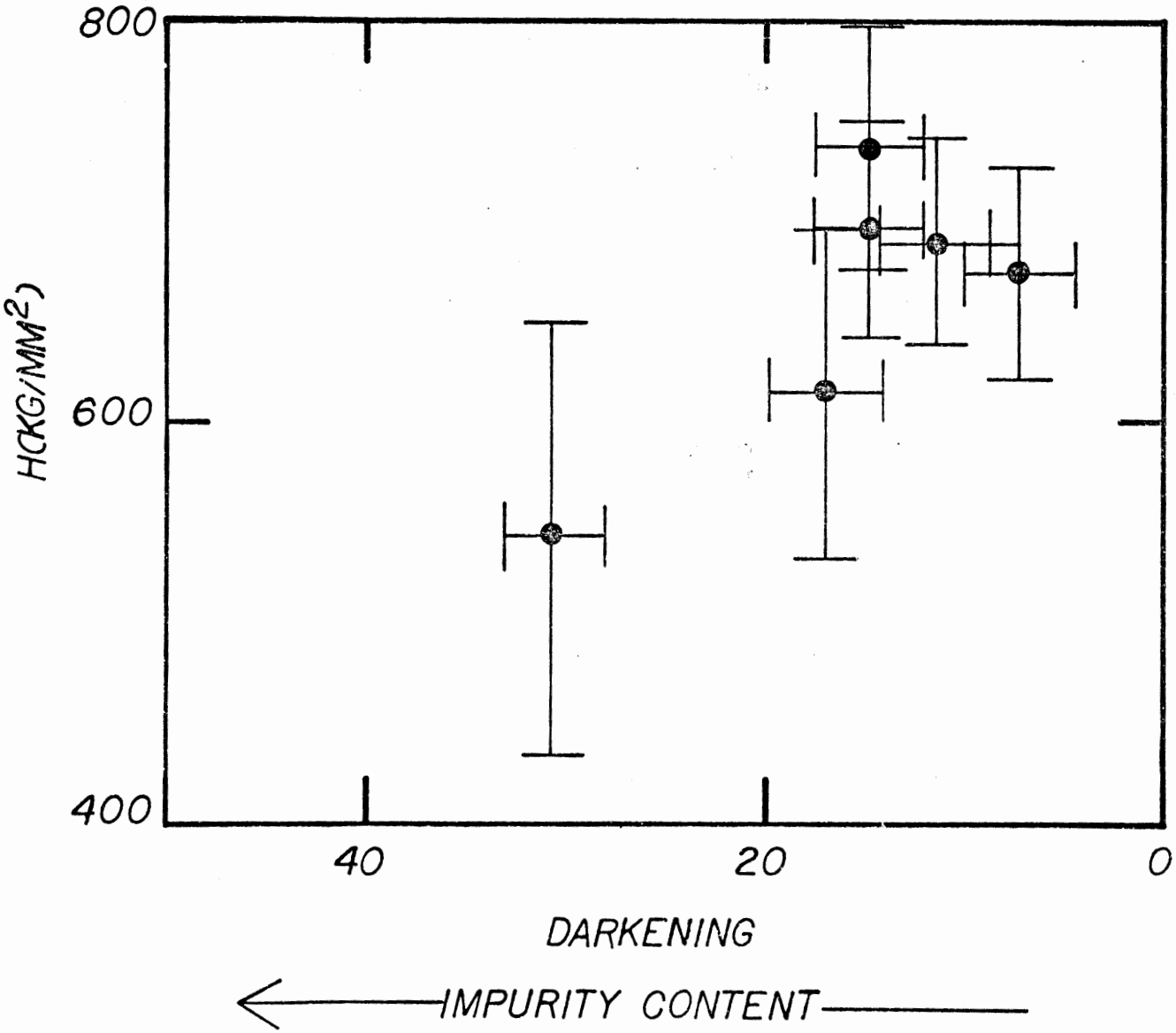
800
600
400
HCKG/MM2)
40
20
0
DARKENING
IMPURITY CONTENT

impurities in the production of color centers in quartz and its colored varieties amethyst, citrine, and smokey quartz (Cohen, 1954, 1956, 1959, 1960; Dennen, 1970; Dennen and Puckett, 1972; Lehmann, 1969; and other more recent authors). Hydroxyl was identified as an impurity in quartz which could give rise to infrared absorption bands by Kats (1961, 1962) and Brunner et al. (1961). The impurities may be incorporated into the quartz lattice as substitutional ions for Si in the case of Al, Fe and Ge and possibly Ti and as interstitial ions in the case of all the above mentioned ions. Hydroxyl ions may be associated as charge compensating ions to a substitutional ion, e.g. an alkali or hydrogen ion compensating a trivalent aluminum which, in turn, is substituting for quadrivalent Si. Hydroxyl ions or water may also occupy a site in the channels of the quartz structure, and in this case, need not be associated with a trivalent substitutional ion. Interstitial ions of this sort may be the charge carriers during electrolytic ionic current flow through quartz (Verhoogen, 1952). A third possibility in the case of water (rather than OH^- ions) is the occlusion during growth to form ordered water (Kats, 1962; Dodd and Fraser, 1965) called gel hydroxyl by Kekulawala et al. (1978). This colloidal water is thought to cause such severe disturbance to the lattice that the mobility of ions under electrolysis is reduced (Dodd and Fraser, 1965).

The earliest studies investigating hydrogen in α-quartz

Figure 8. Comparison Impurity Content of Natural and Synthetic Quartz.

In natural quartz the sum of the atom concentrations of the alkalai impurities including hydroxyl is often observed to equal the atom concentration of aluminum (natural quartz data from Bambauer, 1961). Quartz with large concentrations of water (e.g. HBQ338 of this study) are observed to be weakly biaxial and are termed "lamellar quartz" by Bambauer (1961). Shown for comparison are impurity contents for several synthetic quartzes as given by Chakraborty and Lehmann (1976), for which the correlation clearly does not hold.

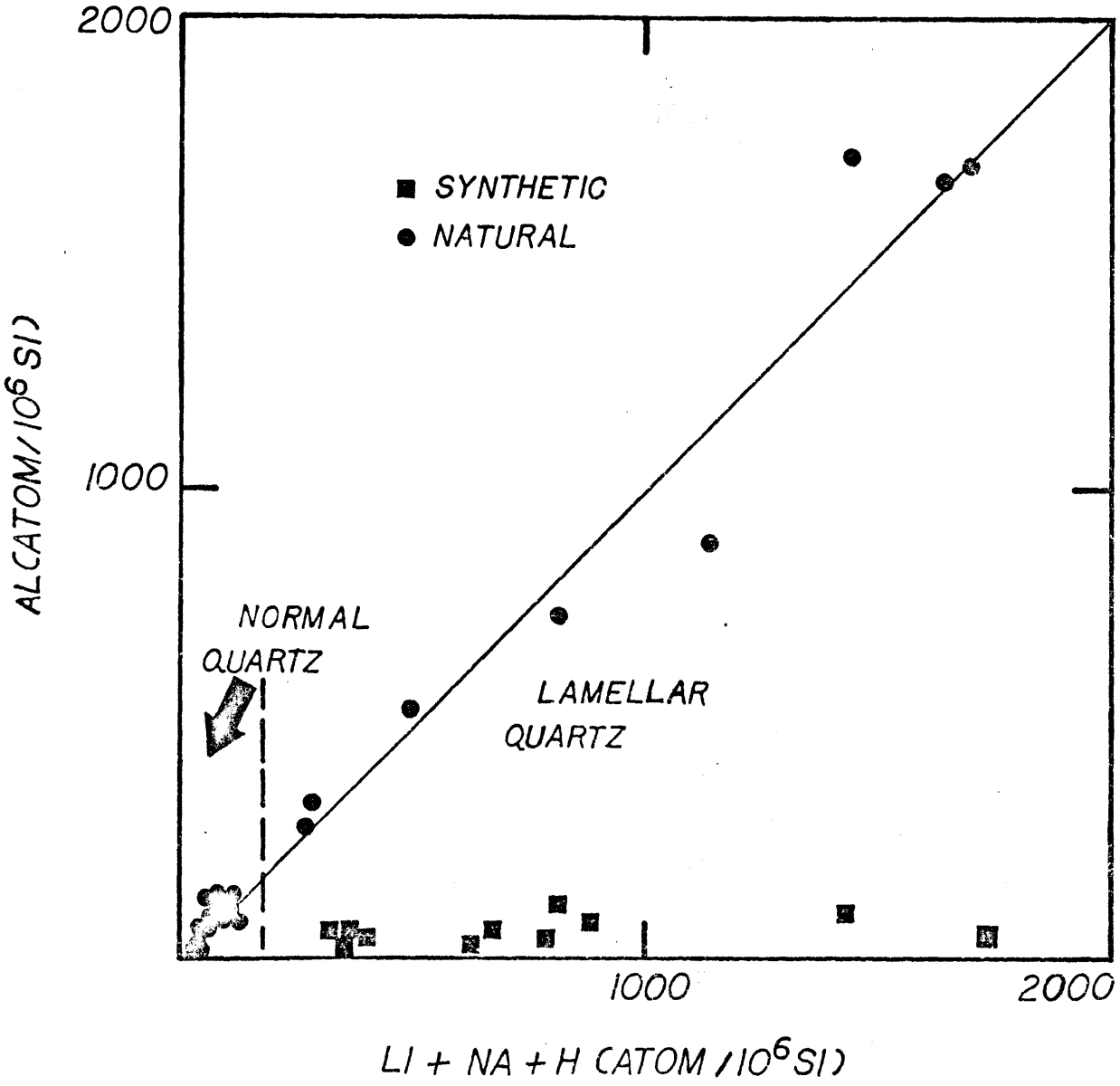
2000
1000
1000
2000
■ SYNTHETIC
● NATURAL
NORMAL
QUARTZ
LAMELLAR
QUARTZ
AL CATOM/10⁶ SI)
LI + NA + H CATOM/10⁶ SI)

were done on large crystals naturally grown in hydrothermal environments (Kats and Haven, 1960; Kats, 1961; Brunner et al., 1961; Bambauer, 1961; Bambauer et al., 1962). Studies by Brunner et al. (1961), Kats and Haven (1960), and Kats (1961) showed that sharp absorption bands in the 3 μm wavelength region of the IR spectrum were due to hydrogen impurity. Shifts in the bands due to deuteration of the crystal confirmed this hypothesis. Bambauer (1961) showed that the concentration of hydroxyl impurity could be associated with other impurities such that the sum of the concentration of the monovalent impurities roughly equalled the concentration of the aluminum impurity (Fig. 8). Furthermore, the concentration of hydroxyl as detected by infrared absorption could be correlated to regional differences in metamorphism. Dennen et al. (1970) extended this idea using the thermodynamics of ideal dilute solutions, showing that for quartz growing in hydrothermal environments with aluminum present in sufficient quantity to saturate the quartz, the aluminum content was a function of temperature (Fig. 9). They presented arguments that this geothermometer should be relatively insensitive to pressure. Some investigations of natural samples from other than hydrothermal environments exist (Dennen, 1964; Bershov et al., 1975) but they do not include hydroxyl contents as well as other impurity concentrations. Bershov et al. (1975) used an electron spin precession resonance technique and also detected increasing aluminum content with

Figure 9. Aluminum Geothermometer (after Dennen et al., 1970).

Measured relation of temperature and aluminum solubility for natural and synthetic quartz crystals grown in aluminum saturated environment (Dennen et al., 1970). Aluminum concentrations were measured by atomic absorption spectroscopy, while the temperature of growth was determined from geologic mineral assemblages, inclusion thermometry, and biotite geothermometers or direct measurement in the case of the synthetic crystals.

The natural samples came from contact metamorphosed and gneissic rocks as well as vein quartzes (Dennen, 1970).

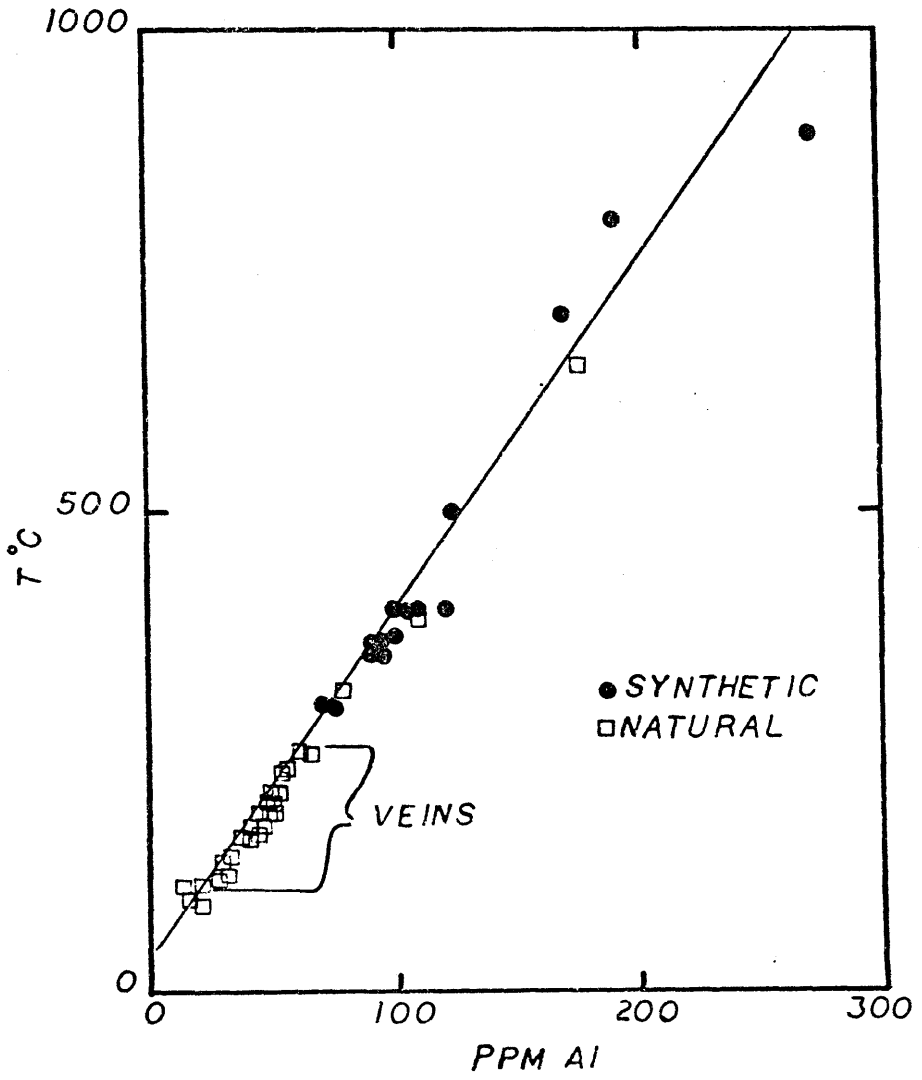
1000
500
0
T°C
0
100
200
300
PPM Al
SYNTHETIC
NATURAL
VEINS

increasing metamorphic grade. However, the impurity levels implied temperatures which were untenable using Dennen's geothermometer.

The detailed structure of the defects of the associated alkali-aluminum impurities, called Al-H, Al-Na,... defects is the subject of continuing research (Kats, 1961; Dodd and Fraser, 1965; Staats and Kopp, 1974; Chakraborty and Lehmann, 1976). Suggestions for the site of the hydrogen ion range from substitutional for O=, to the hydrolysis of the Si-O-Si bond, to more complicated structures involving several ions (Figure 10). Figure 10 is probably not comprehensive, and is only intended to indicate the range of suggestions tendered. Furthemore, no evaluation of the relative merits of any of the models will be given. Clearly further work in this area is needed to delineate the specific structure of the impurity centers in natural quartz.

The defect structure and content of synthetic quartz is strikingly different from that of natural quartz (Dodd and Fraser, 1965; Chakraborty and Lehmann, 1976). Kirby (1975) has reviewed the impurity structure of synthetic quartz and only a brief summary will be given here. Synthetic crystals grown in nutrient solutions relatively free of aluminum, no longer exhibit the Al-alkali correspondence discovered by Bambauer (1961; see Fig. 8). Chernov and Khadzi (1968) have observed trapping of inclusions of colloidal water on the surface of quartz crystals grown above a critical rate. The

Figure 10. List of Some of the Proposed Defect Structures for Quartz.

Some of the proposed defect structures, not including so-called gel or colloidal hydroxyl impurities, are shown in this figure in schematic form to indicate the latitude of the models currently discussed in the literature. Clearly, the exact configuration of the "structural" hydroxyl impurity is not known and probably includes several of the structures shown. (Me stands for a univalent metal ion).

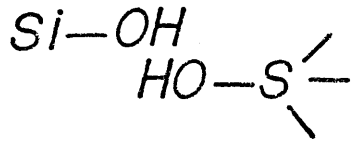

Brunner et al. (1961) and others

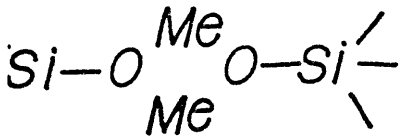

Brunner et al. (1961)

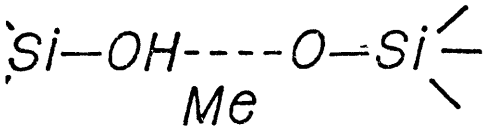

Brunner et al. (1961)

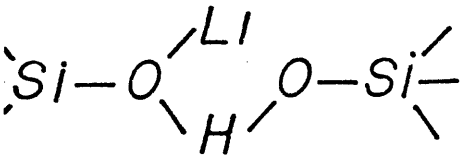

Haven and Kats (1962) and others

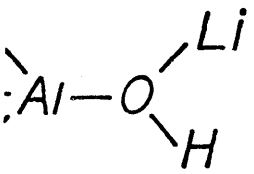

Haven and Kats (1962)

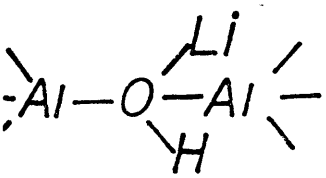

Haven and Kats (1962)

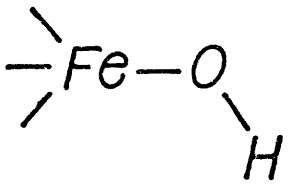

Chakraborty and Lehmann (1972)

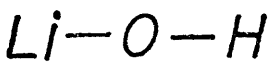

Chakraborty and Lehmann (1972)

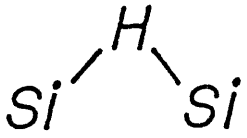

Chakraborty and Lehmann (1976)

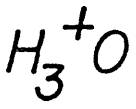

(on Silicon Site) Chakraborty and Lehmann (1976)

Hydrogen in Tunnel Sites Staats anb Kopf (1974)

critical velocity of growth (V_c) is proportional to an Arhennius term

$$V_c \alpha \exp -\frac{U}{RT} \qquad \text{(Eq. 3)}$$

where U is some activation energy for growth.

The threshold rate, V_c, depends also on the crystal form. The order of threshold velocities from least to greatest follows.

$$(0001) < (\bar{1}\bar{1}20) < (\bar{1}\bar{1}22) < (1\bar{1}01) < (10\bar{1}1) < (11\bar{2}0)$$

The sectoral zonation of impurities can thus be explained by an increased number of impurities adsorbed on the face of a growing crystal zone. There seems to be no particuar pressure dependence of the amount of colloidal inclusions (Chernov and Khadzi, 1968; Helgeson, 1967; also see Lias et al., 1973); however, the concentration of alkali ion appears to be larger in the inclusion than in the growth solution. The infrared spectra of synthetic quartz grown above the critical velocity no longer shows the sharp absorption peaks of natural quartz but instead shows a broad band of absorption (Kats, 1962; see also the following section). This suggests that the water impurity is not structurally bound to a specific site. Walrafen and Luongo (1975) have conducted a Raman and infrared investigation in which they suggest that the hydroxyl in hydrothermal quartz is present as H_2O and not the Si-O-H groups proposed by some earlier studies.

Experimental Methods

Characterization of the Samples

The samples used in this study included some crystals which had been carefully characterized in previous studies by several different methods and some crystals which were relatively poorly characterized. A description of the samples, their genesis where known, and their chemical analyses when known are given in Table 5. The impurity contents of three of the samples were reported by Bambauer (1961) and redetermined by Dennen (private communication). A description of the procedures used in the atomic absorption analysis is given by Dennen (1964). Although particular care was used to analyze only fragments which contained no inclusions, some inclusions which were below the size optically detectable may have been present. The accuracy and precision of the determinations is not high owing to the diluteness of the concentrations involved; Dennen (1964) suggests that by replication one may achieve 30-40% variation of the mean of the analyzed quantity. For the purposes of this study, these analyses are certainly sufficient to give a qualitative indication of the impurities present.

Measuring the hydrogen content of minerals has proven to be a difficult task and wide discrepancies often exist when hydrogen contents are measured using different methods. The several methods used include (a) infrared spectroscopy (Brunner et al., 1961; Kats, 1962), (b) ion beam spectroscopy,

TABLE 5: CHARACTERIZATION OF QUARTZ SAMPLES USED IN THIS STUDY

The chemical analysis of some samples was not available at this time, but, when available, the impurity concentration is given in atoms of impurity / 10^6 atoms of Si. Also given are the sources of the crystal, a brief geologic description and the methods of analysis.

137

TABLE 5. CHARACTERIZATION OF QUARTZ SAMPLES USED IN THIS STUDY (Atoms/10^6 atoms Si)

Sample	Source	Genesis	Al	Li	Ca	Na	Mg	H	Fe	Ti	K	Method	Reference
HBQ275	W.H. Dennen	Single crystal hydrothermal vein quartz	60	20	2.1	<1	2.1	9+	1.5	3.2		Atomic absorption infrared	Bambauer (1961)
HBQ329	" " "		23	17		<2	2.1	13+				" "	" "
HBQ338	" " "	from Swiss Alps	750	424	2.0	8.5		352+				" "	" "
C105	Harvard Mineral Museum	Hydrothermal crystal, Hot Springs, Ark.	9	5		4		26*+		1	2	Infrared atomic absorption chemical	Frondel and Hurlbet (1954)
Herkimer diamond	W.F. Brace	Hydrothermal crystal, New York State	Not analyzed									--	Brace (1961, 1963)
R.H. Hoffman (synthetic)	" " "	Synthetic	Not analyzed									--	--
HBQ275(ET1)	W.H. Dennen	As given above (HBQ275)	Annealed in P_{H_2O} = 1.5 GPa, 800°C for 2 days not analyzed after annealing									--	--
HBQ329(ET1)	" " "	As given above (HBQ329)	Annealed in P_{H_2O} = 1.5 GPa, 800°C for 2 days									--	--
UQ	J. Dickey	Unknown massive quartzite	Not analyzed; many small inclusions									--	--

*Qualitative estimate obtained during this study.
+The published hydrogen content was corrected by a factor of .506 as pointed out by Kirby (1975).

137

called IBSCA (Tsong et al., 1976) and a similar, but lower energy technique called SCANIIR (White et al., 1972), (c) an electrolytic technique (Wilkins and Sabine, 1973) and (d) a classical chemical ignition technique (Godbeer and Wilkins, 1977). Godbeer and Wilkins (1977) analyzed a synthetic crystal X-O which had previously been the subject of infrared (Blacic, 1975; Kirby, 1975) mechanical (Griggs and Blacic, 1965; Heard and Carter, 1968; Blacic, 1975; Balderman, 1974; Kirby, 1975; and McCormick, 1976) and ion beam spectroscopic analysis (Tsong et al., 1976). Using both infrared and chemical ignition tests, Godbeer and Wilkins (1977) showed that the IBSCA determined hydrogen impurity contents were approximately fifty times larger than the values given by the classical chemical ignition studies. The infrared determined impurity contents differed by only 30%. One possible cause of the discrepancy between the two types of analysis is an adsorbed and possibly chemically adsorbed surface layer which resists desorption to fairly high temperatures (see the preceding discussions on form anisotropy of hardness and impurities in quartz). It is also possible that because the infrared method measures only C-H bond density, hydrogen may be present in a form which is not analyzed by infrared techniques.

Several infrared spectra were taken in order to complete the characterization of the analyzed samples in this study (see Figure 11). In particular the published analysis of C105 (Frondel and Hurlbert, 1954) did not include hydrogen

Figure 11. Infrared Spectra of Samples HBQ329, C105, and RHH (Synthetic).

11a. Infrared spectrum of sample HBQ329 taken in a liquid N_2 cryogenic holder. The sharp peaks indicate structurally bound hydroxyl impurity with associated alkali impurities (see Dodd and Fraser, 1965). The broad absorption band at ~320 mm^{-1} is due to background contamination in the cold chamber (see 11d).

11b. Infrared spectrum of sample C105 taken in a liquid N_2 cryogenic holder.

11c. Background contamination as shown by the infrared spectrum of a plate of KBr at liquid N_2 temperatures. KBr is transparent to infrared radiation of these wavelengths.

11d. Room temperature spectrum of RHH (synthetic) quartz taken with the radiation path ⊥ to $(1\bar{2}10)$. This synthetic quartz does not show the broad hydroxyl absorption band typical of many synthetic quartzes of high hydroxyl content (cf. Fig. 2 of Blacic, 1975). Because of pleochroism, the magnitude of hydroxyl content of this sample remains uncertain.

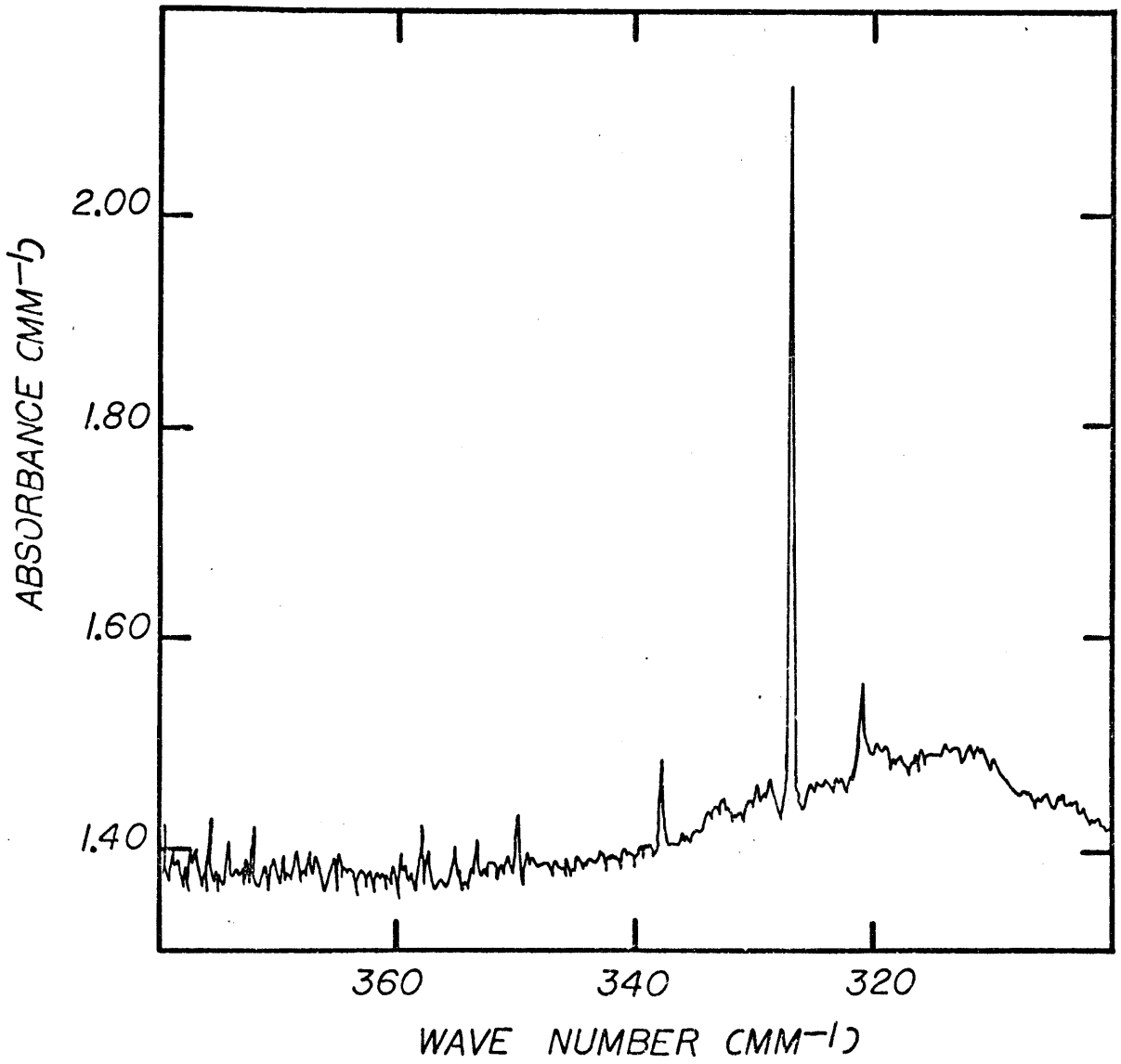

Fig. 11A

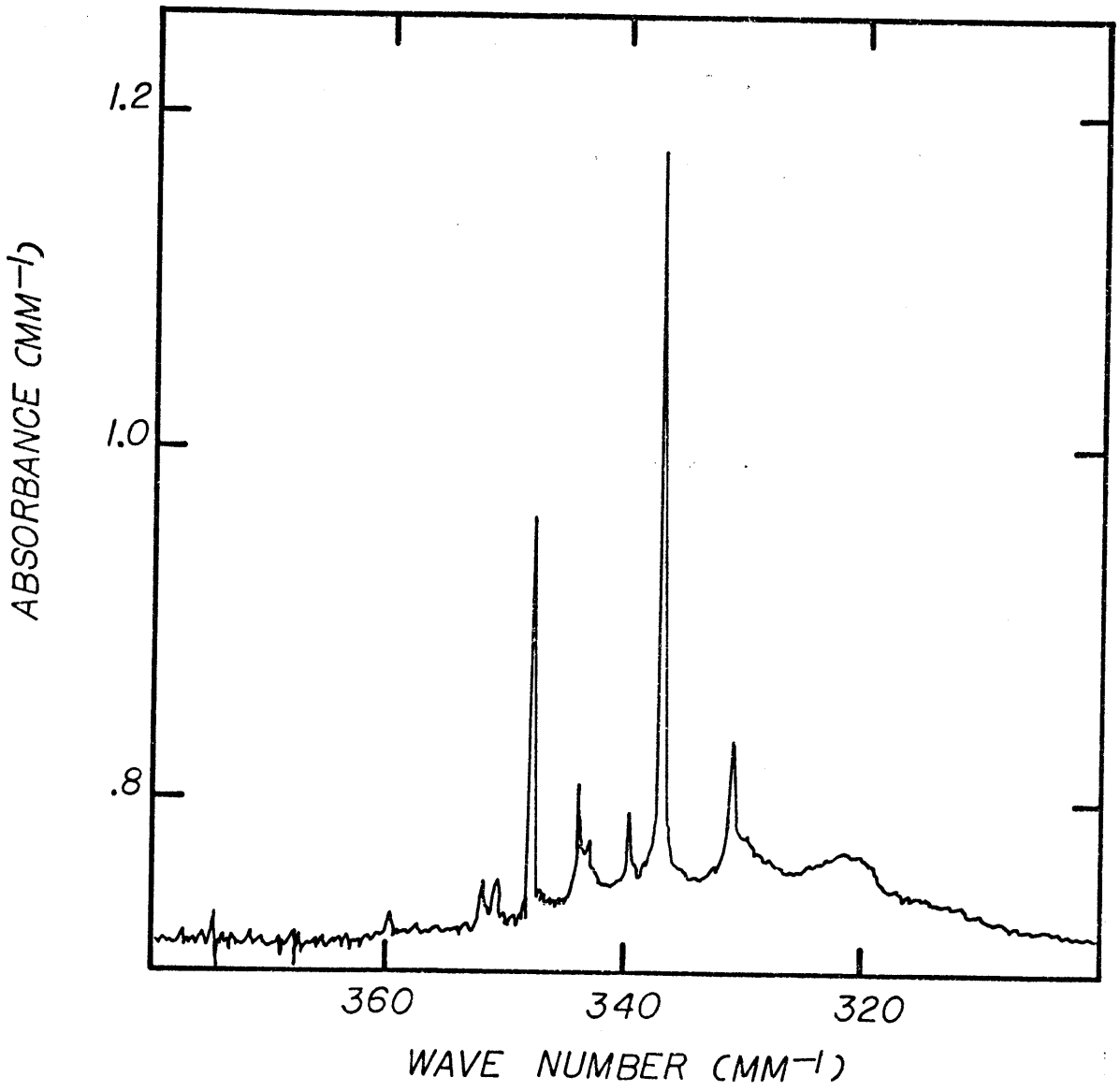

Fig. 11B

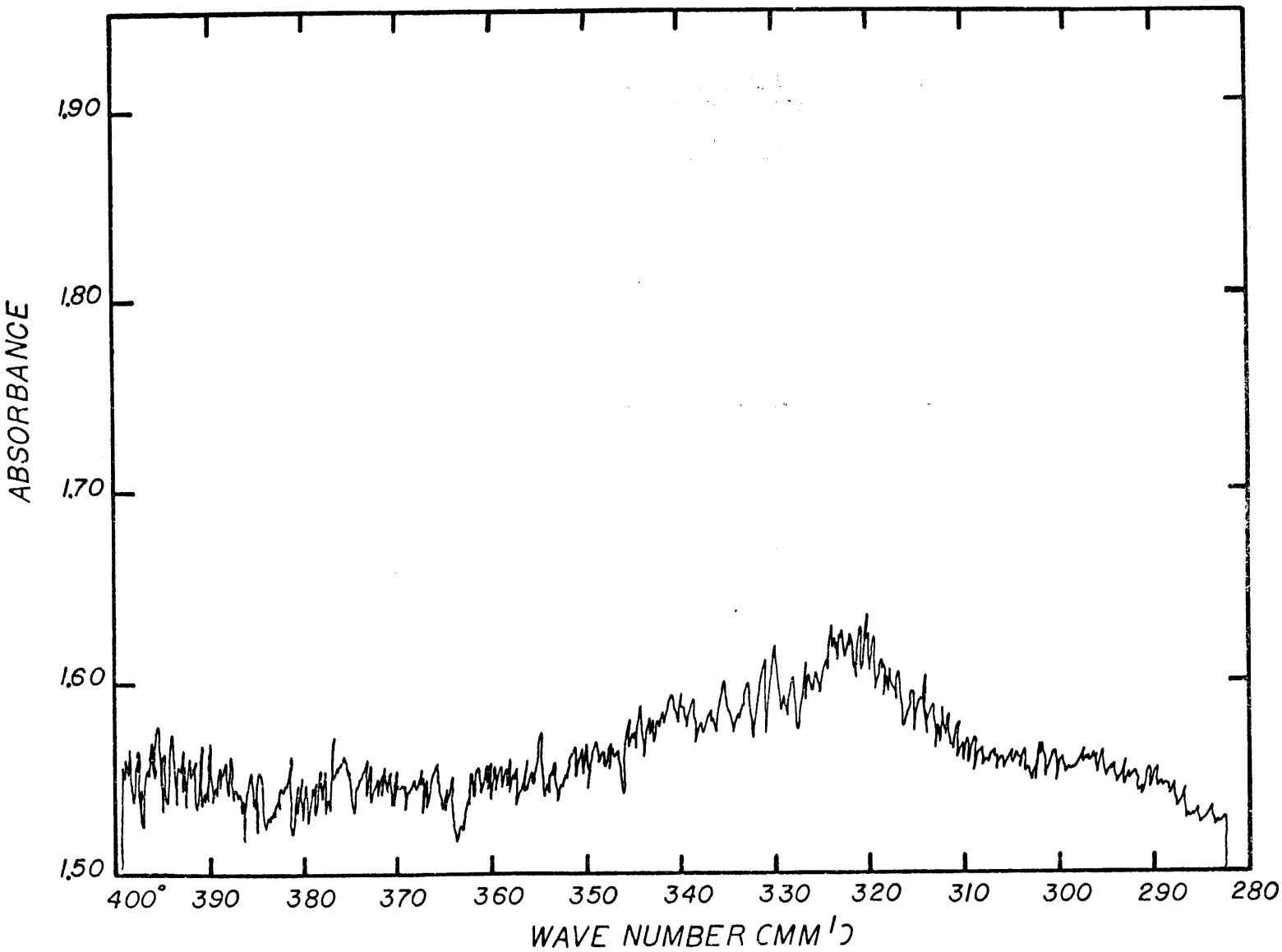
ABSORBANCE
1.90
1.80
1.70
1.60
1.50
400°
390
380
370
360
350
340
330
320
310
300
290
280
WAVE NUMBER CMM⁻¹)

Fig. 11C

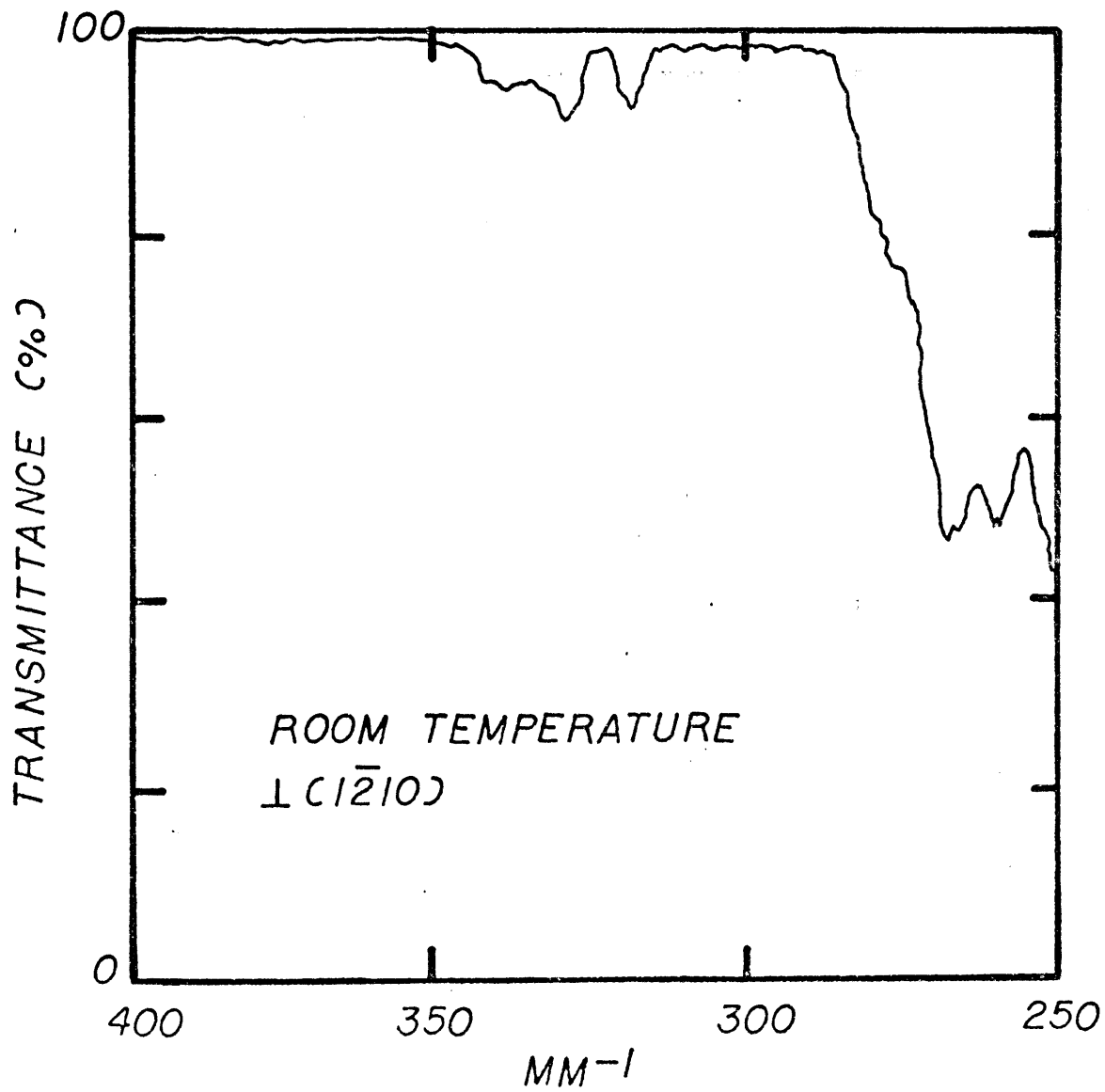
100
0
TRANSMITTANCE (%)
ROOM TEMPERATURE
⊥C(1$\bar{2}$10)
400
350
300
250
MM-1

Fig. 11D

impurity content. The determination of O-H bond content depends on the Lambert-Beer law:

$$c = \frac{\int E d\nu}{\alpha_m t} \qquad \text{(Eq. 4)}$$

where c is the concentration; E is the absorption and is equal to log I_o/I; I_o, the intensity of the reference beam, and I the transmitted beam intensity; α_m, the molar extinction coefficient; t the thickness of the sample, ν is the frequency of the absorption.

Kats (1962) showed that absorption in the bands 347.9, 343.5, 337.1 and 331.1 mm^{-1} were due to O-H stretching vibrations and that these peaks were shifted to lower frequencies by deuterization. In a series of experiments, he was able to electrolytically exchange alkali ions for hydrogen ions and the reverse with the subsequent enhancement or reduction of the bands. The molar absorption coefficient can be calculated by measuring both the current in an electrolytic exchange experiment and the change in the integrated absorption.

As pointed out by Kirby (1975), Bambauer (1961) used an incorrect conversion factor and thus the values reported by Bambauer (1961) are in error by a factor of ~.51. In order to obtain a qualitative estimate of the hydrogen bond content of C105, infrared measurements were made and the following equation was used:

$$C = \frac{22.5 \times 10^3 \int E d\nu}{22.4 \times 10^3}$$

The explanation of the numerical factors is as follows: 22.5×10^3 is the correct conversion factor from $gH/\ell SiO_2$ to atoms $H/10^6$ atoms Si (Kirby, 1975). 22.4×10^3 is the molar extinction coefficient as determined by Brunner et al. (1961). The integrated molar absorbance was calculated using only the peaks at 347.9, 343.5, 337.1, and 331.1 mm^{-1} (Kats, 1962). The spectra were taken on a Digilab 14 Fourier Transform Spectrometer. The resolution was $\pm .4$ mm^{-1}. A standard cryogenic holder was used and the spectra were taken at liquid nitrogen temperatures. The reference beam chamber was purged with dry N_2 and the cryogenic chamber was evacuated. However, it was discovered that the vacuum was not sufficient to exclude all water vapor from the chamber. Included in Fig. 11 is a background spectra obtained on a sample of KBr which is transparent in this region. By measuring only the integral absorbance in the four bands mentioned above, the effect of the background is at least partially negated. However a similar determination of hydrogen bond content for sample HBQ329 differs from the previously determined impurity contents (Bambauer, 1961; and Dennen, private communication) by a factor of two. For the purposes of comparison of hardness in this study, this accuracy is regarded as sufficient, and, in fact, might even result from the zonal variation in impurity content mentioned in the previous section.

Hardness Testing and Sample Preparation

The apparatus used for the hardness testing was described in Chapter 1 and by Mott (1956) and Brace (1961). The specimens were prepared by polishing with grinding powders mixed with water. Nadeau (1970) concluded that within the limits of the scatter of his data there was no difference between the hardness of ground and polished faces of quartz and faces produced by cleavage, etching in HF and chemical polishing in hot KOH. Furthermore, all crystals received very nearly the same preparation. For the comparative tests conducted on quartzes of different impurity contents, surface preparation should have only a very small effect. Throughout the study the loading rate remained constant, ~.8 mm/sec. In order to conduct hardness tests with increased dwell times the loading and unloading cycle could be interrupted to allow the brale and the test surface to be in contact for any desired period. The motion of the brale was measured by a low voltage differential transformer. Thus, the dwell time could be determined to an accuracy of less than 1 sec. At the termination of the test. the brale was then unloaded at the same constant rate. At several times throughout the study, hardness tests were performed on a calibration block of known hardness provided by the Wilson instrument company. All the room temperature tests were made in laboratory humidity; no special effort to desorb the surface water layer was made. However the load use in all tests, 100 grams (weight), for

the VDP tests is probably sufficient to suppress the weakening caused by the surface layer (Westbrook and Jorgensen, 1968). During the Knoop anisotropy tests it was found to be necessary to use a 300 gram load in order to obtain more reproducible results. All the high temperature tests were made in an atmosphere of argon dried by bubbling through magnesium perchlorate. Since the possibility exists that some impurities were removed by annealing during the experiment, several experiments were conducted at constant temperature, to see if hardness was a function of time at temperature. Additionally measurements were made both during heating and cooling cycles. All measurements were done on a reflecting microscope at 500x magnification using a travelling Filar micrometer. Each diagonal was measured five times and thus the average of 10 measurements determined the hardness value. Indents whose diagonals differed by 1.0 μm were excluded.

Results

Room temperature tests

The data for the room temperature hardness tests are presented as averages in Table 4 and Appendix A. The room temperature VDP tests agree well with previously published data. Little form anisotropy is shown by the VDP tests and the values obtained agree with the desorbed values of Westbrook and Jorgensen (1968). Westbrook and Jorgensen (1968) observed that the effect of the adsorbed layer was suppressed by increasing the load and I interpret the agreement with the desorbed values as indicating that the water layer effects have been suppressed by the larger load used here (100 g). Although the 100 g Knoop hardness data also agrees with previously published values, reproducibility was not sufficient for the directional anisotropy studies and therefore a larger load (300 g) was used. It is not known, therefore, if the decrease in hardness when the larger load is used is statistically significant. However, because the depth of the Knoop indentation, approximately .15 of the Vicker's impression, larger relative loads would be needed to suppress surface effects such as surface hardening caused by polishing work hardening or slip band effects (McClintock and Argon, 1966, p. 458), or surface weakening caused by an adsorbed water layer. The room temperature directional anisotropy results are presented in Figure 12.

Figure 12. Knoop Hardness Anisotropy at Room Temperature on a Prism Face of Quartz

θ is the angle between the long indentor axis and <0001>. The room temperature directional anisotropy is a small fraction of the average Knoop hardness, $\frac{\Delta H}{H} = .05$, as compared to .13 for Al_2O_3, (0001); .12 for Ca F_2, .35 for Mg O (001). Since the geometrical factor (τ) predicted by calculations using the Brookes et al. (1971) equation is larger than this for any single slip system (see Figure 5) if the directional anisotropy is controlled by plastic properties, the small variation could be accounted for by flow on two slip systems with roughly equal ease. The form of the curve is consistent with flow on either or both of $(0001)\langle 1\bar{2}10\rangle$ and/or $(\bar{1}2\bar{1}0)\langle 0001\rangle$ in that there is a hardness maximum when $\theta \sim 0°$. The hardness maxima at $\theta = 90°$ are consistent with slip on $(10\bar{1}0)\langle 1\bar{2}10\rangle$. These three slip systems are most frequently mentioned as being the primary low temperature slip systems for quartz (cf. Table 3).

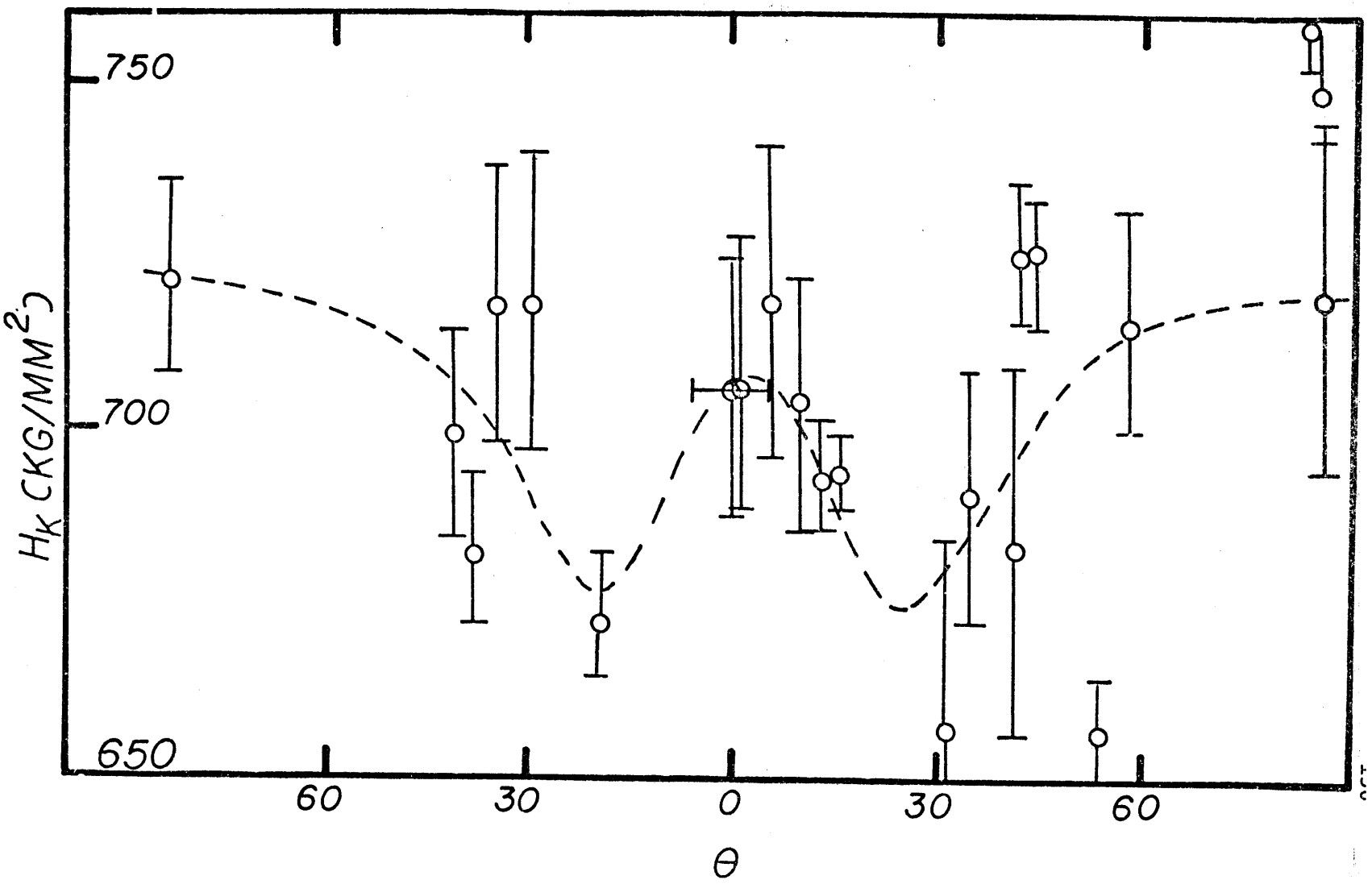
750
700
650
H_K (KG/MM^2)
60
30
0
30
60
θ

Hot hardness data

The hot hardness data for the natural crystals with no heat treatment is tabulated in Appendix B and plotted with the previous hot hardness data in Figure 6. The new data are coherent and show good agreement with previously published data with the exception of Westbrook's 1958 data which is consistently low up to temperatures of ~600°C. No discontinuity was observed at or near the α-β transition temperature (~573°C at 10 MPa). High temperature (>750°C) values for the Herkimer diamond seemed to be higher than either Brace's (1961) data or Westbrook's (1958) curves. This discrepancy may be a manifestation of the hardening with time at temperature which was observed by Nadeau (1970). Therefore several annealing experiments were conducted. In one set, the samples were brought to temperature rapidly (~15°C/min) in the dried argon atmosphere held at a fixed temperature and the hardness measured as a function of annealing time and temperature (Appendix B). A second set of hardness experiments were done on samples that had been annealed for two days at ~850°C and 15 kb confining pressure by Dr. J. Tullis of Brown University in a modified Griggs apparatus (see Tullis and Yund, 1977 for a description of this apparatus). The samples were sealed in a heavy walled platinum capsule with approximately 37 mg of water; however on removal from the apparatus, it was discovered that the samples had lost approximately 33 mg in weight and so the exact partial

pressure of water during the annealing is in some doubt. Finally, one set of hardness data was collected on a sample which had been annealed at 600°C for 3 hours in the dried argon atmosphere. The argon annealed hardness data are discussed below and the hardness of the specimens annealed in the high pressure experiment are plotted in Figure 13.

The relation between yield stress and hardness

The previous chapter discussed the relationship between hardness and yield stress. The constraint factor computed using the methods discussed previously, is presented in Figure 14. At temperatures below the α-β transition, the ratio of Young's modulus to the yield stress is very low, $\sim$20 (see the discussion below), therefore the hardness behavior of quartz is more akin to that of a highly elastic material such as a polymer, as contrasted to that of pure metals which in some cases approach perfectly plastic behavior (cf. Johnson, 1970). The limiting value of H/σ for a cone indenting an elastic material which does not yield plastically is .67 (Sneddon, 1951; Johnson, 1970), if one assumes Poisson's ratio (ν) = .1 and that the "hardness" of an elastically yielding material is defined as the ratio of the load to the actual contact area of the indentor and the specimen. However, in a series of experiments on a range of materials using a VDP brale, Marsh (1964) found that the values of the constraint constant approach 1.1 as more highly plastic materials were indented. 1.1 is the value to be expected

Figure 13. Hardness versus Temperature for Previously Heat Treated Samples.

Samples HBQ329ET1 and H2ET1 were annealed in a sealed platinum capsule containing a few milligrams of water in a modified Griggs apparatus at 825°C for two days under 1.5 GPa confining pressure. Apparently, some water was lost during the experiment and therefore the partial pressure of water is not known, however some water remained in the capsule throughout the experiment. The sample marked "annealed" was HBQ275-127 and had been previously annealed for 2 hours at 600°C in dry argon. The arrows show the path of crystals during the heating and cooling cycle.

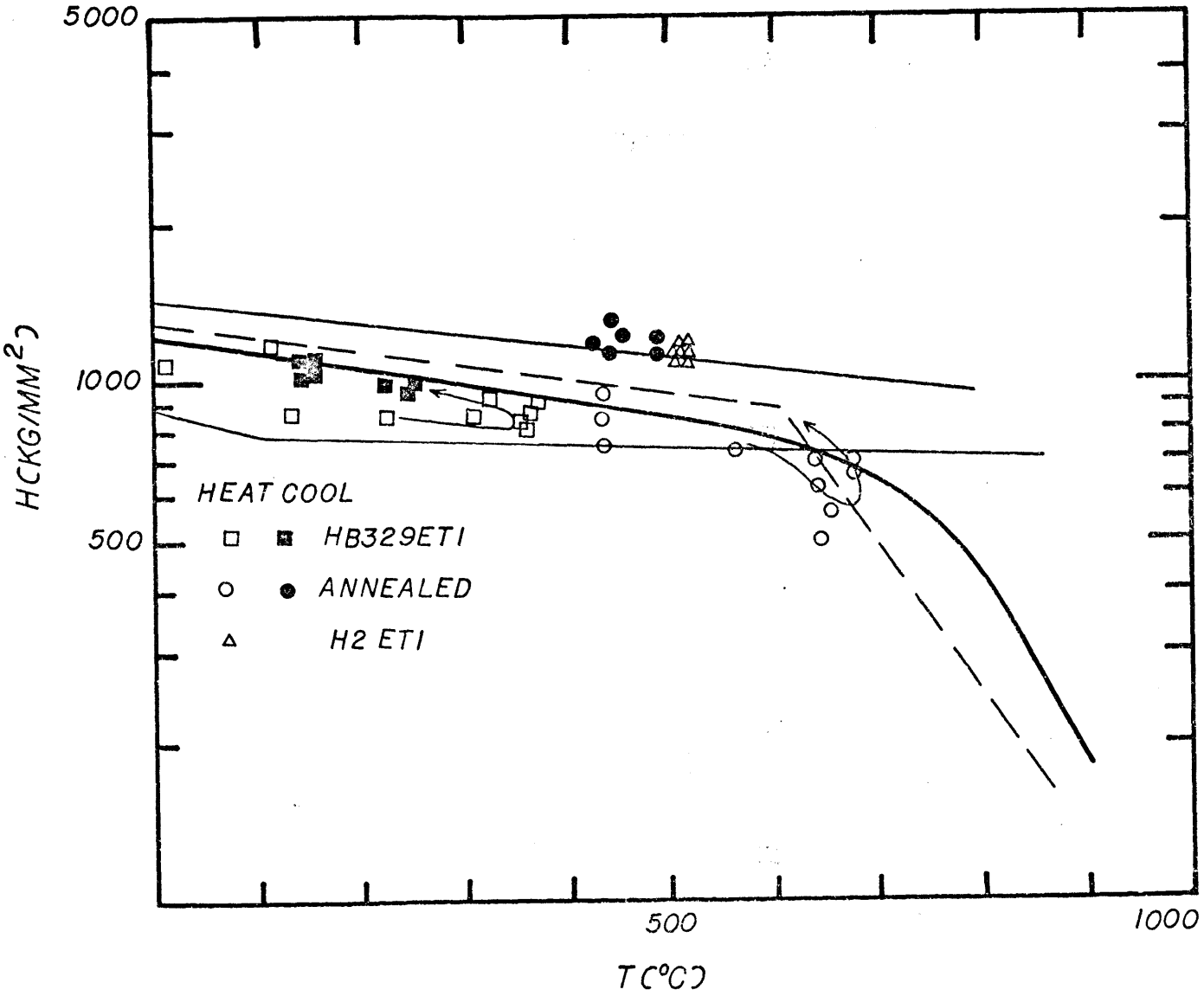
5000
1000
500
HCKG/MM2)
HEAT COOL
HB329ETI
ANNEALED
H2 ETI
500
1000
T(°C)

Figure 14. Constraint Factor for Quartz as a Function of Temperature.

The constraint factor for quartz computed from the hardness and the variation of the elastic modulus (see Chapter I) is shown as a function of temperature. Because the ratio of the Young's modulus to the yield stress increases very rapidly at the α-β transition temperature, the constraint factor increaeses quite rapidly. Below 500°C, the hardness values indicate that the yield stress is an appreciable fraction of the modulus ($E/\sigma \sim 20$) and elastic strains are an appreciable fraction of the total strain. The constraint factor is somewhat uncertain in this range (.7-1.1) but VDP experiments indicate that the best empirical value is 1.1 (see Results and Discussion section).

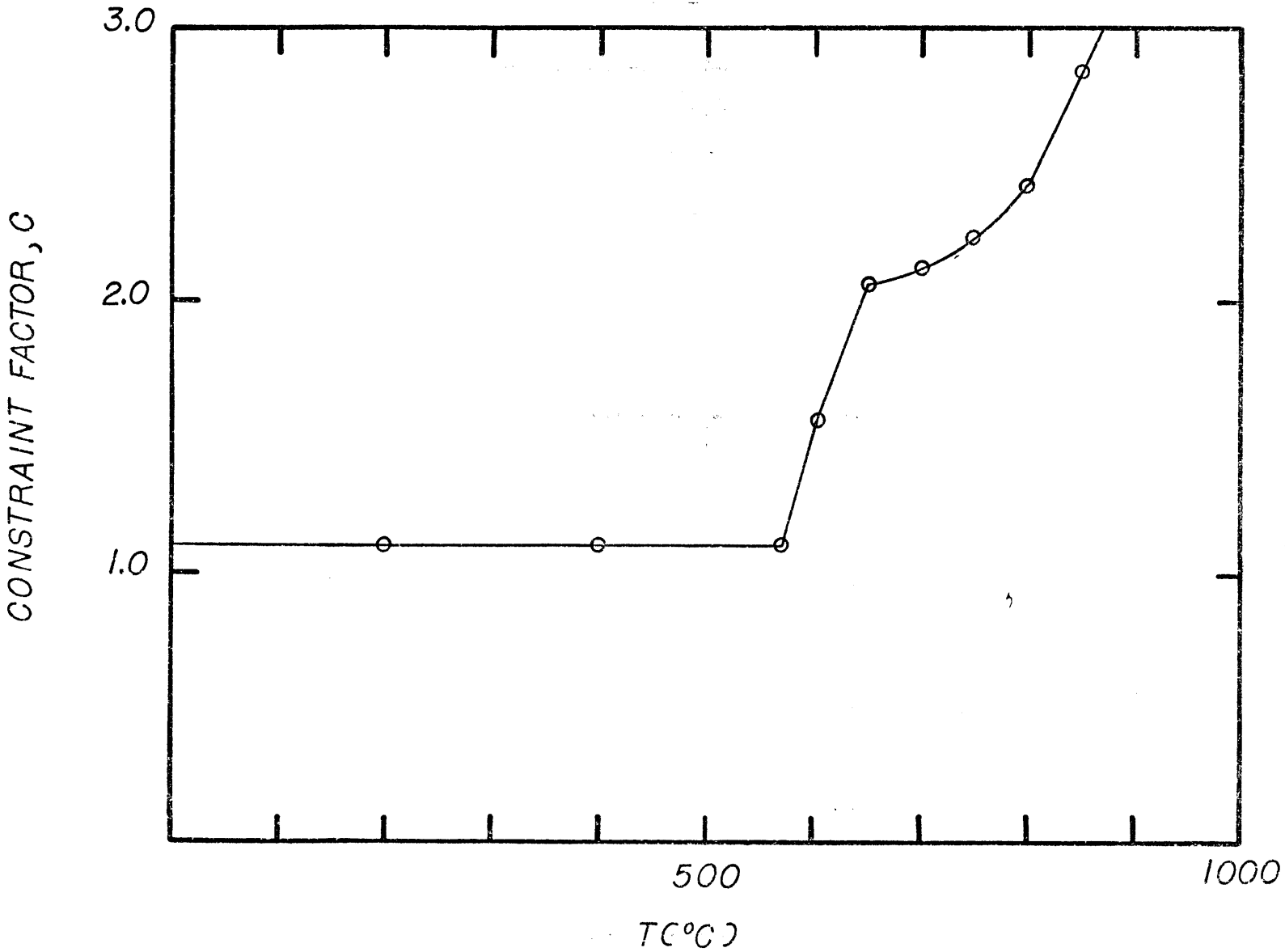
3.0
2.0
1.0
CONSTRAINT FACTOR, C
500
1000
T(°C)

when a sphere indents a perfectly elastic material (Sneddon, 1951). Realizing that the constraint factor may be uncertain by a factor of ~1.6, I have chosen to use the empirically determined value (C = 1.1). The values of the constraint factor as well as the hardness derived yield stresses are tabulated with the hardness temperature and dwell times in Appendix B.

Discussion

Hardness at Room Temperature

As discussed previously, the room temperature hardness values agree well with the desorbed values published by Westbrook and Jorgensen (1968) presumably because a relatively large load was used (100 g). Although the form anisotropy was suppressed in this study, it is instructive to compare the form anisotropy of hardness with the tendency to adsorb hydroxyl impurity as indicated by the critical velocity of growth (Table 6). There are some discrepancies in the data sets, but in a rough way, the two quantities correlate, with (0001) being "softest" and also showing the greatest tendency to adsorb impurities, and the prism planes showing lesser tendency to adsorb impurities and also exhibiting greater hardness.

Considering the aggregated room temperature data the normal or desorbed value of (VDP) hardness for natural α quartz is indicated to be 1200±120 kg/mm^2 at room temperature. From this value, one may set constraints upon the polycrystalline yield stress for quartz at room temperature. For instance Christie et al. (1964) measured rupture strength of quartz at 2.7 GPa confining pressure. Suppose their maximum measured rupture strength (4.5 GPa) represented the yield stress measured in the hardness test, then assuming a value of Young's modulus of 94 GPa, using the empirical and theoretical curves for the constraint factor from Johnson (1970),

TABLE 6. FORM ANISOTROPY OF HARDNESS COMPARED TO CRITICAL VELOCITY OF GROWTH FOR ENTRAPMENT OF IMPURITIES

Smallest Wet Hardness			Greatest Wet Hardness		
		$\{10\bar{1}0\}$	$\{10\bar{1}0\}$	(KHN)	Winchell (1945)
(0001)	$\{10\bar{1}1\}$			(VDP)	Taylor (1949)
(0001)	$\{10\bar{1}0\}$			(VDP)	Young & Millman (1964)
	$\{10\bar{1}0\}$	$\{10\bar{1}1\}$	$\{01\bar{1}1\}$	(VDP)	Westbrook & Jorgensen (1968)
Least Critical Velocity			Greatest Critical Velocity		
(0001)	$(\bar{1}\bar{1}20)$	$(1\bar{1}22)$	$(1\bar{1}01)$	$(10\bar{1}1)$	$(11\bar{2}0)$ Khadzi and Khadzi (1968)

E tan $\beta/Y = 7.5$ and the constraint factor must equal 1.4 which would require the hardness to be 630 kg/mm^2. Since this is in error by a factor of two, the processes occurring during the indentation test must not be the same as those in the test conducted by Christie et al. (1964). Rice (1970) has suggested that the yield property being measured is the polycrystalline flow stress.

At this point, it is instructive to consider the high resolution scanning electron micrographs of Brace (1963; and Figure 3 of this study).

As remarked by Brace (1963) the trend of the features observed on the facets of the indentation are in complete agreement with traces of slip on planes (0001) and $\{1\bar{1}01\}$; comparison of Figures 3a and b also shows that certain of the features observed by Brace (1963) could also be interpreted as slip on the primary prism plane. Slip on these planes with the Burger's vectors as observed by the later TEM studies would form a complete set of 5 independent slip systems, while slip on the basal and unit prism planes with any combination of appropriate Burger's vectors can provide only 2 independent slip systems. This can be verified using the methods outlined by Kelly and Groves (1970, p. 179) but although, the calculations are simple they are relatively tedious and will not be reproduced here. Because the features were so small, no slip steps could be observed and therefore Brace (1963) could not unequivocally prove that

they were slip plane traces, the markings are certainly consistent with the operation of enough slip planes to fulfill the von Mises criterion for homogeneous polycrystalline flow (reviewed by Paterson, 1969). Furthermore, Brace (1963) observed that those traces were best developed which lay on a set of planes that could have been either (0001), $(10\bar{1}0)$, or a particular set of $\{1\bar{1}01\}$ planes. This is consistent with the observation that slip occurs most easily on the (0001) and $\{10\bar{1}0\}$ planes for quartz at low temperatures. To summarize, the yield stress measured by the indentation hardness test corresponds to a process which has a higher yield than the primarily brittle rupture stress measured by Christie et al. (1964) and observations of the details of the indentations made by Brace (1963) are entirely consistent with the hypothesis of Rice (1970) that the indentation process measures polycrystalline flow even at room temperature.

Impurities and Weakening in Natural Quartz Crystals

The ease of specimen preparation and testing has made the hot hardness technique a popular method for comparative studies of materials such as members of solid solution series (UC-PC series, Tokar, 1973; KCl-KBr series, Hopkins et al., 1973); polymorphs (spinels, Dekker and Rieck, 1974); compounds with varying impurity contents (quartz, Nadeau, 1970); members of classes of materials such as carbides, borides and oxides (Kohlstedt, 1973; Koester and Moak, 1967) and changes induced by annealing (galena, Sangwal and Patel, 1974). Many other

examples exist in the metallurgical and ceramics literature. It is important to emphasize that such comparative studies do not depend on the exact value of the ratio of hardness to yield stress, but only on the presumption that the two are proportional for a given temperature, a point that has been abundantly illustrated for a wide range of materials. Thus such comparisons can be used to assess the effect of changing compositional or microstructural parameters on the mechanical strength of materials as was suggested for the case of minerals by Brace (1961).

Kekulawala et al. (1978) have suggested that the weakened state exhibited by synthetic quartz can be correlated with gel-hydroxyl content and not with structurally bound impurities, which may be distinguished from the gel-type or colloidal inclusion hydroxyl by their relatively sharp infrared peaks. All the crystals used in this study had some small inclusions, as is common in natural quartz; however TEM observations of the crystals, which had been heated to 700°C for several hours in dry argon showed no precipitating water at 50,000 power. This included the RHH synthetic crystal, but these observations do not include the pressure annealed specimens. Thus as expected for natural crystals the impurity states tested here were all of the structural impurity type. That this is also true of the synthetic crystal is intimated by the room temperature infrared spectra which does not show the broad hydroxyl absorption band characteristic of synthetic crystals

Figure 15. Comparative Hot Hardness of Natural Quartz.

The hot hardness of the quartz samples tested in this thesis for four temperatures (23°, 350°, 500°, 700°C) do not show a significant variation with increasing hydroxyl impurity. The samples do seem to be affected by different heat treatments: the pressure annealed samples are weakened slightly ~10% for temperatures up to 400°C. However, Sample Herk ET1 which was tested at 500° only, showed an increase in hardness which was similar to that observed by Nadeau (1970). The dry argon annealed sample also showed hardening of a roughly similar magnitude.

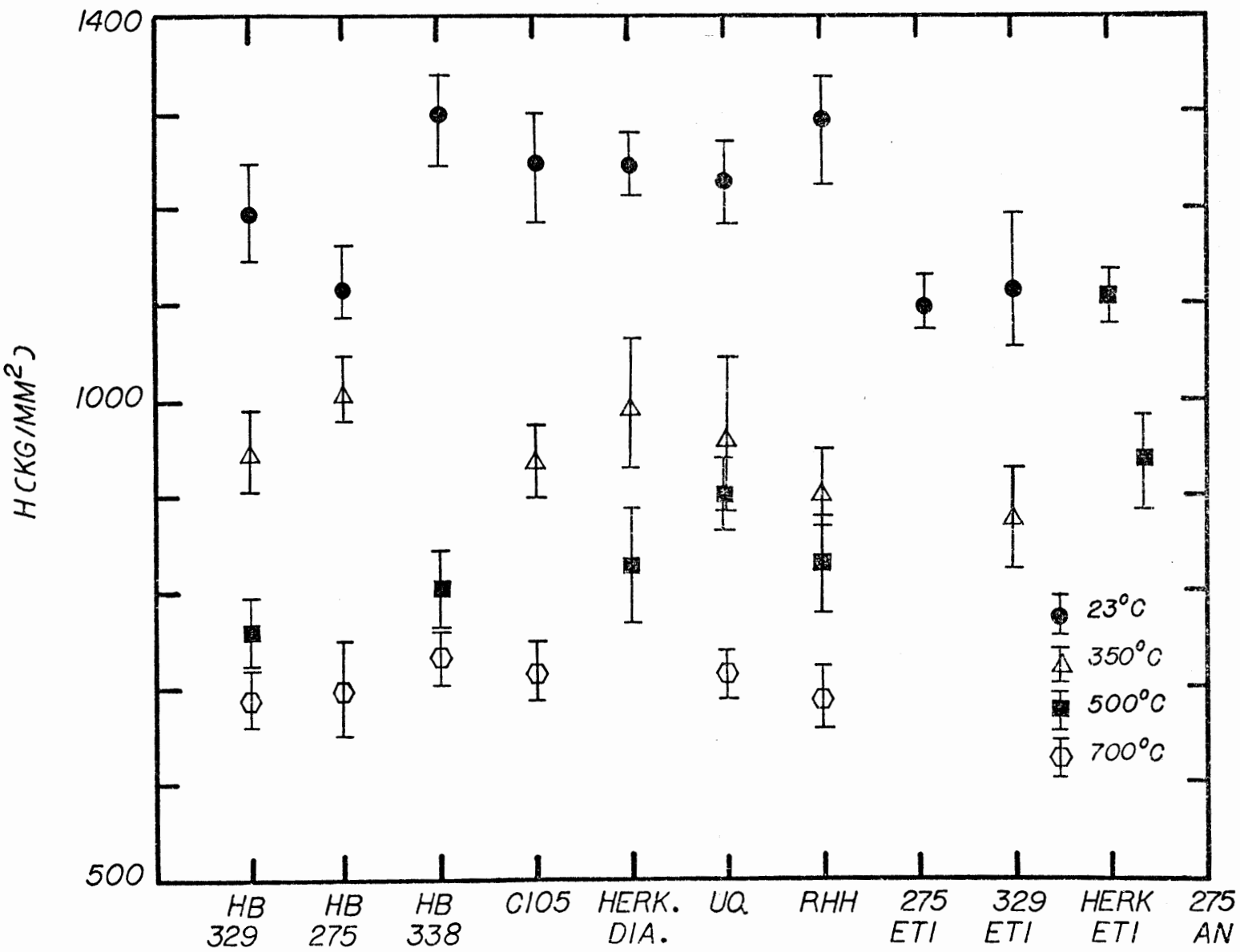
1400
1000
500
H (KG/MM²)
HB 329
HB 275
HB 338
C105
HERK. DIA.
UQ
RHH
275 ETI
329 ETI
HERK ETI
275 AN
23°C
350°C
500°C
700°C

with the gel type impurity (Dodd and Fraser, 1965). High quality synthetic crystals without gel type colloidal inclusions can be grown under the proper conditions (Chernov and Khadzi, 1968; Kolb et al., 1972); it seems likely that the RHH crystal is among that class of high quality crystals. The crystals tested here included previously analyzed crystals whose hydrogen impurity contents were as large as 700 $H/10^6$ si. Because of the correlation of aluminum and alkali content (Bambauer, 1961), consideration of Dennen's (1972) geothermometer shows that this range brackets the concentrations of hydrogen to be expected for reasonable temperatures in the earth. The massive metamorphic quartz was included to show that metamorphic and hydrothermal quartzes do not differ greatly in hardness properties. Therefore, although the suite of samples tested here do not constitute a complete set of natural quartzes they probably represent many of the impurity contents which are found in common quartz bearing rocks. Of course, this excludes such varieties as chalcedony, flint, agate, amethyst and citrine quartz which are known to contain relatively large weight fractions of water (Frondel; 1962, 1978) in the gel state (Katz, 1962). The comparative hardness studies show that within the scatter of the data ($\Delta H < 15\%$) there is no correlation of weakening and impurity content. Brace (1963) observed a qualitative correlation of aluminum color center impurity density as revealed by irradiation and weakening as measured by the Knoop hardness test.

However, this correlation may perhaps be explained by the covariance of aluminum and hydroxyl impurity in synthetic quartz (cf. Cohen, 1960; Chernov and Khadzi, 1968; Chakraborty and Lehmann, 1976). Nadeau (1970) observed some weakening at temperatures from 600°C to 800°C in crystals electrolytically injected with lithium. Upon cooling to room temperature he observed that the indentations in that temperature region had formed a second, denser phase which was unstable over a period of several days at normal laboratory conditions. No such behavior was noted by Westbrook (1958), Brace (1961) or this study. Cohen (1960) has observed precipitation of lithium aluminum silicate in lithium doped synthetic crystals upon cooling quartz through the α-β transition. As stated previously (Chapter 1) the large hydrostatic pressure around the indentor probably would cause β quartz in the region close to the brale to revert to the alpha phase at any temperature below 900°C. Thus the production of the unstable phase around the indentation in a highly lithium doped crystal is probably related to this precipitation. To summarize, this study provides systematic experimental proof of the suggestion of Kirby (1975) and Kekulawala et al. (1978) that the strength of quartz containing hydroxyl incorporated as structural impurities can not be correlated to the amount of hydroxyl present even when it is present in fairly large amounts (700 H/10^6 Si) for temperatures up to ~750°C.

The Effect of Pressure

As pointed out by Kekulawala et al. (1978) it is perhaps possible that the weakened state in natural quartz may be achieved under higher confining pressures than the 300 MPa which they used. The pressure annealing experiment described above represents a tentative step towards resolving the effect of high pressure. Hardness tests conducted in dry argon on the three samples annealed for two days at 15 Kb confining pressure and unknown, but possibly high P_{H_2O} indicated that the weakening effect was small (~15%) and confined to low temperature (<400°C). This agrees with the hardness tests conducted on samples containing electrolytically injected hydrogen impurity (Nadeau, 1970) although the magnitude of weakening of the pressure injected samples was not as large. In neither Nadeau's (1970) study of electrolytically injected hydrogen or the pressure injected samples was a dramatic weakening (>30%) noticed at any temperature. This result is despite the fact that calculations using the diffusion coefficient of hydrogen at 2.5 Mpa (~2.0×10^{-8} sec/cm^2) as determined by Kats and others (1962) and the equation for diffusion of hydrogen into a thin (1 mm) slab (Jost, 1960, p. 37) show that the concentration of hydrogen under the conditions and times of the pressure annealing experiment could have been increased by a factor of 10. However, the samples were cracked badly by the pressure treatment and infrared spectra could not be taken. No increase of hardness was noticed as a func-

tion of time at temperature in dry argon for the low temperature (<400°C) hardness tests on previously pressure annealed samples, but one sample, H2ET1, indented at 500°C appeared to have been hardened relative to the as-received crystal. No TEM or optical observations have as yet been made on the pressure annealed crystals. It is interesting to notice that Chernov and Khadzi (1968) observed no pressure dependence for trapping of colloidal inclusions for pressures up to ~300 MPa (see also Lias et al., 1973).

Although the pressure annealing results agree with Nadeau (1970) and Kekulawala et al. (1978), it is clear from the remarks about the experimental difficulties in the pressure annealing experiment that more tests should be conducted to verify this conclusion.

Hardening of Quartz by Heating in Low P_{H_2O}

In two cases, the hardening mechanism discussed by Nadeau (1970) was observed: One of the early tests of the Herkimer quartz appears to deviate from the trend of the rest of the hardness data (Figure 6). A subsequent sample HBC275/125 (see Appendix B, and Figure 13), which had been annealed at 600° for two hours in dry argon showed hardening during indentation creep runs at ~700°C. The same specimen was hardened upon cooling to 500°C by the same magnitude that Nadeau (1970) observed in his annealed samples (1970). The cause of this phenomenon is essentially unknown. However, Johnson et al. (1973) have observed reduction of

hydrogen solubility in rutile (TiO_2) during annealing in atmospheres with low P_{H2O}. Interestingly enough, the reduction of solubility of hydrogen occurs even if the rutile crystals are annealed in dry hydrogen atmospheres. It is doubtful if this mechanism of hardening has any significance for geologic situations; however, it is clear warning to experimentalists, including those conducting hardness studies, of the subtlety of the behavior of geologic materials at high temperatures. Any further hardness tests, particularly those conducted at very high temperatures would have to take this effect into account.

Polycrystalline Yield Stress of Quartz with Structurally Bound Hydroxyl Impurities

Following the methods outlined previously the polycrystalline yield stress was computed from the hardness data. The data are plotted in Figure 16 along with previously published polycrystalline yield stress data and data thus far obtained by single crystal deformation experiments. When possible the yield data have been selected at 8% strain, which has been shown to be the effective strain for the VDP hardness test for strain hardening metals (Tabor, 1956) and at a strain rate such that $\log \dot{\varepsilon} = -5 \pm .5$. Thus, for the purposes of comparison of the hardness derived yield stress to the polycrystalline yield stress, it is assumed that the strain rate of the indentation hardness test is 10^{-5} sec^{-1} for quartz as was shown to be true for olivine and Maryland diabase (see the previous

Figure 16. Empirical Yield Stress versus Temperature Curve.

Hardness derived-yield stresses from Brace (▽, 1961), Westbrook (Δ, 1958, 1966) and this study (·) are plotted on the same graph as the natural single and polycrystalline yield data (symbols the same as Figure 2). For comparison, the "wet" and dry flow laws of Parrish et al. (1976) are plotted.

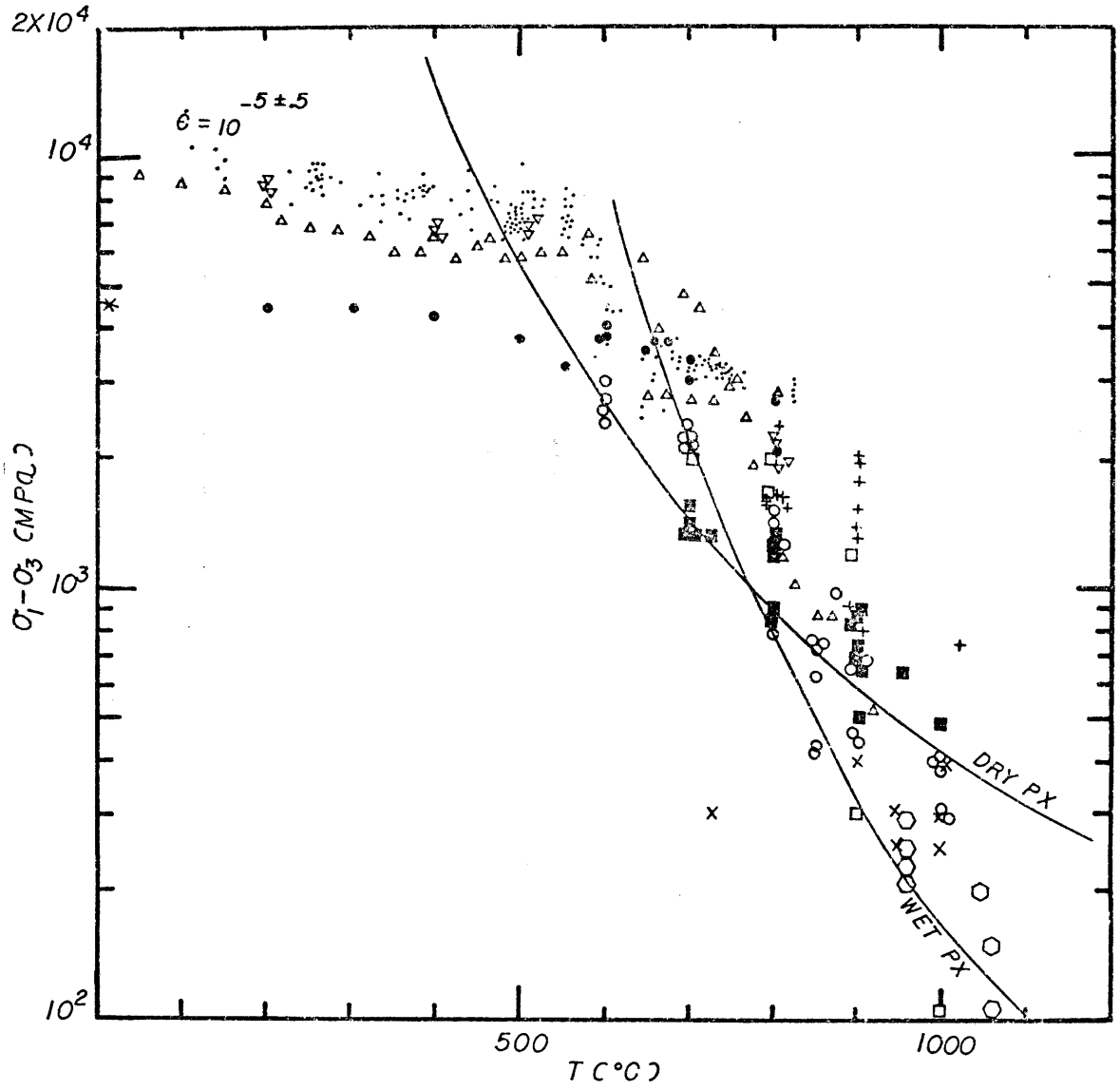
2X10^4
10^4
10^3
10^2
σ1-σ3 (MPa)
ε̇ = 10^-5±.5
DRY PX
WET PX
500
1000
T (°C)

chapter). The plot does not include data determined in polycrystalline experiments in which the differential stress was greater than the confining pressure. Such experiments in quartz at high stresses exhibit a large pressure sensitivity of yield stress (cf. experiments at 500° and 600° at $\dot{\varepsilon} = 5 \cdot 10^{-6}\ s^{-1}$, Heard and Carter, 1968, p. 37). In a similar manner, the single crystal data of Christie et al. (1964), Griggs (1967) and Blacic (1971) fall below the hardness derived yield stresses at temperatures less than 700°C. McLaren et al. (1967), making observations on single crystals deformed by Griggs and Blacic (Griggs, 1967; Blacic, 1971), report that they observed no dislocations of any sort in crystals deformed below 500°-600°C. At intermediate temperatures 600°-700°C, basal dislocations were observed as well as the basal faults characteristic of low temperature failure (Christie et al.; 1964, 1967). At higher temperatures (<750°C) no faults were observed, but only basal plane dislocations. It is not surprising, therefore, that the low temperature single crystal data points diverge from the hardness-derived yield stresses, and in fact they do so exactly in the temperature range at which Christie et al. (1967) observed the formation of basal faults 650°C to 750°C, and lower. This is entirely consistent with the idea that the hardness derived yield stresses are the polycrystalline yield stresses for fully ductile flow. Consideration of Figure 16 shows that with the exclusions of polycrystalline and single crystal data

where fracture processes are occurring, the hardness-derived yield stress and the polycrystalline yield stress form a consistent and coherent data set which may be regarded as the experimentally determined yield stress of natural quartz at 8% strain and a strain rate of 10^{-5} s^{-1}.

One of the primary aims in mechanical studies of geologic materials is the generation of a constitutive equation which may be used to constrain naturally occurring deformation parameters. Typically one presumes to know temperature and pressure and desires to constrain either strain rate or stress of some geomechanical process. The uncertainties in generating a constitutive equation of this sort fall into two categories: uncertainties in the determination of the empirically determined flow law and uncertainties in the application of the empirical flow law as an appropriate constitutive equation. Difficulties in both categories preclude the extrapolation of the empirical flow law for quartz.

Firstly, there appear to be serious discrepancies between the "wet" and "dry" flow laws as published by Parrish et al. (1976) on the one hand and the aggregated polycrystalline and hardness derived data on the other. For instance, Heard and Carter's (1968) data done at 1.0 GPa confining pressure fall consistently below Tullis's (1972) data, and the hardness data in the region 500°-700°C. Thus the "dry" flow law derived from a reanalysis of Heard and Carter's (1968) data also deviates from the body of the data. The reason may perhaps

lie in the increased confining pressure present in the other studies (1.5 GPa in Tullis's experiments and unknown but very high pressure characteristic of the hardness test). Secondly in the dry experiments, strains higher than 10% are seldom achieved. Tullis's study (1972 and Tullis et al., 1973) is notable because even at the relatively large strains of these experiments (up to 60% in some small portions of the sample) the textures developed were extremely inhomogeneous. Because of this inhomogeneity it is difficult to determine when the conditions of steady state deformation are met. The determination of parameters in a flow law such as the familiar power law

$$\dot{\varepsilon} = \dot{\varepsilon}_o \sigma^n \exp -\frac{Q}{RT}$$

become complicated because ε_o, n, and Q may be functions of inadequately described structural parameters such as dislocation density, subgrain size, or grain orientation among others. One result could easily be changing "constants" ε_o, n, and Q.

The addition of water compounds the problem. Its demonstrated effect on recrystallization (Hobbs, 1968; Tullis et al., 1973; and others) and possible effect on dislocation generation, should it enter the lattice in the appropriate impurity structure under the influence of pressure, could profoundly effect the recovery process and influence diffusional deformation through changes in grain boundary diffusivity or reduction in grain size. Clearly such situations render the

extrapolation of the flow law over two orders of magnitude uncertain to a high degree.

Summary and Conclusions

1. Hardness derived yield stresses form a coherent set of data with previously published yield data and can be used to establish an empirical flow law. Below the α-β transition, the hardness data are more uncertain, but indicate that the strength of quartz under high confining pressure reaches values which are at least ~ 8 GPa at temperatures below 200°C.

2. Comparative hardness tests show that structural hydroxyl impurity does not weaken quartz even though it may be present in large amounts. The samples tested spanned the range of hydroxyl impurity contents to be expected in most common crustal environments. A preliminary test of hydrous annealing at high pressures did not show any significant weakening; however the exact partial pressure of water during the experiment is unknown.

3. Room temperature hardness phenomena such as form anisotropy, directional anisotropy and adsorbed layer effects correlate with other studies of mechanical and surficial properties. Observations of the morphology of indents made previously by Brace (1961) are consistent with the idea that hardness properties of quartz are controlled by ductile flow on a complete set of 5 independent slip systems.

APPENDIX A. ANISOTROPY OF KNOOP HARDNESS (300 g) AT ROOM TEMPERATURE ON THE $\{10\bar{1}0\}$ FACE

# Indents	Angle Indentor Axis/(0001)	Hardness (kg/mm^2)
4	-41	701±15
5	-30	720±22
3	-21	674±10
6	0	709±18
4	43	684±27
2	15	695± 5
5	30	658±25
4	52	657± 7
5	34	691±18
4	43	727±11
6	48	727±10
4	-39	720±20
2	-35	684±10
3	-84	724±14
5	+5	720±22
6	+9	705±18
5	+85	720±25
4	+56	716±15

The hardness tabulated is the average value; the maximum variation is also indicated.

APPENDIX B. COLLECTED HOT VDP HARDNESS DATA ON QUARTZ [a]

T (°C)	H(kg/mm^2) [b]	C	σ(MPa)	t_{sec} [c]	Clock Time (mins.)
		Herkimer 1-1			
283	1061±80	1.1	9460	36	
286	1010	1.1	9000	19.2	
288	999	1.1	8910	18	
288	991	1.1	8830	20.4	
440	946	1.1	8439	21.6	
436	928	1.1	8279	14.4	
427	957	1.1	8530	12	
523	786	1.1	7010	18	
525	809	1.1	7210	36	
525	696	1.1	6200	32	
528	758	1.1	6760	16.8	
530	798	1.1	7110	16.8	
530	786	1.1	7010	16.8	
		Herkimer 1-2			
260	1032±60	1.1	9200	11	
260	1035	1.1	9230	11	
260	1077	1.1	9600	11	
260	960	1.1	8560	11	
465	965	1.1	8600	15	
470	890	1.1	7930	13	
465	890	1.1	7930	14	
816	734	2.56	2810	7	
816	754	2.56	2890	28	
820	792	2.60	2990	13.2	
820	842	2.60	3090	12	
820	740	2.60	2790	13	
820	730	2.60	2750	17	
		H2-215 ET1 [e]			
517	1100±60	1.1	9810	31	35
518	1070	1.1	9540	21	41
515	1150	1.1	1030	21	43
513	1060	1.1	9450	21	45
511	1170	1.1	10400	20	47
509	1130	1.1	10100	20	50

(a) All indentations were made with 100 grams load.
(b) Each axis was measured 5 times and the average of all measurements for both axes were used as the hardness value. The variations are an indication of the error of observation.
(c) The dwell time (in seconds) varied because of thermal expansion of the parts.
(d) The running time (in minutes) from the commencement of heat-

T (°C)	H(kg/mm^2)	C	σ(MPa)	t_{sec}	Clock Time (mins.)
		UQ			
251	1061±80	1.1	9460	15	
256	1091	1.1	9730	18	
256	1078	1.1	9610	21	
261	1009	1.1	9000	21	
329	1043	1.1	9300	23	
334	879	1.1	7840	24	
525	883	1.1	7870	23	
518	901	1.1	8030	29	
514	943	1.1	8410	5	
514	855	1.1	7620	22	
510	951	1.1	8480	24	
514	887	1.1	7910	22	
669	782	2.08	3690	5	
673	751	2.09	3520	14	
688	741	2.10	3460	16	
693	657	2.11	3050	13	
743	692	2.20	3080	10	
745	680	2.20	3030	12	
745	724	2.20	3230	10	
747	730	2.21	3240	12	
750	719	2.22	3180	14	
759	678	2.26	2940	8	
440	851	1.1	7590	16	
424	830	1.1	7400	13	
415	897	1.1	8000	12	
405	930	1.1	8290	8	
		HBQ338-1			
726	721±60	2.16	3270	18	85
726	721	2.16	3270	18	
726	728	2.16	3310	18	
726	715	2.16	3250	18	115
726	724	2.16	3290	18	125
760	737	2.26	3200	19	
720	767	2.17	3470	14	
723	750	2.17	3390	14	
730	747	2.18	3360	15.6	160
550	979	1.1	8730	11	175
550	878	1.1	7830	11	
327	918	1.1	8180	12	185

ing is given for some runs.

(e) This sample was annealed in the pressure annealing experiment (see text).

T (°C)	H(kg/mm^2)	C	σ(MPa)	t_{sec}	Clock Time (mins.)
		HBQ338-4			
487	784 ±80	1.1	6990	18	
485	846	1.1	7540	18	
483	802	1.1	7150	18	67
487	815	1.1	7270	19	82
492	850	1.1	7580	18	
495	760	1.1	6780	18	
497	762	1.1	6790	18	
487	766	1.1	6830	18	105
487	822	1.1	7330	19	
487	790	1.1	7040		
487	784	1.1	6990	18	112
492	833	1.1	7430	19	149
497	820	1.1	7310	19	150
497	811	1.1	7230	22	
483	820	1.1	7860	20	160
484	822	1.1	7330	20	
485	756	1.1	6740	19	180
374	946	1.1	8430	10	185
379	911	1.1	8120	19	
264	996	1.1	8080	7.2	195
259	943	1.1	8410	15	
		HBQ275-127 (f)			
495	902 ±60	1.1	8040	19	
495	800	1.1	7130	22	
497	806	1.1	7190	20	
497	835	1.1	7440	20	
497	846	1.1	7540	22	
550	770	1.1	6860	26	
558	820	1.1	7310	13	
565	805	1.1	7180	15	
565	731	1.1	6520	17	
570	711	1.1	6340	18	
584	758	1.30	5720	18	
586	766	1.30	5780	4	
590	782	1.43	5360	7	
593	732	1.43	5020	17	
593	762	1.43	5230	23	
593	715	1.43	4900	162	
597	730	1.43	5010	30	
593-612	675	1.43	4630	786	
617	774	1.70	4460	26	
612-17	670	1.70	3860	1176	
283	1018	1.1	9080	24	
282	1002	1.1	8930	24	
273	1018	1.1	9080	24	

(f) This sample had been annealed at 600°C for 2 hours.

T (°C)	H(kg/mm^2)	C	σ(MPa)	t_{sec}	Clock Time (mins.)
		HBQ275-125			
641	707±40	2.00	3470	25	33
647	492	2.00	2410	26.4	35
652	634	2.00	3110	32	37
664	550	2.08	2590	31	39
687	655	2.11	3040	20	52
683	692	2.10	3230	20	53
683	710	2.10	3320	144	54
683	621	2.10	2900	80	56
683	663	2.10	3100	1470	80
683	701	2.10	3270	20	81
683	672	2.10	3140	1710	110
683	818	2.10	3820	20	111
462	1214	1.1	10800	18	146
454	1320	1.1	11800	18	148
448	1121	1.1	9900	18	150
436	1206	1.1	10800	18	152
		HBQ329-1			
473	726±55	1.1	6470	23	
484	788	1.1	7030	6	
491	756	1.1	6740	28	
507	775	1.1	6910	20	
586	760	1.24	6780	20	
593	712	1.56	4480	18	
603	719	1.56	4520	18	
603	715	1.56	4490	18	
702	691	2.12	3200	25	
735	688	2.19	3080	31	
738	684	2.20	3050	30	
683	730	2.10	3410	7	
662	737	2.07	3490	7	
641	726	1.96	3630	7	
569	734	1.1	6540		
441	752	1.1	6700	24	
436	853	1.1	8370	39	
431	957	1.1	9380	16	

T (°C)	H(kg/mm^2)	C	σ(MPa)	t_{sec}	Clock Time (mins.)
		HB924 (ET1)(g)			
111	1214±80	1.1	10800	18	
138	879	1.1	7840	21	
228	886	1.1	7900	20	
309	870	1.1	7760	34	
334	940	1.1	8380	24	
331	805	1.1	7180	18	
362	837	1.1	7460	19	
367	815	1.1	7270	20	
369	957	1.1	8530	20	
362	912	1.1	8130	16	
255	1005	1.1	8960	22	
241	979	1.1	8730	19	
224	1054	1.1	9400	18	
151	1124	1.1	10000	22	
150	1087	1.1	9690	22	
142	1077	1.1	9600	23	
140	1153	1.1	10300	24	
		C105			
551	754±32	1.1	6720	23	
589	739	1.1	6590	16	
589	714	1.1	6370	16	
704	714	2.13	3290	18	
709	715	2.14	3280	19	
714	676	2.16	3070	20	
695	728	2.11	3380	14	
699	715	2.11	3320	14	
699	715	2.11	3320	15	
687	729	2.10	3400	14	
687	737	2.10	3440	14	
700	739	2.12	3420	17	
707	750	2.13	3450	18	
709	700	2.13	3220	19	
353	952	1.1	8490	15.6	
358	938	1.1	8360	15.6	

(g) The sample had been annealed at high pressure previous to the hardness test (see text).

T (°C)	H(kg/mm^2)	C	σ(MPa)	t_{sec}	Clock Time (mins.)
		RHH-1			
373	813±60	1.1	7250	26	
367	960	1.1	8560	12	
367	880	1.1	7850	14	
367	882	1.1	7860	12	
362	904	1.1	8060	13	
357	851	1.1	7590	13	
556	804	1.1	7170	10	
560	807	1.1	7190	14	
560	807	1.1	7190	13	
565	782	1.1	6970	12	
565	772	1.1	6880	11	
546	840	1.1	7490	9	
702	639	2.12	2960	17	
702	694	2.12	3210	18	
700	697	2.12	3220	18	
697	714	2.12	3300	17	
697	710	2.12	3280	16	
		RHH-3			
381	985±60	1.1	8780	10.8	
382	933	1.1	8310	13.2	
384	940	1.1	8380	14.4	
393	965	1.1	8600	15.6	
391	971	1.1	8660	18	
385	941	1.1	8390	14.6	
384	960	1.1	8560	14.4	
382	1040	1.1	9270	14.4	
551	856	1.1	7630	12	
551	870	1.1	7760	12	
551	910	1.1	8110	13.2	
556	842	1.1	6830	14.4	
556	805	1.1	7180	14.4	
556	825	1.1	7350	14.4	
558	924	1.1	8240	14.4	

T (°C)	H(kg/mm^2)	C	σ(MPa)	t_{sec}	Clock Time (mins.)
		RHH-4			
624	822±60	1.8	4480	11	
629	794	1.84	4230	12	
629	811	1.84	4320	12	
633	732	1.90	3780	13.2	
624-638	744	1.90	3840	180	
624-638	770	1.90	3970	180	
624-638	768	1.90	3960	108	
624-638	754	1.90	3890	66	
624-638	764	1.90	3940	66	
743	719	2.20	3200	12	
743	747	2.20	3300	12	
745	730	2.20	3250	11	
746	730	2.20	3250	12	
749	667	2.22	2950	51	

References

Ave'lallement, H. G., and N. L. Carter, "Pressure Dependence of Quartz Deformation Lamellae Orientations," Am. J. Sci., 270, 218-235, 1971.

Ayensu, A., and K. H. G. Ashbee, "The Creep of Quartz Single Crystals, with special reference to the mechanism by which water accommodates dislocation glide," Phil. Mag., 36, 713-723, 1977.

Baëta, R. D., and K. H. G. Ashbee, "Slip Systems in Quartz: I Experiments," Am. Mineral., 54, 1551-1573, 1969a.

Baëta, R. D., and K. H. G. Ashbee, "Slip Systems in Quartz: II Interpretations," Am. Mineral., 54, 1574-1582, 1969a.

Baëta, R. D., and K. H. G. Ashbee, "Mechanical Deformation of Quartz I. Constant Strain Rate Compression Experiments," Phil. Mag., 22, 601-624, 1970a.

Baëta, R. D., and K. H. G. Ashbee, "Mechanical Deformation of Quartz II. Stress Relaxation and Thermal Activation Parameters," Phil. Mag., 22, 625-635, 1970b.

Baëta, R. D., and K. H. G. Ashbee, "Transmission Electron Microscope Studies of Plastically Deformed Quartz," Phys. Stat. Sol. (a), 18, 155-170, 1973.

Balderman, M. A., "The Effect of Strain Rate and Temperature on the Yield Point of Hydrolytically Weakened Synthetic Quartz," J. Geophys. Res., 79, 1647-1652, 1974.

Bambauer, H. U., "Spurenelementgehalte and γ-Farbzentrenen in Quarzen aus Zerskluften der Schweizer Alpen," Schweiz.

Min. Petrog. Mitt., 41, 335-367, 1961.

Baumbauer, H. U., G. O. Brunner and F. Laves, "Beobachtungen über Lamellenbau an Bergkristallen," Zeitschrift für Kristallographie, 116, 173-181, 1961.

Bambauer, H. U., G. O. Brunner, and F. Laves, "Wasserstoffgehalte in Quarzen aus Zerrkluften der Schweizen Alpen und die Deutung ihrer Regionalen Abhängigkeit," Schweiz. Min. Petr. Mill., 42, 221-236, 1962.

Blacic, J. D., "Hydrolytic Weakening of Quartz and Olivine," Thesis, Univ. of California, Los Angeles, 205 p., 1971.

Blacic, J. D., "Plastic Deformation Mechanisms in Quartz: The Effect of Water," Tectonophysics, 27, 271-294, 1975.

Bershov, L. V., M. D. Krylova, and A. V. Seperanskiy, "Elektronno-dyrochnyye tsentry O^{-}-Al^{3+}+iTi^{3+} v kvartse kak pokazatel' temperaturnykh usloviy regional 'nogo metamorfizma," AN SSR Izvestiya, ser. geol., 10, 113-117, 1975; transl. in Int. Geol. Rev., 19, 741-745, 1975.

Brau, W. F., "Experimental Study of the Indentation of Rocks and Minerals," Unpublished final report to N.S.F., Cambridge, Mass., 81 pp., 1961.

Brace, W. F., "Behavior of Quartz during Indentation," Journal of Geology, 71, 581-595, 1963.

Brace, W. F., "Indentation Hardness of Minerals and Rocks,"

N. Jahrbuch f. Mineralogie. Monatshefte, 9-11, 257-269, 1964.

Brookes, C. A., J. B. O'Neill and B. A. W. Redfern, "Anisotropy in the Hardness of Single Crystals," Proc. Roy. Soc. Lond. A, 322, 73-88, 1971.

Brunner, G. O., H. Wondratschek, and F. Laves, "Ultrarotuntersuchungen über den Einbau von H in Natürlichem Quarz," Zeitschrift für Electrochemie, 65, 735-750, 1961.

Carter, N. L., "Steady State Flow of Rocks," Rev. Geophys. Sp. Physics, 14, 301-310, 1976.

Carter, N. L., J. M. Christie, and D. T. Griggs, "Experimentally Produced Deformation Lamellae and Other Structures in Quartz Sand (Abst.): J. Geophys. Res., 66, 2518-2519, 1961.

Carter, N. L., J. M. Christie, and D. T. Griggs, "Experimental Deformation and Recrystallization of Quartz," J. Geology, 72, 687-733, 1964.

Chernov, A. A., and V. E. Khadzi, "Trapping of Colloidal Inclusions in the Growth of Quartz Crystals," J. Crystal Growth, 34, 641-646, 1968.

Christie, J. M., H. C. Heard, and P. N. LaMoir, "Experimental Deformation of Quartz Single Crystals at 27 to 30 kb Conf. Pressure and 24°C," Am. J. Science, 262, 26-55, 1964.

Cohen, A. J., "Regularity of the F-center Maxima in Fused Silica and α-Quartz," J. Chem. Phys., 22, 570, 1954.

Cohen, A. J., "Color Centers in the α-Quartz Called Amethyst," Am. Min., 41, 874-890, 1956.

Cohen, A. J., "The Role of Germanium Impurity in the Defect Structure," Glastechn. Ber., VI, 53-58, 1959.

Cohen, A. J., "Substitutional and Interstitial Aluminum Impurity in Quartz, Structure and Color Center Interrelationships," J. Phys. Chem. Solids, 3/4, 321-325, 1960.

Cohen, A. J., and E. S. Hodge, "Zonal Specificity and Nonspecificity of Certain Impurities During Growth of Synthetic α-Quartz," J. Phys. Chem. Solids, 7, 361-362, 1958.

Daniels, F. W., and O. G. Dunn, "The Effect of Orientation on Knoop Hardness of Single Crystals of Zinc and Silicon Ferrite," Trans. Am. Soc. Metals, 41, 419-442, 1949.

DeFord, J. W., and O. W. Johnson, "Defect and Impurity Thermodynamics in Rutilelike Systems," J. Appl. Phys., 44, 3001-3007, 1973.

Dekker, E. H. L. J., and G. D. Rieck, "Microhardness Investigations on Manganese Aluminate Spinels," J. of Mat. Sci., 9, 1839-1846, 1974.

Dennen, W. H., "Impurities in Quartz," B. G. S. A., 75, 241-246, 1964.

Dennen, W. H., and A. M. Puckell, "On the Chemistry and Color of Amethyst," Canadian Mineralogist, 11, 448-456, 1972.

Dennen, W. H., W. H. Blackburn, and A. Quesada, "Aluminum in Quartz as a Geothermometer," Contr. Mineral. and Petrol., 27, 332-342, 1970.

Dodd, D. M., and D. B. Fraser, "The 3000-3900 cm^{-1} Absorption Bands and Anelasticity in Crystalline α-Quartz," J. Chem. Phys. Solids, 26, 673-686, 1965.

Evans, B., and C. Goetze, "The Temperature Variation of Hardness of Olivine and Its Implication for Polycrystalline Yield Stress," submitted to J. Geophys. Res., 1978.

Feng, C., and C. Elbaum, "Effect of Crystallographic Orientation and Oxygen Content on Knoop Hardness Values of Iodide," Trans. TMS-AIME, 212, 47-50, 1958.

Frondel, C., The System OF Mineralogy of J. D. Dana and E. S. Dana, Seventh Edition, John Wiley & Sons, New York, 1962.

Frondel, C., and C. S. Hurlburt, Jr., "Determination of the Atomic Weight of Silicon by Physical Measurements on Quartz," J. Chem. Phys., 23, 1215-1219, 1954.

Garfinckle, M., and R. G. Garlick, "A Stereographic Representation of Knoop Hardness Anisotropy," TMS AIME, 242, 809-814, 1968.

Godbeer, W. C., and R. W. T. Wilkins, "The Water Content of a Synthetic Quartz," Am. Min., 62, 831-832, 1977.

Green, H. W., II, D. T. Griggs, and J. M. Christie, "Syntectonic and Annealing Recrystallization of Fine-Grained Quartz Aggregates," in Experimental and Natural Rock Deformation, Springer-Verlag, Berlin Heidelberg, New York, pp. 272-335, 1970.

Griggs, D. T., "Hydrolytic Weakening of Quartz and Other Silicates," Geophys. J. R. Astr. Soc., 14, 19-31, 1967.

Griggs, D. T., and Blacic, J. D., "The Strength of Quartz in the Ductile Regime," EOS Trans. Am. Geophys. Union, 45, 102-103, 1964.

Griggs, D. T., and J. D. Blacic, "Quartz: Anomalous Weakness of Synthetic Crystals," Science, 147, 292-295, 1965.

Griggs, D. T., F. J. Turner, and H. C. Heard, "Deformation of Rocks at 500° to 800°C," G. S. A. Memoir, 79, 39-104, 1960.

Hanneman, R. E., and J. H. Westbrook, "Effects of Adsorption on the Indentation Deformation of Non-Metallic Solids," Phil. Mag., 19, 73-88, 1968.

Hannink, R. H. J., D. L. Kohlstedt, and M. J. Murray, "Slip System Determination in Cubic Carbides by Hardness-Anisotropy," Proc. Roy. Soc. (London) A, 326, 409-421, 1972.

Haven, Y., and A. Kats, "Hydrogen in α-Quartz," Revue Silicates Industriels, N° de Mars, 1-4, 1962.

Heinisch, H. L., Jr., G. Sines, J. W. Goodman, and S. H. Kirby, "Elastic Stresses and Self Energies of Dislocations of Arbitrary Orientation in Anisotropic Media: Olivine, Orthopyroxene Calcite, and Quartz," J. G. R., 80, 1885-1896, 1975.

Hobbs, B. E., "Recrystallization of Single Crystals of Quartz," Tectonophysics, 6, 353-402, 1968.

Hobbs, B. E., A. C. McLaren, and M. S. Paterson, "Plasticity of Single Crystals of Synthetic Quartz," Geophys. Monograph 16, Flow and Fracture of Rocks.

Heard, H. C., I. Y. Borg, N. L. Carter, and C. B. Raleigh, Am. Geophys. Union, 1972.

Hopkins, J. R., J. A. Miller, and J. J. Martin, "Flow Stress, Vickers Hardness and Wing Size for KCl and KCl:KBr," Phys. St. S., A., 19, 591-595, 1973.

Phys. St. S., A., 19, 591-595, 1973.

Johnson, O. W., J. DeFord, and J. W. Shoner, "Experimental Technique for the Precise Determination of H and D Concentration in Rutile (TiO_2)," J. Appl. Phys., 44, 3008-3011, 1973.

Jost, W., Diffusion in Solids, Liquids, and Gases, Academic Press, New York, 1960.

Kats, A., and Y. Haven, "Infrared Absorption Bands in -Quartz in the 3μ-Region," Physics and Chemistry of Glasses, 1, 99-102, 1960.

Kats, A., "Hydrogen in Quartz," Thesis, University of Delft, 148 pp., 1961.

Kats, A., "Hydrogen in α-Quartz," Philips Research Reports, 17, 133-195, 201-279, 1962.

Khlapova, A. N., "X-Ray Data on the α-β Quartz Phase Transition," Sov. Phys.-Crystallogr., 7, 458, 1963.

Kelly, A., and G. W. Groves, Crystallography and Crystal Defects, Addison-Wesley, Reading, Mass., Chapt. 6, 179 pp., 1970.

Kirby, S. H., "Creep in Synthetic Quartz," EOS, Trans. Am. Geophys. Union, 56, 1062, 1975.

Kirby, S. H., "Micromechanical Interpretation of the Incubation Stage of the Creep of Hydrolytically Weakened Synthetic Quartz Single Crystals," (Abs.), EOS, Trans. Am. Geophys. Un., 58, 1239, 1977.

Kirby, S. H., J. W. McCormick, and M. Linker, "The Effect of Water Concentration on Creep Rates of Hydrolytically-Weakened Synthetic Quartz Single Crystals," (Abs.), EOS,

Trans. Am. Geophys. Un., 58, 1239, 1977.

Knoop, F., C. G. Peters, and W. B. Emerson, "Sensitive Pyramidal Diamond Tool for Indentation Measurements," J. Res. Nat. Bur. Stds., 23, 39-61, 1939.

Koester, R. D., ank D. P. Moak, "Hot Hardness of Selected Borides, Oxides and Carbides to 1900°C," J. Am. Ceramic Soc., 50, 290-296, 1967.

Kohlstedt, D. L., "The Temperature Dependence of Microhardness of the Transition-Metal Carbides," J. Materials Sci., 8, 777-786, 1973.

Kolb, E. D., D. A. Pinnow, T. C. Rich, R. A. Landise, A. R. Tynes, N. C. Lias, and Mrs. E. E. Grudenski, "Low Optical Loss Synthetic Quartz," Mat. Res. Bull., 7, 397-406, 1972.

Lehmann, G., "Interstitial Incorporation of Di and Trivalent Cobalt in Quartz," J. Phys. Chem. Solids, 30, 395-399, 1969.

Lias, N. C., Mrs. E. E. Grudenski, E. D. Kolb, and R. A. Landise, "The Growth of High Acoustic Q Quartz at High Growth Rates," J. Crystal Growth, 18, 1-6, 1973.

McCormick, J. W., "Transmission Electron Microscopy of Experimentally Deformed Synthetic Quartz," Thesis, University of California at Los Angeles, 1977.

McLaren, A. C., R. G. Turner, J. N. Boland, and B. E. Hobbs, "Dislocation Structure of the Deformation Lamellae in Synthetic Quartz, a Study by Electron and Optical Microscopy," Contr. Mineral. and Petrol., 29, 104-115, 1970.

McLaren, A. C., J. A. Ritchford, D. T. Griggs, J. M. Christie, and J. D. Blacic, "Transmission Electron Microscope Study of Brazil Twins and Dislocations Experimentally Produced in Natural Quartz," Physicus Status Solidi, 19, 631-644, 1967.

von Mises, R., "Mechanik der Plastichen Formanderung von Kristallen," Z. angew. Math. Mech., 8, 161-185, 1928.

Morrison-Smith, D. J., M. S. Paterson, and B. E. Hobbs, "An Electron Microscope Study of Plastic Deformation in Single Crystals of Synthetic Quartz," Tectonophysics, 33, 43-79, 1976.

Mott, B. W., Micro-Indentation Hardness Testing, Butterworth's Scientific Publications, London, 1956.

Mügge, O., "Über Translationen und verwandte Ersheinungen in Kristallen: Neues Jb. f. Min., Geol., Paläont., Teil 1, 71-159, 1898.

Nadeau, J. S., "Influence of Hydrogen and Alkali Impurities on the High-Temperature Indentation Hardness of Natural Quartz Crystals," J. Amer. Cer. Soc., 53, 568-573, 1970.

Paterson, M. W., "The Ductility of Rocks," in Physics of Strength and Plasticity, ed. by A. S. Argon, M.I.T. Press, Cambridge, pp. 377-392, 1969.

Rice, R. W., "The Compressive Strength of Ceramics" in Ceramics in Severe Environments Mater. Sci. Res., Vol. 5, ed. by W. W. Kriegel and H. Palmour III, Plenum Press, New York, pp. 195-229, 1971.

Saksena, B. D., "Interpretation of the Infrared Spectrum of α-Quartz in the 3μ Region on the Basis of Localized Modes Due to Substitutional Impurities," J. Chem. Phys. Solids, 26, 1929-1937, 1965.

Sangwal, K., and A. R. Patel, "Change in Dislocation Distribution and Hardness of Galena in Air-Annealing," J. Phys. D: Appl. Phys., 7, 2031-2035, 1974.

Taylor, E. W., "Correlation of the Moh's Scale of Hardness with the Vicker's Hardness Numbers," Mineral. Mag., 28, 718-721, 1949.

Thibault, N. W., and H. L. Nyquist, "The Measured Knoop Hardness of Hard Substances and Factors Affecting Its Determination," Trans. Am. Soc. Metals, 38, 271-323, 1947.

Tokar, M., and J. A. Leary, "Compressive Creep and Hot Hardness of U-Pu Carbides," J. Amer. Ceramic Soc., 56, 173-177, 1973.

Tsong, I. S. T., A. C. McLaren, and B. E. Hobbs, "Determination of Hydrogen in Silicates Using the Ion Beam Spectrochemical Analyzer: Application to Hydrolytic Weakening," Am. Mineral., 61, 921-926, 1976.

Tsong, I. S. T., and R. B. Liebert, "The Use of Sputter-Induced Emission Spectroscopy for the Analysis of Hydrogen in Solids," Nuc. Inst., 149, 523-527, 1978.

Westbrook, J. H., "Temperature Dependence of Strength and Brittleness of Some Quartz Structures," J. Amer. Ceramic Soc., 41, 433-440, 1958.

Westbrook, J. H., "The Temperature Dependence of Hardness of Some Common Oxides," Rev. Hautes Tempér. et. Réfract., 3, 47-57, 1966.

Westbrook, J. H., and P. J. Jorgensen, "Indentation Creep of Solids," Trans. AIME, 233, 425-428, 1965.

Westbrook, J. H., and P. J. Jorgensen, "Effects of Water Desorption on Indentation Microhardness Anisotropy in Minerals," Am. Mineralog., 53, 1899-1909, 1968.

White, C. W., D. L. Simms and N. H. Tolk, "Surface Composition by Analysis of Ion Impact Radiation," Science, 177, 481-486, 1972.

Wilkins, R. W. T., and W. Sabine, "Water Content of Some Nominally Anhydrous Silicates," Am. Min., 58, 508-516, 1973.

Winchell, H., "The Knoop Microhardness Tester as a Mineralogical Tool," Am. Mineralogist, 30, 583-595, 1945.

Young, B. B., and A. P. Millman, "Microhardness and Deformation Characteristics of Ore Minerals," Trans. Inst. Min. and Met. (London), 7, 437-466, 1964.

Yu, F. C., and J. C. M. Li, "Impression Creep of LiF Single Crystals," Phil. Mag., 36, 811-825, 1977.

CHAPTER III

LIMITATIONS OF THE METHOD AND ADDITIONAL SUGGESTIONS FOR FURTHER WORK

Abstract

The application of indentation hardness is limited by several factors. Uncertainties in the determination of the constraint factor (C) caused by errors or lack of knowledge in the values of the temperature variation of the elastic modulus, and uncertainties in the constraint factor theory near the elastic limit; difficulties in observing the developing microstructure; and difficulties in the interpretation of indentation creep tests.

The hardness technique seems particularly appropriate for surveys of mechanical behavior of solid solution series such as the feldspars and as a tool combined with yield studies to extend the range of stresses achievable.

Introduction

Much of the foregoing material has attempted to convince the reader that hardness is a useful tool for the investigation of the mechanical properties of minerals. The technique has the advantage of being relatively rapid as compared to other creep tests. In addition, it is fairly reproducible, and one may achieve an accuracy of 4% with some effort. Only small amounts of material are necessary, which increases the efficiency of the samples used. For instance, many hardness tests were conducted on one single solid medium test sample

(see the discussion of pressure annealing samples HBQ 329 ETI). In addition, the hardness test can be used to explore a region of stress-temperature space which has only been attained heretofore in the diamond cell apparatus.

This chapter attempts to provide a more neutral perspective of the hardness technique and discusses some of the limitations of the test, a way in which its usefulness could be extended, and some problems of geologic interest to which it could be usefully applied.

Some limitations of the hardness technique

As is true of any experimental method, indentation hardness testing is not without its limitations. For example, in quartz at temperatures below 573°, the amount of elastic strain can be a significant fraction of the total strain during indentation. In terms of Johnson's (1970) constraint theory, the ratio of E/σ may be surprisingly small (10-15) for quartz at room temperature. In this region, because of the departure of experimental data from the Johnson theory, the determination of the constraint factor may be somewhat uncertain. Secondly, some knowledge of the variation of the elastic constants with temperature is required and error in those values has concomitant error in the reduction of hardness data to hardness-derived yield stresses.

There are, however, other limitations to the use of hardness data, which if overcome, would greatly increase the efficacy of the method: difficulties in interpreting indentation creep tests and difficulties in tracing microstructural

development. The former problem is discussed in some detail below. Microstructural observations are invaluable in postulating constitutive equations. Without their aid, one has a much more difficult time establishing that an empirical relationship may be extrapolated from regions of laboratory accessibility to regions of theoretical (and particularly geological!) interest. The advent of the decoration technique for olivine (Kohlstedt et al., 1976) made rapid and detailed observations of the dislocation structure possible. Unfortunately, such a happy circumstance does not emerge for quartz. Several attempts have been made to observe indented and ion-thinned sections of quartz, but they have not yet been successful due to the small size of the indents and the intensity of the deformation in the yielded region.

Indentation creep

In order to compare creep and hardness tests, one needs to determine an effective strain rate for the hardness test. In this thesis, that problem was approached by an empirical determination. High quality stress-strain rate data happened to be available for two readily accessible and geologically interesting materials: olivine (Kohlstedt et al., 1974) and Maryland diabase (Yves Caristan, unpublished data). The empirical determination is interesting in several respects. The olivine hardness data were obtained using the mutual indentation technique. During those experiments no cracking at all was observed. The hardness points also partially span a region where the dislocation mechanism has been demonstrated

to be changing from glide, cross slip and climb processes to predominantly glide alone (Durham, 1975). Yet, except for a single anomalously low data point, the empirically determined strain rate remains reasonably constant. The Maryland diabase (VDP) experiments show at least coincidental agreement of two different materials. It should be recognized, however, that both the diabase and the higher temperature peridot experiments were conducted in roughly similar temperature regimes ($\frac{T}{T_m}$ = ~.55 to .8 for olivine and $\frac{T}{T_m}$ = ~.8 for the diabase, assuming T_m = 1250°C). There is, therefore, some uncertainty in extending the empirical correlation of strain rate into the region where the power law is not likely to apply, e.g., the high stress "power law breakdown" region. This uncertainty is lessened by the fact that such high strength regions are quite likely to be relatively athermal and thus less strain rate sensitive.

However, to fully exploit the hardness test, it would be desirable to be able to discover the yield properties using indentation creep. Hargreaves (1928) reported for several metals that the effect of increasing dwell time (t) could be expressed as an equation of the form

$$\log H = A_1 - B_1 \log t \qquad (1)$$

where A_1 and B_1 are constants for a given temperature.

Subsequently Ito (1923) and Nunes and Larson (1963) published similar equations of empirical correlations of log hardness and temperature and hardness and the reciprocal of the temperature. It now seems clear that the proper relationship of hardness and temperature is

$$H = A_2 \exp + \frac{Q_H}{nRT} \quad \text{(Sherby and Armstrong, 1971)} \quad (2)$$

where n may be identified as the exponent of strain rate sensitivity of stress, Q_H is an apparent activation energy which may be identified with the operative deformation mechanism, and A_2 is a pre-exponential "constant" factor which contains a modulus of elasticity dependence.

From the discussions above concerning the variation of the constraint factor, it is clear that a better method of describing the hardness-temperature relationship would be

$$\sigma_H = A_3 \exp + \frac{Q_H}{nRT} \quad (3)$$

where $\sigma_H = H/C$ and is the hardness-derived yield stress discussed above. A_3 might still contain an elastic modulus term (Johnson, 1970; see also Chapter I and Sherby and Armstrong, 1971). Sherby and Armstrong (1971) indicate that Q_H is correlated with the appropriate activation energy for plastic deformation for many materials. Thus by determining an empirical strain rate for indentation as was done in the case of olivine and diabase, the hardness derived yield curve can be used with data collected at constant temperature and varying strain rate to determine the material and deformation process parameters of a

flow law such as

$$\dot{\varepsilon} = \dot{\varepsilon}_o \, \sigma_H^{\,n} \exp - \frac{Q}{RT} \qquad (4)$$

as was done in the case of olivine (although a different form of the flow law was indicated).

During the investigation of flow regimes which are unattainable by ordinary deformation experiments, it would be highly desirable to be able to determine flow law parameters using only the hardness test. In this regard, the indentation creep test appears to be extremely attractive. Several attempts to exploit this test have been made (Atkins and others, 1966; T. Evans and Sykes, 1973; Yu and Li, 1977). However, the interpretation of the indentation creep test differs in these studies. Atkins et al. (1966) describe the process as involving the expansion of a growing plastic hemisphere into an elastic half space, assuming that the effective strain behaves as though it were proportional to the diameter of the indent cubed (d^3). The following indentation creep relation obtains after further assuming that the material deforms according to a transient strain relation:

Transient relation: $$\dot{\varepsilon}_{tr} = \dot{\varepsilon}_{otr} \, \sigma^{m/3} \exp\left(- \frac{Q}{3RT}\right) \, t^{-\frac{2}{3}} \qquad (5)$$

Indentation creep relation: $$H^{-m/3} - H_o^{-m/3} = A_4 \exp\left(- \frac{Q}{3RT}\right) \cdot \left(t^{\frac{1}{3}} - t_o^{\frac{1}{3}}\right) \qquad (6)$$

where $\dot{\varepsilon}_{otr}$ and A_4 are constants.

T. Evans and Sykes (1973), using equation (6) (Atkins et al. (1966), determined creep parameters for diamond at 1500°C to 1850°C, but they conclude that the correct stress exponent (m)

to use in equation (6) is the steady state exponent (i.e., n in equation (4)). Yu and Li (1977) have developed an indentation punching experiment which shows excellent agreement with single crystal studies on lithium fluoride. They use still another method to determine the strain rate-dwell time relation, namely the correspondence that the velocity of punching is directly proportional to $\dot{\varepsilon}$ in a single crystal test. The punching experiment uses a cylindrical flat tipped brale as the indentor.

Some indentation creep experiments were done on olivine and quartz. They are insufficient to distinguish between the various approaches to indentation creep, however, for the following reasons: Indentation creep tests are needed at several different temperatures in order to determine Q and m in equation 6. Experiments in quartz at temperatures ~700-800°C were plagued by the hardening mechanism discussed earlier. In the case of olivine, many replications of the tests are necessary to achieve precision in the data since the deformation regime under investigation is relatively insensitive to strain rate ($T < 1000°C$, $\sigma_H > .2$ GPa). Furthermore, it will be necessary to reconsider the problem of a plastic sphere expanding into an elastic material which deforms by a stress activated flow law (see Chapter I, Conclusions). Several attempts were made to duplicate the punching experiments of Yu and Li (1977). They were unsuccessful because stress concentrations around the blunt punch caused fracture of the specimens. With further effort some of these problems are probably surmountable; however, for the present, I merely summarize the results obtained.

(1) Both quartz and olivine appear to approximately obey the Hargreaves (1928) relation.

For olivine (500°C): $\log[H(Kg/mm^2)] = 2.908 - 2.2 \times 10^{-3} \log[t(s)]$

For quartz (600°C): $\log[H] = 2.914 - 3.0 \times 10^{-3} \log[t]$

(2) For the correct exponent (m), equation 6 predicts linear plots of $(H^{-m/3} - H_o^{-m/3})$ and $(t^{\frac{1}{3}} - t_o^{\frac{1}{3}})$ with slope of unity where t_o is 1.00 and H_o is determined from the Hargreaves relation. These two conditions are not satisfied by the present data set on quartz at 600°C by any of the exponents: 10 (suggested for MgO by Atkins et al., 1966), 6.5 (suggested for the flow of "dry" quartz, Parrish et al., 1976) or 3 ("wet" flow law exponent, Parrish et al., 1976).

(3) The data sets are inadequate in quality and quantity to distinguish the appropriate approach to indentation creep or to determine flow law parameters.

Further work on this problem could develop a potentially useful technique.

Some suggestions for future applications of indentation hardness

Many common minerals are members of solid solution series which may contain several components. Two examples of great geologic interest are the plagioclase and alkali feldspar series, $Na[Al\ Si_3O_8] - Ca[Al_2Si_2O_8]$ and $K[Al\ Si_3O_8] - Na[Al\ Si_3O_8]$. Since it would take an inordinate amount of time to perform creep tests on an inclusive range of minerals in these series, the method of indentation hardness testing suggests itself as a viable alternative. Although little data on the variation of

elastic constants exist, comparative strength measurements could be made without this data. Unfortunately, the effort necessary to measure the elastic moduli as a function of temperature would be considerable because of the low symmetry of these materials, even though it would also be very useful. In the absence of the elastic moduli-temperature variation, an estimate could be made using a "typical" temperature variation of Young's modulus computed using an average of values for other minerals. I have done this and used the Johnson (1970) theory to compute hardness derived yield stresses for hardness data obtained on feldspars in two samples of anorthitic rocks from Split Rock, Minnesota, and Essex City, New York. Young's modulus was assumed to vary according to $\frac{1}{E}\frac{\partial E}{\partial T} = 3 \times 10^{-4}/K$, which is an intermediate value between quartz ($\frac{1}{E}\frac{\partial E}{\partial T} = 4 \times 10^{-4}/K$) and olivine ($\frac{1}{E}\frac{\partial E}{\partial T} = 2 \times 10^{-4}/K$) (Simmons and Wang, 1971). The applicability of polycrystalline indentation data is not well established, but may depend on the likelihood of impingement on pre-existing cracks. Frederick diabase is very fine-grained and is known to have a very low density of cracks (Feves et al., 1977). It may be that, in such materials, polycrystalline VDP experiments are controlled by ductile flow. Figure 1 shows the reduction of this data using the methods described above.

For comparison the yield stress from Y. Caristan's experiments on Frederick diabase at .5 GPa confining pressure and 990°C is shown. It goes without saying that the curves shown in Figure 1 should be regarded only as estimates, there being uncertainty in the elastic moduli and the applicability of the polycrystalline indentation test. Furthermore, the

Figure 1. Hardness Derived-Yield Stress as a Function of Temperature for Two Anorthitic Rocks (solid triangles) and Frederick, Maryland Diabase.

The diabase is a very fine-grained rock, primarily bimineralic (pyroxene and feldspar) and with very low crack density. Brace's (1961) hardness indentations (open triangles) spanned many mineral grains. Shown for comparison is data from Y. Caristan, conducted at confining pressure of .5 GPa and at a strain rate of 10^{-5}/s.

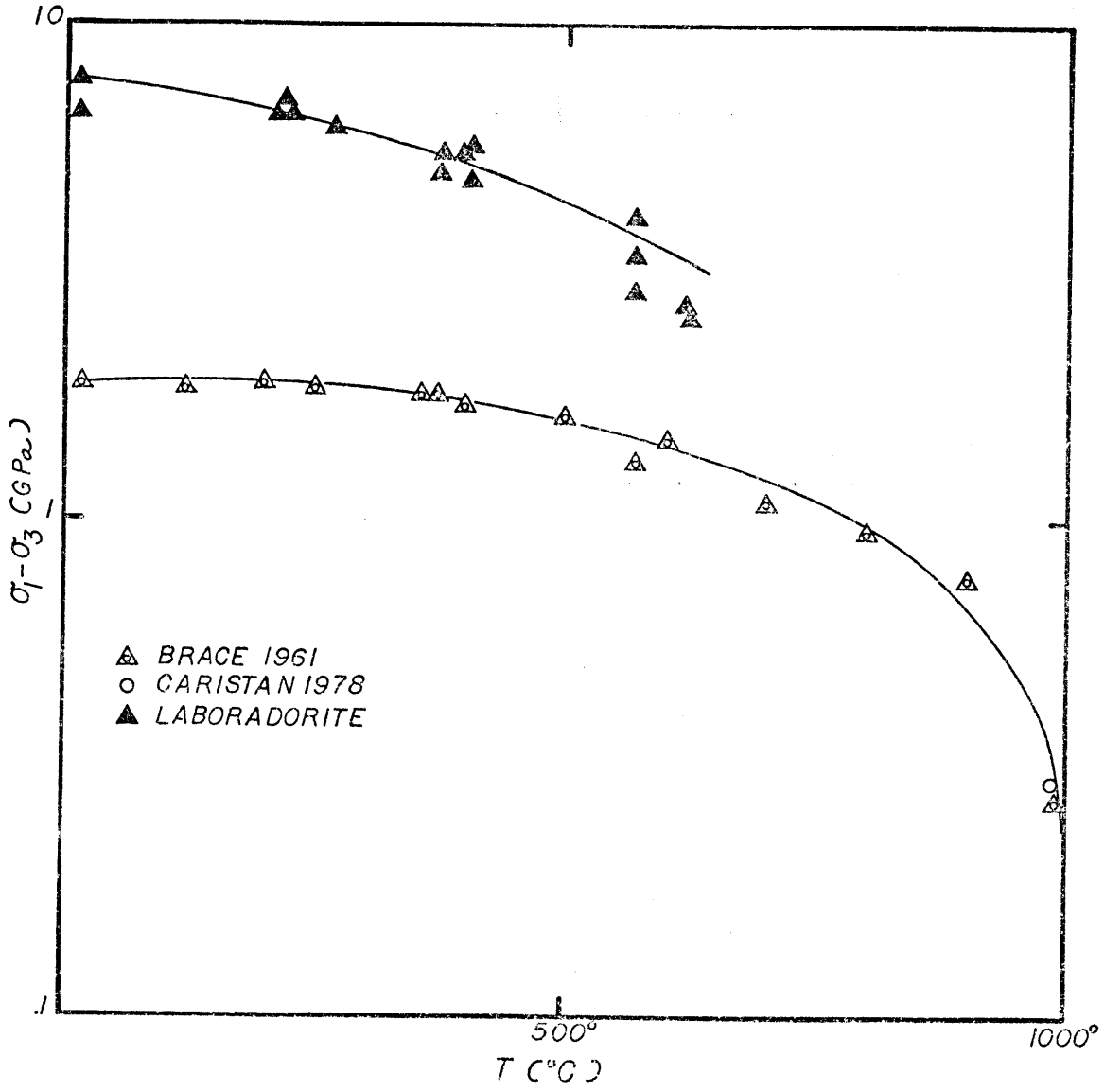
10
1
.1
$\sigma_1-\sigma_3$ (GPa)
500°
1000°
T (°C)
BRACE 1961
CARISTAN 1978
LABORADORITE

hardness points on the feldspar samples scatter rather widely because in some cases the crystals contain pre-existing cracks which perturb the stress field around the indentation. The intention of presenting this data has been simply to indicate fruitful avenues of investigation using the indentation method. These experiments could be extended without great difficulty and the results used to guide a thorough investigation of the mechanical properties of the feldspar series.

REFERENCES

Atkins, A.G., A. Silverio, and D. Tabor, Indentation hardness and the creep of solids, J. Inst. Met., 94, 369-378, 1966.

Durham, W.B., Plastic flow of single-crystal olivine, Doctoral dissertation, M.I.T., September 1975, 253 pp.

Evans, T., and J. Sykes, Indentation hardness of two types of diamond in the temperature range 1500°C to 1850°C, Phil. Mag., 29, 135-147, 1973.

Feves, M., G. Simmons, and R.W. Siegfried, Microcracks in crustal igneous rocks: Physical properties, in Geophysical Monograph 20, The Earth's Crust, Amer. Geophys. Union, Washington, D.C., pp. 95-117, 1977.

Hargreaves, F., The ball hardness and the cold-working of soft metals and eutectics, J. Inst. Met., 39, 301-327, 1928.

Ito, K., The hardness of metals as affected by temperature, Sci. Rep. Tohoku Imp. Univ., Series 1, 12, 137-148, 1923.

Johnson, K.L., The correlation of indentation experiments, J. Mech. Phys. Solids, 18, 115-126, 1970.

Kohlstedt, D.L., C. Goetze, W.B. Durham, and J. Vander Sande, New technique for decorating dislocations in olivine, Science, 191, 1045-1046, 1976.

Kohlstedt, D.L., C. Goetze, and W.B. Durham, Experimental deformation of single crystal olivine with application to flow in the mantle, in Strens, R.G.J. (ed.), The Physics and Chemistry of Minerals and Rocks, John Wiley & Sons, London, 1974, pp. 37-49.

Nunes, J., and F.R. Larson, Low temperature hardness and flow-stress relationships of metals, J. Inst. Met., 91, 114-117, 1962-63.

Parrish, D.K., A.L. Krivz, and N.L. Carter, Finite element folds of similar geometry, Tectonophysics, 32, 183-208, 1976.

Sherby, O.D., and P.E. Armstrong, Prediction of activation energies for creep and self-diffusion from hot-hardness data, Met. Trans., 2, 3479-3484, 1971.

Simmons, G., and H. Wang, Single Crystal Elastic Constants and Calculated Aggregate Properties: A Handbook, M.I.T. Press, Cambridge, Mass. 1971, 370 pp.

Yu, E.C., and J.C.M. Li, Impression creep of LiF single crystals, Phil. Mag., 36, 811-825, 1977.